DETERMINATION OF THE NORTH RUKURU RIVER FLOODING EXTENT IN KARONGA DISTRICT, MALAWI

MASTER OF SCIENCE DEGREE IN WATER RESOURCES MANAGEMENT

THESIS

GEOFFREY GOMBOZA MLITA MANDA

MZUZU UNIVERSITY, MALAWI

DECEMBER 2025

DETERMINATION OF THE NORTH RUKURU RIVER FLOODING EXTENT IN KARONGA DISTRICT, MALAWI

GEOFFREY GOMBOZA MLITA MANDA

A THESIS SUBMITTED TO THE FACULTY OF ENVIRONMENTAL SCIENCES, DEPARTMENT OF WATER AND SANITATION IN FULFILMENT OF THE REQUIREMENTS FOR THE AWARD OF A MASTER OF SCIENCE DEGREE IN WATER RESOURCES MANAGEMENT

MZUZU UNIVERSITY

DECEMBER 2025

DECLARATION

I hereby declare that this thesis titled, "*Determination of the North Rukuru River flooding extent in Karonga District, Malawi"* has been written by me and is a record of my research work. All citations, references, and borrowed ideas have been duly acknowledged. It is being submitted in fulfilment of the requirements for the award of a Master of Science Degree in Water Resources Management and Development at Mzuzu University. None of the present work has been submitted previously for any degree or examination at any other University.

_____ _____

Student's name **Date**

Geoffrey Gomboza Mlita Manda

CERTIFICATE OF COMPLETION

The undersigned certify that this thesis is a result of the author's work and to the best of our knowledge, it has not been submitted for any other academic qualification within Mzuzu University or elsewhere:

Signature: _____ Date: _____

Main Supervisor: Dr. Brighton Chunga (Ph.D.)

Signature: _____ Date: _____

Co-supervisor: Dr. Frank Mnthambala (Ph.D.)

Signature: _____ Date: _____

Postgraduate Coordinator: Dr. Russel Chidya (Ph.D.)

Signature: _____ Date: _____

Head of Department: Mr. Willy Chipeta

ABSTRACT

Karonga district has experienced devastating floods since 1946, and it was the worst-hit district in Malawi in 2017. The district faces an increasing flood risk due to the downstream overflow of the North Rukuru River (NRR) and dyke failure. A reliable mitigation strategy involves using flood inundation maps to assess flood extent and dyke effectiveness. This study aimed to determine North Rukuru River flooding extent. Flood frequency analysis using streamflow data (1979–2022) from Mwakimeme gauge station applied Gumbel's and Log-Pearson Type III (LP3) distributions to estimate peak flows for various return periods from NRR. Chi-square, Anderson-Darling, and Kolmogorov-Smirnov tests identified LP3 as the best-fit distribution. Peak flows for 2, 5, 10, 25, 50, and 100-year return periods were 1028 m^3/s, 1306 m^3/s, 1474 m^3/s, 1675 m^3/s, 1815 m^3/s, and 1950 m^3/s, respectively. These were input into a HEC-RAS model to simulate flood depths along river reaches. Maximum channel flood depths at Mwakimeme gauge station were 5.15 m, 6.00 m, 6.47 m, 6.99 m, 7.33 m, and 7.65 m for the respective return periods. ArcGIS was used with HEC-RAS outputs to generate flood inundation maps. Flooded areas under the same return periods were 254,209.5 m^2, 289,555.8 m^2, 309,817.3 m^2, 332,673.4 m^2, 348,384.7 m^2, and 362,771.7 m^2. Inundation maps developed showed Peter Mwangalaba, Mwanyesha, Mwamatope, Mwanganda, Mwanyongo, Mwahimba, Mweniyumba, Mwanjabala, and Katolora as consistently affected by all flood magnitudes. The 1.5 m height dyke was breached across all flood magnitudes. Household survey was conducted to further evaluate effectiveness of the dyke. Notably, 96.70% (381 out of 394) supported reinforcement and extension of the dyke, confirming persistent vulnerability despite its presence. Therefore, this study recommends the use of flood inundation maps developed as a

flood control measure to demarcate safe zones, and to reinforce, and extend the dyke height to 2-4.6 m according to a 100 year flood depth.

Keywords: Flood inundation mapping, Flood frequency analysis, Karonga, HEC-RAS, ArcGIS

DEDICATION

This work is dedicated to my loving and caring parents, Mr. and Mrs. Manda for their love, support and guidance. It is heartbreaking that my father is no longer with me in this earthly world to witness this success. The fond memories of him continue to shape my life. Continue resting in peace dad. To my brothers, sisters, niece, nephew, and to you friends who have encouraged and supported me throughout this journey, this is for you. I love you all, strive always to be good people out there.

ACKNOWLEDGEMENT

Firstly, I would like to render my profound gratitude to my supervisors Dr. Brighton Chunga and Dr. Frank Mnthambala for their guidance and insightful criticisms. This work would not have been accomplished without their mentorship and assistance.

To members of staff and supporting staff of the Department of Water and Sanitation, I am truly grateful for the encouragement, assistance and support, especially Mr. Aimloce Banda.

This research was supported by the Norwegian Program for Capacity Development Higher Education and Research for Development (NORHED) under the Climate change and ecosystems management in Malawi and Tanzania project (# 63826). I fondly recognize them for funding my work. To my loving and caring colleagues Mrs. Stella Jossiah and Eng. Jeremiah Nkowani thank you for pushing and encouraging me. You made my stay at Mzuzu University wonderful, may God richly bless you. To the project management team, Dr. Brighton Chunga, Dr. Benjamin Kondowe, Dr. Russel Chidya, Dr. Kumbukani Mzengereza, and Professor Wales Singini, the Vice Chancellor and indeed my fellow students from the Fisheries department, thank you all. Special thanks to Dr. Russel Chidya and Dr. Kumbukani Mzengereza for always encouraging me to soldier on. Here we are finally, at the last mile and we are all smiles. May God bless you all.

Table of Contents

LIST OF TABLES

LIST OF FIGURES

ACRONYMS

ALOS	Advanced Land Observing Satellite
DCCMS	Department of Climate Change and Meteorological Services
DoDMA	Department of Disaster Management and Affairs
GEV	Gumbel Extreme Value
FFA	Flood Frequency Analysis
GDP	Gross Domestic Product
GIS	Geographic Information System
GOM	Government of Malawi
HEC-RAS	Hydrologic Engineering Centre's River Analysis
SRTM	Shuttle Radar Topography Mission
SWAT	Soil and Water Assessment Tool

CHAPTER 1 : INTRODUCTION

1.1 Background

Flooding is among the most prevalent natural hazards affecting people around the world. For the past 20 years, floods have been the most common natural hazards, accounting for 43 percent of all disasters and causing the most concern among the global population (Rangari *et al.* 2021; UNDRR 2020). It is estimated that 1.47 billion people, or 19 percent of the world population, are directly exposed to substantial risks during 1-in-100-year flood events (Rentschler and Salhab 2020).

Africa has not been spared; the destruction of vital amenities such as power lines, roads, schools, health facilities, as well as farmlands and livestock, lead to untold economic costs to the already poverty-stricken continent. For instance, in 2022, West and Central Africa experienced one of the worst years in terms of flooding, with 8.5 million people affected, 1,567 reported dead, and 4,401 injured in 20 countries of the region (OCHA 2023). The most affected countries were Nigeria, Chad and the Democratic Republic of Congo, with 4.5 million,1.5 million and 946,000 people affected, respectively. Of the 132 million people who are estimated to live in both extreme poverty and in high flood risk areas, 55 percent are in Sub-Saharan Africa (Rentschler and Salhab 2020).

Malawi is highly vulnerable to the impacts of extreme weather events given its location along the Great African Rift Valley, rapid population growth, unsustainable urbanization, climate variability and change, and environmental degradation (Garcin *et al.* 2025; GoM 2019). Districts such as Karonga, Phalombe, Chikwawa, Sanje, Zomba, and Salima have faced recurrent floods, causing severe losses of property, lives, and crops (DoDMA 2023). Over the

past five decades, Malawi has experienced more than 19 major floods, with these events increasing in frequency, magnitude and scope over the years (DoDMA 2019). The 2023 floods alone, mostly caused by Cyclone Freddy, affected over 2.2 million people, killing 679, over 530 people were declared missing and caused estimated damages of over $500 million (GoM 2023). Floods and droughts together result in annual losses of at least 1.7 percent of the country's GDP (Šakić *et al.* 2017).

Table 1. Frequency of flood occurrence in notable flood-prone areas in Malawi

Area	**Period of occurrence**
Karonga	2001,2012,2013,2015,2017,2023,2024
Phalombe	1991,2023
Lower-shire (Chikwawa & Nsanje)	1956,1984,2012,2015,2019,2022
Zomba	1946,2023
Salima	2010,2012,2019,2021,2022,2023

Source: DoDMA (2023)

Karonga district has experienced devastating floods since 1946 (Manda *et al.* 2016). The district registered the largest number of disasters in Malawi between 1946 and 2008 (Runduka *et al.* 2010). In particular, extreme were the floods in 1979-1980, which damaged most of the old town and led to the relocation of the commercial center to the current site (Manda 2014). In 2017, Karonga was the district that was worst hit by floods, with an estimated 41,430 people affected, more than 5,000 displaced, killing 4 people and injuring six with three people missing (UNICEF 2017).

A number of local factors intensify the risks of flooding in Karonga. The low altitude of the district, its high-water table and the increasing amount of construction in low-lying areas raise the potential for damage from flooding (Manda 2014). Numerous studies have been done to understand the nature of flooding in Karonga. Critical studies and recordings started in 1981 following the 1979/1980 floods which damaged most of the old town and led to the relocation of the town to the current site in 1987 (Manda *et al.* 2016). The 1979/1980 floods came about because of the rise in water level in Lake Malawi from 471m above Karonga reference level in 1915 to 477.8m in 1980 (Macheyeki *et al.* 2015). The location of the new town center was deemed as a much safer place from Lake Level rise related floods and riverine floods. Nevertheless, flooding has continued with varying degrees of impact. The feasibility study conducted by Gitec Consult in 1981 showed that Karonga district was at risk mainly due to riverine flooding of North Rukuru River.

In an effort to mitigate the adverse impacts of flood disasters on human life and property, societies have accumulated and refined water control practices over thousands of years (Wang *et al.* 2022). In the early years, flood control was given primary emphasis. Flood control refers to modifying the natural behavior of floods through engineering interventions to minimize disaster impacts. For instance, the use of leeves and dykes to contain floodwaters, and the use of diversion channels like canals to redirect floodwaters away from vulnerable areas. Flood control was initially implemented when humans recognized that floods, though inevitable, could be managed. Severe flooding in the United States during the 1920s, in China throughout the 1930s to 1950s, and across Europe in the late 1950s compelled societies to build resilient dams, and elevate dikes (Chiu *et al.* 2022). In the era of climate change, flood risks are intensifying, necessitating higher standards for flood control infrastructure. Nevertheless,

despite the implementation of numerous flood management projects, flood disasters have persisted, gradually revealing to societies the inherent limitations of structural flood defenses (Kundzewicz *et al.* 2019). For example, flood events in the 1990s on the Rhine River in Switzerland and in the UK, the Asia tsunami in 2004, and 2005 floods in New Orleans, USA despite the presence of well-engineered flood control structures like levees (Sayers *et al.* 2015). As a result, societies are now learning more towards risk-based flood management which aims to keep humans away from flood waters than flood control which aims to keep flood waters away from humans through structural measures (Wang *et al.* 2022; Mudashiru *et al.* 2021). Flood inundation mapping is one of the prominent risk-based flood management strategy globally promoted (Garcin *et al.* 2025; Xing *et al.* 2021; Dotori *et al.,* 2013; Coles *et al.* 2017).

A number of directives, frameworks, and theories have been developed to support the concept of flood inundation mapping as a flood resilience strategy. Notably, the EU directive which provides an overall framework for integrated flood risk management and requires EU Member States to identify Areas of Potential Significant Flood Risk (APSFRs) using detail flood hazard and risk maps (European Council 2007); the U.S National Flood Insurance Program (NFIP) established in 1968 in order to provide appropriate protection against the perils of floods losses by minimizing exposure of property to floods through flood insurance maps indicating different levels of risks (NFIP 2021); the Danube Flood Risk Management Plan established in 2015, a directive which focuses on flood risk mapping along the Danube river (ICPDR 2021); the DOST-UP Disaster Risk and Exposure Assessment for Mitigation (DREAM) Program, a cutting-edge research project framework in the Philippines, promotes the use of flood hazards maps for major river systems (Santillan *et al.* 2016; UP DREAM 2016); the Hyogo Policy Framework advocates for the resilience of communities and nations through the development

and dissemination of flood risk maps (UNISDR 2005). There is a growing need to adopt these frameworks and strengthen advocacy for flood inundation mapping in the era of accelerating climate change and rapid urbanization, particularly in developing countries across Africa.

There is clearly much work to be done in flood inundation mapping as a flood risk management tool in Africa. For instance, a study in 2016 done by Lumbroso and his colleagues found that of the 54 countries in Africa, there were only 7 stakeholders who deemed risk assessment for floods to be effective (Lumbroso *et al.* 2016). Out of these seven countries, South Africa has produced flood hazard maps for high-risk flood zones for over two decades, while Mozambique began major flood mapping after the 2000 floods (Lumbroso *et al.* 2014). Considerable emphasis has been placed on structural flood management measures, notably the establishment of dykes along the Nile River, the construction of barrages and large-scale dams, as well as the deployment of check dams and sandbags within vulnerable communities (Brasa 2023). Despite extensive investments in physical flood control structures, Africa continues to experience severe flooding. Between 2008 and 2018, floods accounted for 65% of disaster events and 24% of deaths (Dal. 2024). This underscores the urgent need for African states to integrate risk-based flood management tools like flood inundation maps alongside physical infrastructures to safeguard lives and property.

This is also the case with Malawi and its communities, flood mapping is not perceived as particularly effective in reducing the impacts of floods. A lot of effort is put on structural flood mitigation measures such as canals and dikes which comes with their failures. In Karonga district, the primary and most common means of local defense against floods are dykes and canals. Following the devastating floods of 1979–1980 that severely impacted Karonga District, major structural flood control measures were introduced, including the construction

of a dyke along the North Rukuru River and artificial drainage channels to direct floodwaters into Lake Malawi (Manda 2014). Despite their continued use as primary protective infrastructure, recurrent flooding in various parts of the district highlights their limitations. With the global advancement and adoption of flood inundation mapping, there is a growing need to integrate these non-structural tools with existing physical structures to enhance flood risk mitigation. Flood inundation maps provide a reliable means to identify flood prone areas across different return periods and assess the performance of the dyke against varying flood depths. This study was therefore undertaken to identify safe and flood prone areas, determine the efficacy of the dyke and to some extent explore alternative mitigation strategies that complement or improve upon the existing infrastructure. By integrating flood mapping with structural measures, Karonga District can strengthen its capacity for flood prevention and community protection.

1.2 Problem Statement

Karonga district is prone to several natural hazards, but floods are locally regarded as the most serious (Manda and Wanda 2017). The frequent overflowing of the North Rukuru River, which is further aggravated by human settlements in the floodplain, poses a significant threat to Karonga Town and surrounding communities. 60% of informal houses are built on flood plains (Gondwe *et a/* 2017). The floodplains of North Rukuru River, spanning up to 125 meters from the riverbank are home to many informal settlements, vulnerable to flooding even frequent low impact events. Flooding of the North Rukuru river occurred almost every wet season between 2009 and 2016 (Manda and Wanda 2017). In 2017 alone, a total number of 8,286 households, representing 55,921 people, were affected by floods, mainly due to overflowing of North Rukuru river (IFRC 2018). In 2024, flooding from the North Rukuru River affected 911

households, resulting in the displacement of 516 individuals and in 2025, the magnitude of the disaster intensified in Karonga, with 7,740 people affected and 2,138 displaced (MRCS 2024; ACT 2025). The council and people of Karonga have tried to protect themselves from floods, and dykes and artificial channels have remained the primary local defense against floods since 1980 (Manda 2014). Despite the use of these physical structures, flooding from North Rukuru River continues to affect people significantly, damaging their houses, crops and other infrastructures. In an attempt to identify an effective mitigation strategy apart from the dykes and artificial channels which have shown massive weaknesses, a land use planning tool has also been used, however instead of mitigating flood risks, it has divided the district into informal and informal settlements, exacerbating flood risks to the poor who usually settle in informal settlements which are customarily considered flood prone areas (Gondwe *et al.* 2017). The use of flood inundation maps has gained world promotion and recognition in this era of climate change and rapid urbanization, core drivers of flooding, as these flood inundation maps identify cross-sections where flooding phenomenon is prominent and offers insights in containing floods within the river by providing reliable designs of embankments, or flood walls heights according to simulated flood depths (Wahba *et al*. 2024; European Council 2007; UP DREAM 2016; Pathan and Agnihotri 2019). Despite, flood inundation maps being extensively used and promoted worldwide, its use as an alternative flood mitigation measure has been neglected in Karonga, as much priority has been given to physical control structures such as dykes, even with their evident weaknesses.

Flood inundation maps provide better insights in planning for flood risk management strategies. They precisely indicate the extent to which floods of different return periods or severities would affect different areas. This promotes a targeted flood risk management

strategy where people are settled in safe areas, infrastructures to withstand floods of different severities are built and embarkments to withstand floods of highest possible depths are built. The integration of the flood inundation maps and physical flood control structures like dykes in Karonga offers a reliable flood mitigation strategy which demarcates safe zones preventing people from settling in flood prone areas, and provides an opportunity for the right height to which the dyke built along North Rukuru River could be raised. This study addresses this by exploring the flood frequency analysis in the North Rukuru river using Log-Pearson Type 3 and Gumbel Extreme Value statistical models, identifying flood-prone areas using flood inundation maps generated through a combination of HEC-RAS model and ArcGIS, and evaluating the efficacy of the dyke in withstanding designed flood depths of different return periods, as simulated by the HEC-RAS model. It also gathers feedback from local stakeholders on the effectiveness of the dyke in protecting them against floods, through focus group discussions, surveys, and key informant interviews.

1.3 Research Aim and Objectives

1.3.1 Main Objective

This research study aimed to determine the extent of flooding of the North Rukuru River in Karonga district.

1.3.2 Specific Objectives

The specific objectives were as follows:

a. To estimate the North Rukuru River discharges for different return periods in Karonga District.
b. To simulate flood water depths for North Rukuru River in Karonga District.

c. To develop flood inundation maps for the downstream North Rukuru River in Karonga District.
d. To evaluate the effectiveness of the dyke as a flood control structure along the North Rukuru River.

1.4 Research Questions

The following key research questions were raised about the extent of flooding in Karonga under different return periods:

a. What are the resultant flood magnitudes (Q) of 2, 5, 10, 25, 50, and 100 years return periods?
b. What are the flood depths for simulated 2, 5, 10, 25, 50, and 100 year design floods?
c. To what extent would flood depths of 2, 5, 10, 25, 50, and 100 year design floods reach?
d. What is the effectiveness of the dyke as a flood control measure against simulated flood depths of different return periods and according to community perception?

1.5 Significance of the Study

The study was important because among other things, it offers reliable spatial data for development planning in Karonga District. The research produces trustworthy geospatial information that can assist in land-use planning, urban growth, and infrastructure projects, helping to avoid building in areas that are highly susceptible to flooding. This is in line with sustainable development goal (SDG) 11, which advocates for sustainable cities and communities as well as Malawi Vision 2063, which promotes a Malawi that has cities and communities in a safe, clean, and secure environment. Data realized from the effectiveness of the dyke gives a clue to Karonga council and DoDMA if the flood control structures currently

in place is able and capable of protecting people from floods of different magnitudes and any recommended improvements.

1.6 Summary of the introduction chapter

This chapter examines the global extent of flooding, with a particular focus on Africa and subsequently Malawi. It explores societal responses to flood hazards, tracing the shift from reliance on engineering-based flood control structures to the adoption of risk-based management approaches such as flood inundation mapping. The discussion highlights the limited use of inundation maps by institutions such as the Karonga District Council, despite their widespread promotion as effective tools for flood mitigation worldwide. The chapter further outlines the study's objectives in alignment with the research questions and provides a justification of the study, emphasizing the value of flood inundation maps in supplying spatial data crucial for development planning.

CHAPTER 2 : LITERATURE REVIEW

2.1 Introduction

This chapter reviews frequency distributions used to to estimate river discharges for various return periods, and scenarios around the world where HEC-RAS model has been used to simulate river flood depths on gauge stations. Further, it also discusses the development and use of flood inundation maps around the world as a risk-based flood management strategy and lack of its use in Karonga district. Lastly, it tackles on the use of flood inundation maps to evaluate effectiveness of the dyke, as well seeking perception of the communities to evaluate effectiveness of the dyke. In such a way, it illustrates the use of flood inundation maps and physical flood control structures like dykes to complement each other.

2.2 Estimating River discharges for different return periods

Estimating river discharge is an important component of flood management, serving as the initial step in understanding flood behavior and severity of rivers. There are several methods by which to estimate river discharges. Some of them are purely empirical and some are based on statistical analysis of historical records (Ghosh 2014). In this study a statistical analysis of the previous streamflow records was done. The whole process is termed flood frequency analysis, and the two statistical models or frequency distributions used were log Pearson Type III distribution and the Gumbel Extreme value distribution.

In detail, flood frequency analysis is a technique used to predict flow magnitudes corresponding to specific return periods (T) or exceedance probabilities (EP) along the river. The return period of a flood is the average time interval (in years) between floods of a certain magnitude, while the exceedance probability is the likelihood that such a flood will occur in

any given year. The information from flood frequency analysis is essential for defining flood hazard areas, for managing floodplains, and for designing bridges, culverts, dams, levees (dykes), and other flood control structures (Vivekanandan 2015). Fundamental to flood frequency analysis is the selection of frequency distribution fitted to the data set (Zhang *et* al. 2021).

A multitude of distributions have been used in flood frequency analysis. The Log-Pearson type three (LPT3) distribution is used in the U.S and Australia (Benameur *et al.* 2017); the Pearson type three (P3) distribution is recommended in China by the Ministry of Water Resources Republic of China as studies have shown that it has the most satisfactory results when compared to that of Weibull and copula-based distributions due to its ability reliability in estimating larger return periods and flexibility of skewness which is common in flood peak flows (Zhang *et al.* 2015; Zhan and Ye 1987; Song *et al.* 2018); and the generalized extreme value (GEV) distribution is usually used in Europe (National Research Council 1999). Recently, some generalized distributions have also been used for flood frequency analysis, for instance, Chen *et al.* (2017) used the generalized gamma (GG), Adguna (2020) used Gumbel max, Log Pearson III, Logistic and Log normal distribution at Horeta river, Ethiopia. However, no single distribution has been accepted as a global standard (Chen *et al. 2*017).

A regional frequency analysis study of annual maximum streamflow data compromising 407 stations from 11 countries of Southern Africa used Pearson type 3 (P3), lognormal 3-parameter (LN3), Log Pearson type 3 distribution (LP3) and General Extreme Value (GEV) to select the most suitable flood frequency distribution, and Log Pearson type 3 (LP3) and Pearson type 3 (P3) were found to be more suitable to the region as its simulations were not far from the observed data (Mkhandi *et al*. 2000). A number of studies have also utilized the Gumbel

distribution in Africa, such as Diop *et al* (2025) used the annual maximum flow (AMF) time series, covering 246 river basins in West Africa, between 1975 and 2018 to perform flood frequency analysis focusing on Generalized extreme value (GEV) and Gumbel probability distributions; Izinyon and Igbinoba (2013), conducted a comparison of flood frequency analysis of Log-Pearson Type III and Gumbel probability distributions for flood frequency analysis of Ikpoba River Catchment at Benin City, where they found that the river peak flows can be satisfactorily modeled by any of the two methods of analysis and that at lower return periods of up to 5 years, the Gumbel distribution predicts lower peak discharge values better, and for higher return periods of 10 years and above, the Log Pearson Type III distribution predicted peak discharge values better; Mujere (2011) analyzed the frequency of Nyanyadzi River floods in Zimbabwe using the Gumbel distribution, covering 30 water years (1969-1999) of flow data.

In this study, Log Pearson Type III and Gumbel distribution were used to calculate flood magnitudes of North Rukuru River because they have extensively used in Africa including the Sub-Saharan region as they offer robust statistical frameworks for estimating flood magnitudes across a wide range of return periods, especially estimating rare, high-magnitude floods, which are critical for flood risk management, and handles skewed data well. The analysis was done for 5-, 10-, 25-, 50-, and 100- year return periods by using annual maximum discharge data from 1979 to 2022 (44 years). Three goodness of fit tests wrer applied to the fitted distributions: Kolmogorov–Smirnov, Anderson–Darling, and Shapiro Wilk to choose the best statistical distribution in estimating North Rukuru River discharges between the two. To understand the reliability and precision of results of the two statistical distributions, confidence limits are calculated at 95% confidence interval. Flood frequency analysis in conjunction with hydraulic

models like HEC RAS and geographical software's like ArcGIS offers a reliable tool in form of flood inundation maps.

2.3 Simulating flood water depths for rivers

Simulating flood water depths using hydraulic models, particularly by translating river gauge data into spatial inundation patterns, is a vital component of flood risk management. Gauge stations provide measurements of discharge which is integrated into hydraulic models. This enables the generation of flood depth at the gauge station which is later transformed into flood inundation maps for surrounding floodplains. This process provides spatial data for supporting floodplain zoning, infrastructure design, and emergency preparedness.

Hydraulic models such as HEC-RAS have been extensively used to translate river gauge discharge data into flood depths and inundation maps. Kumar *et al.* (2022) emphasize that gauge-driven hydraulic simulations improve the accuracy of floodplain delineation, while Kiba *et al.* (2023) highlight the integration of HEC-RAS with GIS platforms to produce detailed hazard maps. In Europe and Asia, HEC-RAS has been widely applied to simulate return-period floods at the river gauge station into inundation extents that guide land-use planning and disaster risk reduction.

In Africa, where flood risk is exacerbated by rapid urbanization and climate variability, HEC-RAS has been increasingly adopted to simulate flood depths and extents from gauge data. Falade (2024) applied HEC-RAS integrated with GIS to Nigeria's Ogbese Catchment, using gauge-derived flows to generate inundation maps that informed vulnerability assessments. Similarly, studies in Ethiopia's Baro–Akobo basin employed flood frequency analysis and HEC-RAS simulations to translate gauge records into return-period flood depths, supporting

regional floodplain management and infrastructure design (Minywach 2024). In South Africa, HEC-RAS has been used to delineate floodplains along the Hennops River, where gauge-based discharge data were converted into spatial inundation maps for urban flood risk planning (Mawasha 2021). These examples demonstrate the growing reliance on hydraulic modeling to transform river discharge data on the river gauge station into flood depths capable of identifying spatial flood risks along the river.

Despite recurrent flooding in Malawi, particularly in districts such as Karonga, the use of flood hydraulic models to simulate flood depths in river gauge stations remains limited. Institutions such as the Karonga District Council continue to rely primarily on physical flood control structures, with minimal integration of risk-based tools such as HEC-RAS. By transforming gauge station data into flood depth and extent maps, HEC-RAS could provide spatially explicit information for development planning, disaster preparedness, and community resilience. This gap highlights the urgent need for Malawi to adopt hydraulic modeling practices that are already widely promoted globally and regionally, thereby complementing physical flood control measures with risk-based strategies.

2.4 Flood inundation maps

Flood maps come in various forms, each serving different purposes. The Canada Federal Flood Mapping Framework proposes four types of flood maps, namely, the inundation map, flood hazard map, flood risk map and flood awareness map (Natural Resources Canada 2018). A number of scholars have classified flood maps into flood extent maps, flood depth maps, flood danger maps, flood damage risk maps, flood vulnerability maps, flood insurance rate maps and maps displaying other flood parameters such as flow velocity, duration, propagation and the rate of rising of the water (Aerts *et al*. 2009; Di Baldassarre *et al.* 2010; Thieken and Gocht

2014). The most common category of a map that illustrates a flood hazard is a map that shows inundation area or flood extent for different flood events with different return periods (Adugna, 2020).

Moel *et al*. (2009) noted that the type of a flood map may depend on the user/target group and their interest of using flood maps. Van Alphen *et al.* (2009) highlighted that the use of flood maps serves at least one of these three purposes of flood risk management, preventing the buildup of new risks (land use planning and zoning), reducing existing risks (flood control infrastructure design and flood resistant construction) and adapting to changes in risk factors. While, Moel *et al*. (2009) divided the use of flood maps to two main entities, flood map use by government agencies for emergency planning (e.g. evacuation) and spatial planning (flood zones), as well as flood use map by the private sector mainly in insurance industry to differentiate premiums between the different flood zones and to determine in which areas, or under which condition, buildings can be insured.

This study focusses on flood inundation maps, which are a visual representation of the extent and depth of flooding in a specific area. Flood inundation maps show boundaries of flooded zones, depth of flooded waters in affected areas, areas affected by flooding events of different return periods, and flood sources such as rivers. A need for more accurate flood inundation maps has arisen because of the increasing frequency and magnitude of flood events around the world (Merwade *et al.* 2008). Consequently, there is a growing emphasis on avoiding exposure to flood hazards through flood inundation maps, rather than relying solely on physical infrastructure to confront them (Patel and Srivastava 2013; Kvočka *et al.* 2015; Malik and Abdalla 2016; Kumar and Singh 2021). A number of studies have been done promoting the

use of flood inundation maps in flood risk management (Iosub *et al.* 2015; Shahzad *et al.* 2015; Pathan and Agnihotri 2019; Khan *et al.* 2022; Vashist 2023).

Flood inundation mapping in the United States began in 1968 with the establishment of the National Flood Insurance Program (NFIP), and these flood maps were based on the 100-year flood (NFIP 2021). The primary objective of these maps was to reduce loss of life and property while facilitating the benefits of flood insurance. Authorities recognized that floods were becoming increasingly severe and difficult to control, and that as societies expanded and land scarcity intensified, populations were compelled to settle in hazard-prone zones. Although structural measures such as dykes and dams were implemented, they proved insufficient as standalone solutions, thereby reinforcing the need for flood mapping as a non-structural risk management tool. In recent years, hydraulic models such as HEC-RAS, integrated with ArcGIS, have been widely applied across U.S. states to generate flood inundation maps, with numerous studies demonstrating their effectiveness in safeguarding communities against floods of varying magnitudes. Similarly, in Asia, where floods remain the most frequent natural disaster, datasets from 48 countries reveal that while flood frequency has increased due to climate change, mortality rates have declined significantly (Wang 2021). This reduction is attributed to the adoption of risk-based flood management strategies, particularly the use of flood risk maps to delineate safe zones amidst rapid urbanization and population growth, the primary drivers of flood vulnerability in the region.

Despite the low adoption of flood inundation mapping as a flood mitigation strategy in Africa, a number of scholars have studied many major rivers in Africa and have produced flood inundation maps. They have promoted the use of these flood inundation maps so that floods which could have been avoided should not be repeated in the future. Martin *et al.* (2012)

applied HEC-HMS/HEC-RAS and GIS to the Sironko River in Uganda, producing inundation maps for 10, 50-, 100-, 250-, and 500-year return periods and identifying flood-prone zones that had experienced severe events in 2007 and 2011. These flood events could have been avoided if the flood inundation maps were in place. Similarly, in Ethiopia's Oromia Region, where over half a million people are exposed to flood hazards, HEC-RAS and GIS have been used to delineate inundation extents along the Fetam River, providing insights into embankment performance and safe zone demarcation (Erena *et al.* 2018; Desalegn and Mulu 2021). These examples highlight the growing recognition of flood inundation maps as essential tools for complementing structural measures and enhancing resilience, despite their limited adoption across the continent. This study replicates this through flooding events of different return periods from North Rukuru river. Eventually, benefiting the surrounding communities, the government and other relevant stakeholders in flood plain identification, protection and restoration, land use planning and zoning, levee (dyke) design, flood risk assessment and risk mitigation strategies.

Research on flood inundation mapping in Malawi remains limited, with only a few studies focusing on the lower Shire River (Sekani 2024; Atkins 2011) and urban vulnerability assessments of buildings and populations (Kamanga *et al.* 2020; Mwalwimba *et al.* 2024). Karonga District, in particular, faces persistent challenges in flood risk management due to the absence of comprehensive flood inundation maps, a critical tool for informed land-use planning. The continued expansion of informal settlements into low-lying floodplains has heightened vulnerability, as many communities are unknowingly established along natural flood pathways. Existing interventions have relied primarily on structural measures such as dykes and artificial channels, yet these have frequently failed, resulting in recurrent inundation

of residential areas. Land-use planning tool has also been employed to address flooding, however, Gondwe *et al.* (2017) observed that socio-economic inequalities force marginalized groups to occupy flood-prone zones, thereby exacerbating risks. This situation underscores the urgent need for flood inundation maps to offer reliable spatial data for sustainable development and land-use planning.

2.5 Evaluating effectiveness of the dyke

Recurring floods in Karonga District have prompted a range of mitigation measures aimed at alleviating their devastating impacts. Immediate responses have largely prioritized humanitarian assistance to affected households, many of which are located within the floodplains of the North Rukuru River. This pattern of settlement has contributed to a dependency on relief aid, as communities anticipate support whenever disaster strikes. Several studies have noted that flooding in Malawi is primarily driven by settlement in close proximity to rivers and low-lying areas, with post-disaster interventions often emphasizing relief provision rather than relocation (Gondwe and Shukla 2020; Trogrlić *et al.* 2019; Reliefweb 2020).

Structural measures, particularly dykes, have been the main form of protection for Karonga Town and its surrounding floodplains. The first dyke along the North Rukuru River was constructed in 1980, followed by a second in 2022. Despite these interventions, challenges persist. The dykes only protect portions of the town, leaving hundreds of houses exposed in flood-water holding zones and on the opposite bank where no dyke exists. In 2011, floodwaters overtopped the dyke, inundating the district assembly, market, offices, and residential areas, affecting 105 villages, displacing 27,995 people, and destroying 504 houses (Larson 2011).

Such events underscore the need to assess the effectiveness of flood control structures in terms of flood depth, duration, and frequency, to determine areas requiring improvement.

Comparative studies provide useful insights into dyke performance. Murtaza *et al.* (2025) evaluated a dyke as a composite defense system against flooding from the Indus River, finding that 58% of floodwater was prevented from reaching residential areas. In Malawi, Sekani (2024) assessed the effectiveness of dams and embankments along the Shire River using a Rainfall-Runoff Inundation model. The study demonstrated that combined countermeasures significantly reduced inundated areas and the number of affected buildings and populations across return periods, highlighting the importance of integrating hydraulic modeling with structural defenses.

These findings emphasize the necessity of combining structural and non-structural measures for sustainable flood management. Flood inundation maps, generated through hydraulic models such as HEC-RAS and integrated with GIS, provide accurate spatial data on flood depths and extents for different return periods. Such maps are critical for evaluating the effectiveness of dykes and informing the design of future flood control structures (Wang *et al.* 2021). In the context of Karonga, this study integrates flood inundation mapping with existing dykes to assess exposure to floods of varying magnitudes, particularly the 100-year flood as the worst-case scenario. In such a case the dyke is tested against flood depths from different flood inundation maps, and its best possible design in terms of height is realized from flood depths in its vicinity on a 100-year flood map. Furthermore, a household survey is employed to capture community perceptions of dyke effectiveness on flood depth, duration, and frequency before and after dyke's construction.

2.6 Summary of the literature review chapter

In this review, scenarios of river discharge estimations using frequency distributions such as Log Pearson Type III and Gumbel distributions are explained in detail, and simulations of flood depths using HEC-RAS model is also well articulated. The development and use of flood inundation maps around the world are also covered in detail and the need to evaluate the effectiveness of the dyke along the North Rukuru River through flood inundation maps of different return periods and perception of the people residing in the direction of the dyke is also discussed.

CHAPTER 3 : MATERIAL AND METHODS

3.1 Introduction

This chapter describes the research methodology used to generate data. Aspects of study area, research design, sampling design, materials used, data collection, preparation and processing, methods, and ethical considerations have been highlighted.

3.2 Description of the study area

The study was mainly conducted in the North Rukuru River basin. The basin's area is about 1970 km^2 and stretches between the two districts, Rumphi and Karonga district (Kingdon *et al.* 1999). The North Rukuru River is the main river in this basin. It originates in the Nyika Plateau, meanders through the basin, entering Karonga Town, and eventually drains into Lake Malawi. The basin experiences a sub-tropical climate with two distinct seasons, the dry season and wet season, from June to October and November to May, respectively (DCCMS 2020). The North Rukuru River manifests a strong seasonal pattern in streamflow, with a wet season commencing in November/December, reaching a high peak before moderately declining from May onwards to a discharge of nearly 0 (Mokkenstorm *et al.* 2021).

In this study, much of the interest was in the low-lying region of the basin, situated in Karonga district, which experiences frequent flooding. Karonga experiences a sub-tropical climate with two distinct seasons, the dry season and wet season, from June to October and November to May, respectively. The dominant soil types in the district are lixisols, cambisols and fluvisols. The overflowing of the downstream of the North Rukuru River causes a lot of destruction to adjacent areas such as Mwahimba, Fwira, Lwayo, Karonga Airport and other localities. Even

during low rainfall events in the downstream, riverine floods occur as floods originate from the upper stream. Riverine flooding of the North Rukuru River has occurred every wet season between 2009 and 2016, where the 2010 and 2016 floods were classified as severe (Manda and Wanda 2017). The floodplains (up to 125m wide from the river to the end) are home to many informal settlements, which are prone to flooding, even frequent low-impact events (Manda and Wanda 2017).

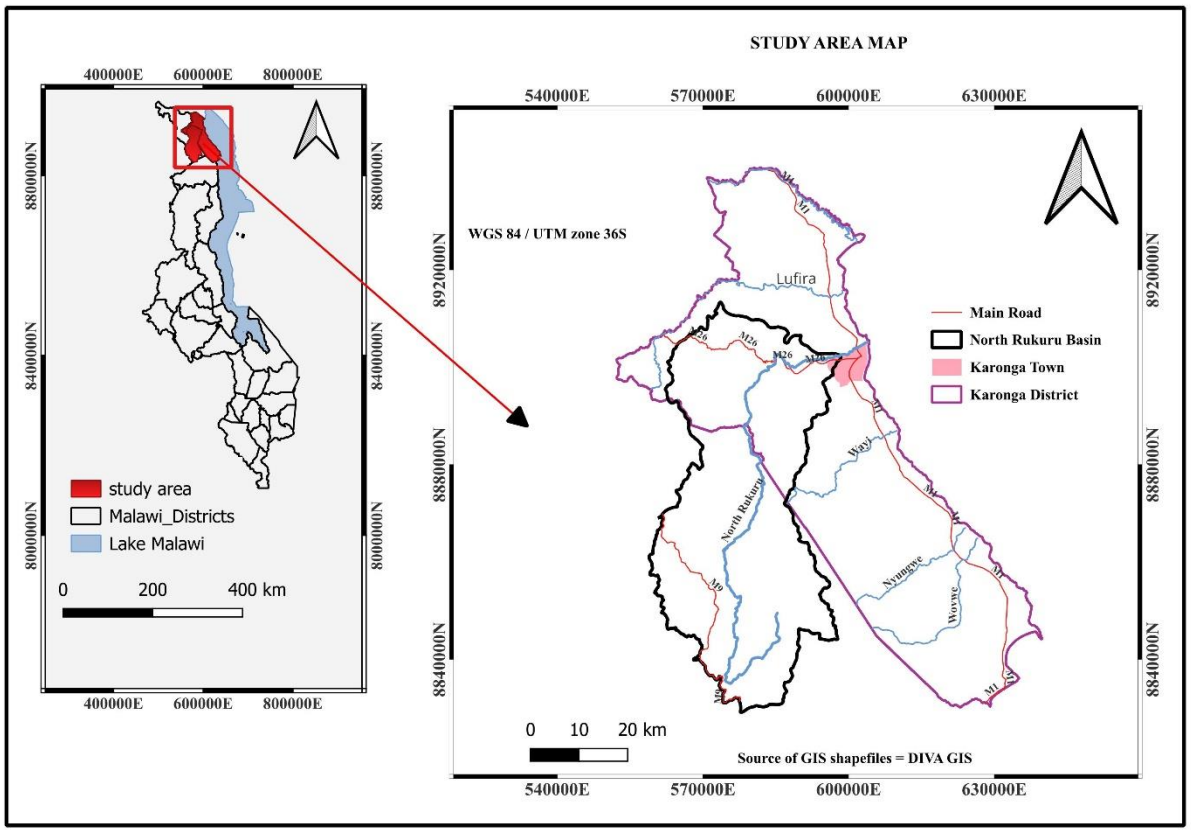

Fig 1. Study Area

3.3 Research Design

This study adopted a mixed-methods sequential explanatory research design to estimate peak flood discharges, simulate flood inundation extents, validate model outputs through

community-based field data and evaluate effectiveness of the dyke. The design integrates quantitative hydraulic modeling with qualitative field verification to enhance the reliability and contextual relevance of flood risk assessments. A quantitative approach was employed to conduct flood frequency analysis using the Log Pearson Type III and Gumbel probability distributions. The estimated discharges were then used as boundary conditions in the HEC-RAS hydraulic model to simulate flood extents, which were subsequently mapped using ArcGIS. A qualitative approach was also adopted where interview guides and discussion guides were conducted through key informant interviews with the disaster officer and water officer, and the village civil protection committees, respectively, to get clear information on flooding experiences on the ground, areas prone to floods, flooding patterns of North Rukuru River and validation of the flood inundation maps. Household surveys was also done to evaluate effectiveness of the dyke and semi-structured questionnaires were purposively administered to villages situated along the dyke as they received direct protection from the dyke, and in the process GPS coordinates were collected to verify whether the villages were situated in the floodplain or not and also to verify the accuracy of the flood inundation maps generated from HEC-RAS and ArcGIS by comparing them with local flood experiences. The questionnaire included open-ended questions, and so yielded both qualitative and quantitative information. Ground observations were also done to get familiar with the state of the dyke, and contributing factors, to get Manning's values in reachable areas, to get GPS coordinates confirming the floodplain, and also to assess the artificial channel which was meant to convey runoff water from the town center to the lake. This design allowed triangulation of results, where modeled outputs were cross-checked with community observations, making the findings more actionable for flood risk management and infrastructure planning in Karonga District.

In this research study, both quantitative and qualitative methods were adopted to address the limitations of each method. The use of mixed methodology improves the overall validity and depth of research findings (Creswell 2013).

3.4 Sampling design

According to Kativhu (2016), a sample refers to a finite subset of a statistical population in any research, selected for the purpose of examining specific properties, to gain information about the entire population. This enables the researcher to assess the extent to which the findings can be generalized beyond the study participants. Given the mixed-methods research design adopted in this study, both purposive sampling and simple random sampling techniques were employed. Purposive sampling was used to strategically select villages which were situated along the dyke and the simple random sampling method facilitated unbiased data collection by ensuring each household in these areas had an equal chance of selection. Further information was obtained from people and groups who hold key positions in issues related to flooding in the district; the district water officer, district disaster officer, and village civil protection committees. The focus group discussion required 8 people from civil protection committees to have an in-depth understanding about areas facing flooding, causes and trends in order to validate the flood inundation maps. The number of years chosen for streamflow data was 44 years, exceeding the minimum recommended 30 year for flood frequency analysis.

3.5 Materials used

For a proper implementation of this study, materials and software's used were based on the availability, and capability on achieving the set objectives.

Table 2. Materials and software used

Models, Software and Materials	**Application**	**Objective Addressed**
ArcMap 10.5	Used to map flood inundated areas	Object 3
HEC-RAS 6.3.1	Used to create river cross sections, river channel, river banks, flow paths, as well as simulate the hydraulics of water flow through the North Rukuru River	Objective 2
Statistical models, Log Pearson Type III and Gumbel Max	Used to select the best probability distribution for flood frequency analysis	Objective 1
Microsoft excel	Used to calculate the statistical parameters of hydrological data for flood frequency analysis and evaluate effectiveness of the dyke in terms of flood depths, flood duration and flood frequencies in areas protected by the dyke	Objective 3 and 4
SWAT model	Used to create a floodplain of the North Rukuru River for validation of flood inundation maps	Objective 3

3.6 Data collection, preparation and processing

Defining a clear and efficient methodology is important for the quality of the findings of the study (Adugna 2020). Different data inputs were required to achieve the objective of this study. Secondary data like streamflow data were downloaded from GEOGLOWS Hydroviewer, a streamflow data source currently used by the Karonga District Council and partners in M-climate project called Community Based Flood Early Warning System (CB-FEWS). The early

warning system designed based on this data source is able to operate accurately, warning people in time and saving a lot of lives.

One of the most important inputs in flood inundation mapping is the geometric description of the floodplains and river channels that is often derived from the digital elevation models (DEMs). In this study the recently released Advanced Land Observing Satellite (ALOS) was used. Azizian and Broca tested different remotely sensed DEMs for flood inundation mapping in data-sparse regions using 1D Hydrologic Engineering Centre-River Analysis System (HEC-RAS) (Azizian and Brocca 2020).Their findings indicated that using ALOS-30 m for hydraulic simulation approximately leads to similar results as ground-based DEM (GDEM), surpassing the usefulness and efficiency of Shuttle Radar Topography Mission (SRTM-90 m), SRTM-30 m, and Advanced Spaceborne Thermal Emission and Reflection Radiometer (ASTER-30 m). To create a floodplain of the North Rukuru River, the Soil and Water Assessment Tool (SWAT) model was used. This was done to differentiate between the floodplain and residential areas. Data input needed for this task was ALOS-30 m DEM. To gain a deeper understanding on community perceptions regarding the extent of flooding and dyke effectiveness, household surveys, key informant interviews and focus group discussions were conducted with affected residents, local leaders, water officers, disaster officers, and village civil protection committees. Field observations were also done to get a glimpse of flooding extent, Manning's roughness, dyke's dimensions and state of flood control structures.

Table 3. Data sources

Data	**Source**
Digital Elevation model (30m by 30m) (ALOS DEM)	Open Topography (Japan Aerospace Exploration Agency)
Streamflow	GEOGLOWS Hydroviewer (Version 1)
Geographic coordinates	Survey
Manning's (n) values	USGS online data based on physical characteristics of the river
Land use/cover	Soil and Water Assessment Tool (SWAT (Data))
Hydrologic soil	Soil and Water Assessment Tool (SWAT (Data))

North Rukuru river outlet is gauged near Karonga Town at Mwakimeme Mwakenja Bridge-Karonga-Chitipa Road (M26 Road). The Mwakimeme streamflow gage coordinates were retrieved from the Ministry of Water and Sanitation. The code for the station was 8A5, with a latitude (in decimal) of -9.9454462° and a longitude (in decimal) of 33.7757021°.

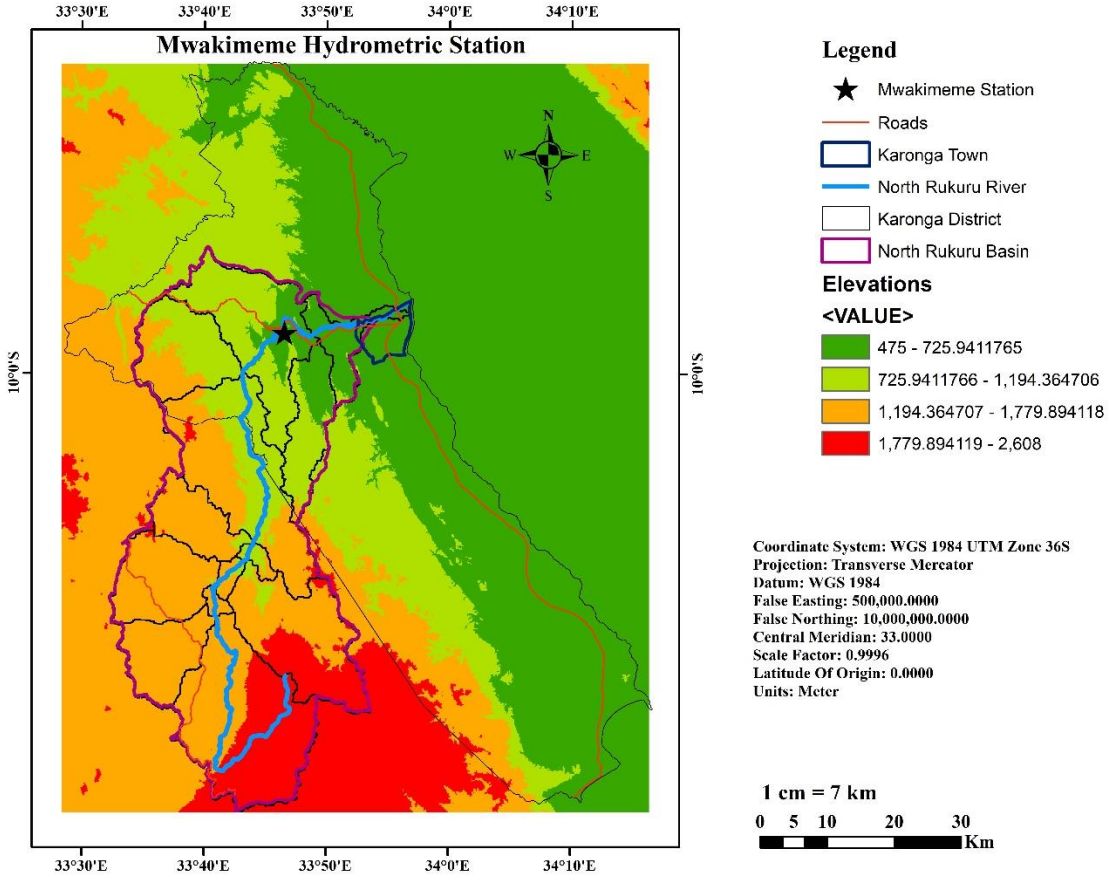

Fig 2. Mwakimeme Streamflow Station situated in the study area and elevation

3.7 River discharges estimation at Mwakimeme gauge station

To estimate river discharges at the Mwakimeme gauging station on the North Rukuru River, a flood frequency analysis was conducted using both the Log-Pearson Type III and Gumbel probability distributions. The suitability of these distributions was evaluated through goodness-of-fit tests, specifically the Kolmogorov–Smirnov, Anderson–Darling, and Chi-square tests. In addition, confidence limits were established to assess the reliability and accuracy of the results. Based on these procedures, the distribution that demonstrated the most consistent and robust performance was selected. The following steps were done:

3.7.1 Flood Frequency Analysis

Flood frequency analysis (FFA) is a technique that relates the magnitude of extreme streamflows to their frequency of occurrence through distribution functions (Pakhale *et al.*, 2024). How frequently a flood event of a given magnitude may be expected to occur is important, as almost every activity in a particular flood-prone area might depend on it (Hosking and Wallis 1997). Flood frequency analysis with various risks of exceedance is therefore needed for a wide range of land use planning, engineering, environmental and social problems; assessing flood risk and making informed decisions about land use and infrastructure in flood-prone areas, the design capacities of bridges, culverts, spillways, levees and other flood control structures, and insurance risk calculations (Chen *et al.* 2010, 2012; Pakhale *et al.* 2024).

In flood frequency analysis, two time series of streamflow data are mostly used: the annual maximum series and the partial duration series. In an annual maximum series, the maximum streamflow is picked for each year, while in a partial duration series, a threshold is defined and all the values above that threshold are picked for that year. As a result, in annual maximum series the number of data points equals the number of years of data, while in partial duration series the number of data points may or may not be equal to the number of years of data. In partial duration series, there is a possibility of picking streamflow data in a year that is not independent, while the annual maximum series offers the independence of data; hence, this study used the annual maximum series for frequency analysis.

Annual maximum series is usually used with Gumbel and Log Pearson Type III probability distributions for flood frequency analysis. Executing flood frequency analysis needs a good understanding of probability theory and statistics. The probability distributions are the basic

concepts of statistics and are fundamental in determining a suitable probability distribution to a given dataset. Selecting appropriate probability distributions most closely fitted to the observed data depends on the underlying characteristics of the data, such as the nature of occurrence and distribution of the data (Athulya and James, 2017). The probability distribution models used for this study are Gumbel and Log Pearson Type III. Normally, there is no single universally accepted model choice (Bedassa, 2016). Numerous studies have been done using Gumbel and Log Pearson type III models to perform flood frequency analysis (Solomon and Prince 2013; Ganamala and Sundar 2017; Samantaray and Sahoo 2020; Kumar *et al.* 2021).

3.7.2 Log-Pearson Type-III (LP3) Distribution

Among the well-known extreme distributions Log Pearson Type III method is commonly used in hydrology to express statistics of streamflow (Bea *et al.* 2006). The Log- Pearson Type-III is used for estimating peak flood magnitudes in engineering hydrology (US Water Resources Council, 1976). In Log-Pearson Type-III (Pearson,1916) probability distribution, the annual peak discharge series is first transformed to the base 10 logarithm of the discharge, Q, and the transformed data is analyzed for the random hydrological series at selected exceedance probability, P, and return period, T. The mean logarithm, the standard deviation of the logarithm, and the skewness coefficient are later computed to estimate peak discharge for a given return period for a specific event (Gogoi and Patnaik 2023).

The mean, standard deviation, and skew coefficient of the transformed data are also computed. To address issues of uncertainty of computed flood magnitudes using Log-Pearson Type-III distribution, confidence limits are also computed in this study using the Bulletin 17B Formula. Confidence limits estimate a measure of uncertainty of the discharge at a selected exceedance

probability or return period. It indicates the limits of the calculated value between which the true value can be said to lie. The narrower the difference between the upper and lower bounds of discharges at a selected exceedance probability or return period the lower the uncertainty. To estimate flood magnitudes for different return periods or exceedance probabilities using Log-Pearson Type-III (LP3) distribution, the following steps were followed with respective equations;

Step 1: The annual maximum series of discharges is converted to logarithm base 10.

$Z = \log Q$ ..... (1)

Q = Variate/streamflow data of a random hydrologic series.

Z = Log transformed streamflow data

$Z_T = \bar{Z} + K_z \sigma_z$ ..... (2)

Z_T = Flood magnitude of log transformed data under a specific recurrence interval, T.

$\bar{Z}$ = Mean of Log transformed data

σ_z = Standard deviation of log transformed data

K_z = Frequency factor which is a function of recurrence interval, T, the coefficient of skew, C_s.

Step 2: Computed the mean, standard deviation and coefficient of skewness of log transformed data.

$\bar{Z} = \frac{1}{N}\sum_{i=1}^{N} Z$ ..... (3)

N= Number of years for discharge data from 1979 to 2022, a span of 44 years

$\sigma_z = \sqrt{\frac{\sum_{i=1}^{N}(Z-\bar{Z})^2}{(N-1)}}$ ..... (4)

$C_s\ (skewness) = \frac{N\sum_{i=1}^{N}(Z-\bar{Z})^3}{(N-1).(N-2).(\sigma_z)^3}$ ..... (5)

Step 3: The frequency factors K of the return periods 2, 5, 10, 25, 50 and 100 years are determined from the Log Pearson Type III Distribution table based on the skewness coefficient value.

$T = \frac{N+1}{m}$ …….. (6)

This is a Weibull formula where;

T = Return period or recurrence interval, an average time or an estimated average time between events such as river flows of a certain magnitude to occur and it is expressed in years.

m = the rank of observed streamflow when arranged in a descending order.

$P = \frac{m}{N+1}$ ……. (7)

This is a Weibull plotting formula where;

P = Exceedance probability, P, a reciprocal of recurrence interval, a probability of a flood exceeding or surpassing a particular flood magnitude or return period in a year and it is expressed in percentages.

$P = \frac{1}{T}$ …… (8)

The variations of $K_z = f(Cs, T)$ were given by the Log Pearson Type III distribution table for frequency factors under different coefficient of skewness and return period.

Step 4: The logarithms of flood discharges, Z_T, for different return periods, were computed using equation 1.1.

Step 5: After finding Z_T by equation 2, the expected flood discharge was computed by the anti-logarithms of equation 2, hence the corresponding value of Q_T was:

$Q_T = antilog(Z_T)$ …….. (9)

3.7.3 Confidence Limits of Log-Pearson Type III (LP3) Distribution

Confidence limits provide a range within which flood estimates are likely to fall. Confidence limits are a very important part of flood frequency analysis because they clearly provide a clear way of understanding the accuracy of the estimates, dealing with the uncertainty of the results. In indicating the reliability and precision of estimates, they provide a concise margin of error, the narrower the range between the upper and lower confidence limits the smaller the margin of error of estimates. The following Bulletin 17B (Log Pearson III) formula indicates how these confidence limits were computed;

$$Upper\ lim. = \bar{Z} + K_{up}\sigma_z \quad \text{.....(10)}$$

K_{up} = Upward bound K statistic of log Pearson type III distribution.

$$Q_{up} = 10^{Z_{up}} \quad \text{..... (11)}$$

Q_{up} = Upper bound limit, a function of confidence interval, and return period.

$$K_{up} = \frac{K_T + \left(K_T^2 - ab\right)^{1/2}}{a} \quad \text{..... (12)}$$

$$Lower\ lim. = \bar{Z} + K_{low}\sigma_z \quad \text{..... (13)}$$

$$Q_{up} = 10^{Z_{low}} \quad \text{..... (14)}$$

$$K_{low} = \frac{K_T - \left(K_T^2 - ab\right)^{1/2}}{a} \quad \text{..... (15)}$$

K_T is a K statistic for a return period of T, if it is a 100-year flood, it is a K statistic for a 100-year flood and, a and b are just constants. These constants are a mostly a function of Z statistic and a number of records, N.

$$a = 1 - \frac{2^2}{2(n-1)} \quad \text{..... (16)}$$

$$b = K_T^2 - \frac{2^2}{n} \quad \text{..... (17)}$$

2 is this case is referred to as a Z statistic.

$$K_{low} = \frac{K_T - \left(K_T^2 - ab\right)^{1/2}}{a} \quad \text{..... (18)}$$

3.7.4 Gumbel Extreme Value Distribution

Gumbel extreme value distribution as a statistical tool is commonly used in forecasting extreme hydrological occurrences such as floods (Handique *et al.* 2024). The Gumbel extreme value distribution is also known as the Gumbel distribution or the Gumbel maximum. The largest flow that occurs in a given year, also known as the annual maximum flow, is analyzed using the Gumbel extreme value distribution. For streamflow data that is less than 50 years old, the Gumbel extreme value distribution also performs well (Cunnane 1989). According to Gumbel's theory, the probability of an event occurring is greater than or equal to a certain number, x_o (Ahad, *et al.* 2022).

Numerous studies have used the Gumbel Extreme Value distribution to predict and evaluate extreme flood events (Asad 2013; Vivekanandan, 2017; Islam and Sarkar 2021; Khwairakpam *et al.* 2024). The following steps describe in detail on how to find flood magnitudes of different return periods using the Gumbel extreme value distribution;

Step 1: From 1979 to 2022, the annual maximum discharge is tallied in descending order and each is assigned an order number ranging from 1 to 44.

Step 2: The mean ($\overline{x}$) and standard deviation (σ_{n-1}) of the annual maximum discharge data for N years are calculated as follows:

$$\bar{X} = \frac{1}{N}\sum_{i=1}^{N} X_i \quad \text{..... (19)}$$

$$\sigma_{n-1} = \sqrt{\frac{1}{(N-1)}\sum_{i=1}^{n}(x_i - \bar{x})^2} \quad \ldots\ldots\ldots\ldots\ldots\ldots\ldots\ldots\ldots\ldots\ldots\ldots\ldots\ldots\ldots\ldots\ldots\ldots\ldots\ldots \quad (20)$$

Step 3: The values of Y_n and S_n are obtained from Gumbel's extreme value distribution table depending on sample size, N, and in this case the sample size is 44.

Step 4: Computing of the reduced variate (Y_T) from the designated return period T, leads to the calculation of flood frequency function (K) is by using table values of reduced mean, $\bar{Y}_n$, and reduced standard deviation, S_n, both are functions of sample size, N, as follows:

$$Y_T = -\left[\ln.\ln\left(\frac{T}{T-1}\right)\right] \quad \ldots\ldots\ldots\ldots\ldots\ldots\ldots\ldots\ldots\ldots\ldots\ldots\ldots\ldots\ldots\ldots\ldots\ldots\ldots\ldots\ldots \quad (21)$$

$$K = \frac{Y_T - \bar{Y}_n}{S_n} \quad \ldots\ldots\ldots\ldots\ldots\ldots\ldots\ldots\ldots\ldots\ldots\ldots\ldots\ldots\ldots\ldots\ldots\ldots\ldots\ldots\ldots\ldots\ldots\ldots\ldots\ldots \quad (22)$$

Step 5: The magnitude (X_T) of the flood for the return period (T) of 2, 5, 10, 25, 50 and 100 years is computed using Gumbel's extreme value equation:

$$X_T = \bar{X} + K.\sigma_{n-1} \quad \ldots\ldots\ldots\ldots\ldots\ldots\ldots\ldots\ldots\ldots\ldots\ldots\ldots\ldots\ldots\ldots\ldots\ldots\ldots\ldots\ldots\ldots\ldots \quad (23)$$

3.7.5 Confidence Limits of Gumbel Extreme Value Distribution

The value of the variate for a given return period, X_T, determined by Gumbel's Extreme Value distribution can have errors due to the limited sample data used. An estimate of the confidence limits of estimates is recommended to deal with such errors, eventually getting a clear understanding of the uncertainty of results. The confidence interval indicates the limits of the calculated value between which the true value can be said to lie with a specific probability based on sampling errors only.

For a confidence probability c, the confidence interval of the variate X_T is bounded by values X_1 and X_2. Taking X_1 as the upper bound and X_2 as the lower bound, the boundaries are calculated as follows:

$$X_1 = X_T + f(c)S_e \quad \text{..... (24)}$$

$$X_2 = X_T - f(c)S_e \quad \text{..... (25)}$$

In this case f(c) is the function of the probability c determined by using the table of normal variates. In this study the confidence probability of 95% was used which directly relates to the function of probability (f(c)) of 1.96. S_e is the probable error given by the following equations:

$$S_e = b\frac{\sigma_{n-1}}{\sqrt{N}} \quad \text{..... (26)}$$

$$b = \sqrt{1 + 1.3K + 1.1K^2} \quad \text{..... (27)}$$

Where K is a frequency factor given by equation (19).

3.7.6 Goodness of fit test

Goodness of fit is a measure employed to evaluate how well expected data values realized from a statistical model fit observed data. A high goodness of fit indicates that the model accurately represents the data, while a low goodness of fit suggest that the model may not be suitable for the task. In flood frequency analysis, goodness of fit is crucial for model selection, prediction accuracy and uncertainty assessment.

Three different types of goodness of fit tests were conducted in this study: Anderson-Darling, Kolmogorov-Smirnov, and Chi-squared.

3.7.7 The Kolmogorov-Smirnov Test

The Kolmogorov-Smirnov Test compares the distribution of a sample with a reference probability distribution. Mostly, it is used to determine whether two probability distributions differ. It is more powerful in detecting differences near the median rather than in the tails. In this study it was used to compare an observed sample distribution and a theoretical distribution by using the following formula:

$$D = Max|F0(x) - Ft(x)| \quad \text{..... (28)}$$

Where:

D = Kolmogorov-Smirnov Test

FO(x) = Observed cumulative frequency

Ft(x) = Theoretical frequency

3.7.8 The Anderson-Darling Test

The Anderson-Darling Test was used to determine if the sample data came from a population with a specific distribution. This test gives more weight to the tails compared to other tests, such as the Kolmogorov-Smirnov Test. This makes it more sensitive to deviations in the tails, which is a crucial area in determining extreme flows. The following equation was used to compute the Anderson-Darling Test in this study:

$$AD = -n - \sum_{i=1}^{n}(2i-1)\left(\ln F(X_i) + \ln\left(1 - F(X_{n-i+1})\right)\right) \quad \text{..... (29)}$$

Where:

AD = Anderson-Darling Test

n = The sample size

F(x) = Cumulative distribution function for a specified distribution

i = The ith sample, calculated when arranged in ascending order

3.7.9 The Chi-square Test

The Chi-square Test was used to measure how the expected data values compared to the actual observed data. In general, it checked if the observed data fitted a specific distribution between Gumbel extreme value and Log-Pearson Type III distribution. It was determined by the following equation:

$$X^2 = \sum \frac{(Q_i - E_i)^2}{E_i} \quad \ldots\ldots\ldots\ldots\ldots\ldots\ldots\ldots\ldots\ldots\ldots\ldots\ldots\ldots\ldots\ldots\ldots\ldots\ldots\ldots\ldots\ldots\ldots\ldots \text{(30)}$$

Where:

X^2 = Chi-squared

Q_i = Observed value, and

E_i = Expected value

3.8 Flood depth simulation at Mwakimeme gauge station

To simulate flood depths at the Mwakimeme gauging station on the North Rukuru River, a Digital Elevation Model (DEM) together with the Hydrological Engineering Center's River Analysis System (HEC-RAS) model was utilized. The HEC-RAS model was used to generate the North Rukuru River geometry from the DEM. River discharge values were then introduced into the HEC-RAS model, and simulations were performed under a steady flow regime to estimate flood depths at the gauging station. The following steps were done:

3.8.1 HEC-RAS model

The Hydrological Engineering Center River Analysis System (HEC-RAS) developed by the United States Army Corps of Engineers (USACE), is a one-dimensional steady flow hydraulic model designed to aid hydraulic engineers in channel flow analysis and flood mapping (Brunner and Bonner 2010). HEC-RAS has three main components: (a) the geometry data which consists of a description of the size, shape and connectivity of river cross-sections; (b) the flow data which contain discharge rates; (c) the plan data which consists of information suitable to the run specifications of the model such as description of the flow regime. The main aim is for HEC-RAS to compute water surface profiles, and it assumes a steady, gradually varied flow scenario. The primary computational procedure is based on the energy equation (Butler and Davies 2004).

$$H = Z + \frac{P}{\rho g} + \frac{V^2}{2g} \quad \text{..... (31)}$$

Where:

H = Total energy head (m)

Z = Potential head (m)

$P/\rho g$ = Pressure head (m)

P = Pressure (N/m^2)

ρg = Unit weight (N/m^3)

$\frac{V^2}{2g}$ = Kinetic (velocity) head (m)

V = Velocity of flow (m/s)

g = Acceleration due to gravity (m/s^2)

The following steps were followed to fully produce flood inundation maps in HEC-RAS and later in ARC-GIS:

3.8.2 Stationing in HEC-RAS

The first part is assigning stations and reaches to the river, which is called stationing. The tributaries divide the river into a number of reaches, one tributary divides it into two reaches. The upstream is called Reach 1 when there is a tributary in between and the downstream is called Reach 2. While station starts from the downstream of the river, it is assigned in terms of the distance between two or more reaches and the distributaries that divides them. For example, a downstream reach of 13km long, the first station will start at 0 km, will be called Station 0, the second at the end of the reach, 13 km, and it will be called Station 13. If there is a second upstream reach of 12 km long with no any tributary dividing it in between, the third station would be put at the end of this reach which would be called Station 25, the name is coming in after adding 13 km of reach 2 and reach 1 of 12 km, assuming the tributary joins these two reaches at 13 km length of the river. In this study, we only have one reach, as the focus is only on the downstream of North Rukuru river and has no any major tributaries which divides it into two or more reaches. When assigning the names of cross-sections, the name comes first, seconded by the name of the river, then the name of the reach and lastly the station name. In my case because I was dealing with the downstream of North Rukuru river with no any major tributary in the downstream, what is changing is the name of the cross-section and the station number, the river and the reach, the river name remains the same, also assuming the upstream has no any tributary as I was mostly interested in the downstream.

3.8.3 RAS pre- processing

The RAS pre-processing is the task done to analyze the river geometry. In this study, river geometry analysis is done by Ras Mapper. In previous versions of HEC-RAS river geometry analysis was being done by an external GIS software called HEC-Geo RAS but this current version is embedded with a GIS tool called RAS MAPPER to conduct the river geometry analysis. The RAS MAPPER is a GIS extension with a set of procedures, tools and utilities for the preparation of river geometry. RAS MAPPER uses Digital Elevation Model (DEM) to create river geometry. The Advanced Land Observing Satellite (ALOS) DEM (30 by 30) was downloaded from Japanese Aerospace Exploration Agency (JAXA) aimed at observing and monitoring disaster-hit areas. The river center line, River bank, flow path; XS cross-section are developed by the RAS MAPPER. The river reach (river segment between junctions), cross-section and other related data is stored in the geo-database file of HEC-RAS. The following section describes how each individual layer was created (digitized).

Creating River Centre line

The river centerline layer is very important, because it represents the river network for HEC-RAS. The digitizing of stream centerline starts with selecting the sketch tool from the Editor Toolbar and digitization proceeds in the direction of a river flow (Slobodan, 2009). The process started from Mwakenja Village, considered as upstream and ended to the downstream end of North Rukuru River. After digitizing all of reaches, the name of the river was assigned. This was accomplished by the selection of Assign River code menu item and assigning appropriate names.

Creating River bank

The bank lines layer is used to define river channel from overbank areas. This definition is important because Manning's n values are different for channel and for floodplain areas. Usually, the overbank areas have higher values of Manning's n due to vegetation or presence of residential areas. Since Manning's n values influence the accuracy of HEC-RAS modeling, this task is very important. The bank lines are created in similar fashion as the river centerline. On the Edit toolbar, select "Editor" "Start Editing". The digitizing of bank lines starts from the Mwakenja Village considered as upstream, with the left bank (looking in downstream direction) being digitized first. The task window of the Edit toolbar is set to "Create New Feature" and the target is set to "Banks" (Slobodan 2009).

Creating Flow paths

The flow path layer is a set of lines that follows the center of mass of the water flowing down the river, during the flood event (Meyer and Olivera 2007). For the main channel, the flow path centerline is defined to be the same as the stream centerline. For floodplains, the flow path centerlines are digitized to represent assumed water flow within the floodplain. The flow path layer is used to determine the length between two neighbouring cross-sections (required by HEC-RAS). Flow path centerlines are also created in the upstream to downstream direction. To create left and right flow paths, it is necessary to start Editing, then choose Create New Feature as the Task, followed by Flow paths as the Target. By using the Assign LineType button, the Flow path is labelled Right, Channel, Right looking in downstream direction. In this study flow path centerlines are created from Mwakenja Village considered as upstream to downstream of North Rukuru river following the flow direction.

Creating cross-sections

Cross-sections are one of the most important inputs to HEC-RAS. Cross section cut lines are used to extract the elevation data from the terrain and to create a ground profile across the flow (Slobodan 2009). The intersection of cut lines with other RAS layers such as centerline and flow path lines are used to compute HEC-RAS attributes such as bank stations (locations that separate main channel from the floodplain), and downstream reach lengths (distance between cross- sections).

A few basic rules were followed during the process of drawing cross section cutlines (Meyer and Olivera 2007; Slobodan 2009):

- ✓ Cut lines are drawn perpendicular to the direction of flow.
- ✓ Cut lines are drawn directionally from left to right bank, looking at downstream direction.
- ✓ Cut lines are extended far enough on either side of the channel to encompass the entire portion of the floodplain.
- ✓ Cut lines are spaced close enough to account for notable changes in the hydraulics or geometry of the stream, such as changes in discharge, slope, cross section shape, roughness or presence of hydraulic structures (bridges, levees, weirs.)

In this study, a number of cut lines were created from Mwakenja Village considered as upstream to downstream of North Rukuru river.

3.8.4 RAS post-processing

Hydraulic models are there to simulate the behavior of the flow in the main channel and the flood plain of a river. The peak flood discharge which was generated from Log Pearson type 3 probability distribution method is used as the main input for hydraulic modeling. The other important input for RAS Post processing is geometry data of the river which was prepared by using RAS MAPPER. HEC-RAS has the ability of performing the analysis in steady state (simplicity approach; flow does not change through time) and unsteady state (more complex and realistic approach) (Alaghmand *et al.* 2010).

HEC-RAS software accomplishes this by following these steps:

1. Create a new project
2. View and Edit Geometric Data
3. View and Edit steady or unsteady Flow Data
4. Perform a steady or an unsteady flow simulation

3.8.5 Import RAS Geometry

The RAS geometry was imported to HEC-RAS in GIS format using the geometric editor from RAS mapper. This geometry file contains stream network, cross-section information and head (Hirtan 2015). Launched HEC-RAS by double clicking on HEC-RAS 6.3.1 on the desktop; then saved the new project by going to File, Save Project as North Rukuru River Flood Study.prj in the working folder, clicked OK.

To import the GIS data into HEC-RAS; went to the geometric data editor by clicking on Edit, Geometric Data. In the geometric data editor, clicked on File, Import Geometry Data, GIS

Format. Browsed to GIS2RASImport.sdf file created in ArcGIS (DEM), and clicked OK. The import process asked for some inputs to complete. In the Intro tab, confirmed SI (Metric) Units (this converted the US customary units to the SI metric units) for Import data and clicked next. Confirmed the River/Reach data, made sure all import stream lines boxes are checked, and clicked next.

Confirmed cross-sections data, made sure all Import data boxes are checked for cross-sections, and clicked OK (accepted default values for matching tolerance, round places, etc) and, clicked Finished-Import data. The data was then imported to the HEC-RAS to be worked on by the RAS MAPPER.

Manning's roughness coefficient (n) values were used in the model to define roughness for each cross-section. It is influenced by various factors such as topographic heterogeneity, the bed material, the surface irregularity on the floodplain, obstructions, the variation in shapes and size and the vegetation for floodplain (Cowan 2018).

3.8.6 Steady Flow Analysis

The steady and unsteady flow analysis is the computation of hydraulic results by taking the input river geometry data for flow simulation (Dewberry 2012). Usually, a steady flow approach is used for floodplain management and flood insurance studies whereas unsteady flow approach is used for subcritical flow regimes (Lamichhane and Sharma 2017). In this study steady flow analysis was done, all the river reaches were subjected to the same flow related to a particular return period at a time.

In the main HEC-RAS window, clicked on Edit, Steady Flow Data. Entered 6 for number of profiles, and clicked Apply Data. Edited profile names from options of the Steady flow data

window, Edited profile names to 2 Year, 5 Year, 10 Year Flood, 25 Year Flood, 50 Year, and 100 Year Flood, and then entered the corresponding flow data, clicked apply Data to save the entered flow data. To define downstream boundary conditions; clicked on Reach Boundary Conditions. Set boundary conditions for all the profiles and then selected Downstream for North Rukuru River Lower Reach, clicked on Normal Depth, and entered slope of the North Rukuru River Lower reach and clicked ok. Saved the steady flow data and closed the Steady Flow editor window.

3.8.7 Running North Rukuru River RAS model

In the main HEC-RAS window, clicked on Run and then Steady Flow Analysis. Selected the Subcritical Flow Regime, and clicked on the COMPUTE button. Simulation runs were performed for these six profiles (2, 5, 10, 25, 50, and 100 year floods), closed the computation window and the steady flow window after successful simulation. Later on, the generated flood depths at Mwakimeme gauge station were realized and they were observed through a cross-sectional editor.

3.9 Flood inundation maps development

The flood depths simulated at the Mwakimeme gauging station on the North Rukuru River using the HEC-RAS model were translated into spatial representations of inundation across the surrounding floodplain. Within HEC-RAS, the RAS Mapper was used to generate GIS layers corresponding to various flood magnitudes. These GIS files were subsequently imported into ArcGIS software, where flood inundation maps were produced to illustrate the spatial extent and distribution of flooding. The following steps were done:

3.9.1 Exporting North Rukuru River RAS model output data

The HEC-RAS results were export ed to ArcGIS by clicking on File, and then Export GIS Data in the main HEC-RAS window. Clicked on Select Profiles, and selected all the profiles (2, 5, 10, 25, 50, and 100 year floods) for export, and accepted the default export options; clicked on Export Data button; which created a SDF file in the working directory folder. Saved the HEC-RAS project and exited.

In ArcGIS (ArcMap) opened North Rukuru river file created by RAS MAPPER and clicked on Import RAS SDF file button to convert the SDF file into an XML file. In the Convert RAS Output File to XML window, browsed to 2_100 SteadyFlow. RASexport.sdf, and clicked OK. The XML file was saved with the input file name in the same folder with an xml extension. The SDF files from RAS Mapper were in Raster formant and they were converted into shapefiles in the ArcMap 10.5 and flood inundation maps were produced in relation to the study area.

The methodological flow chart shown in Figure 3 describes the steps that were followed to achieve the main objective of this research project.

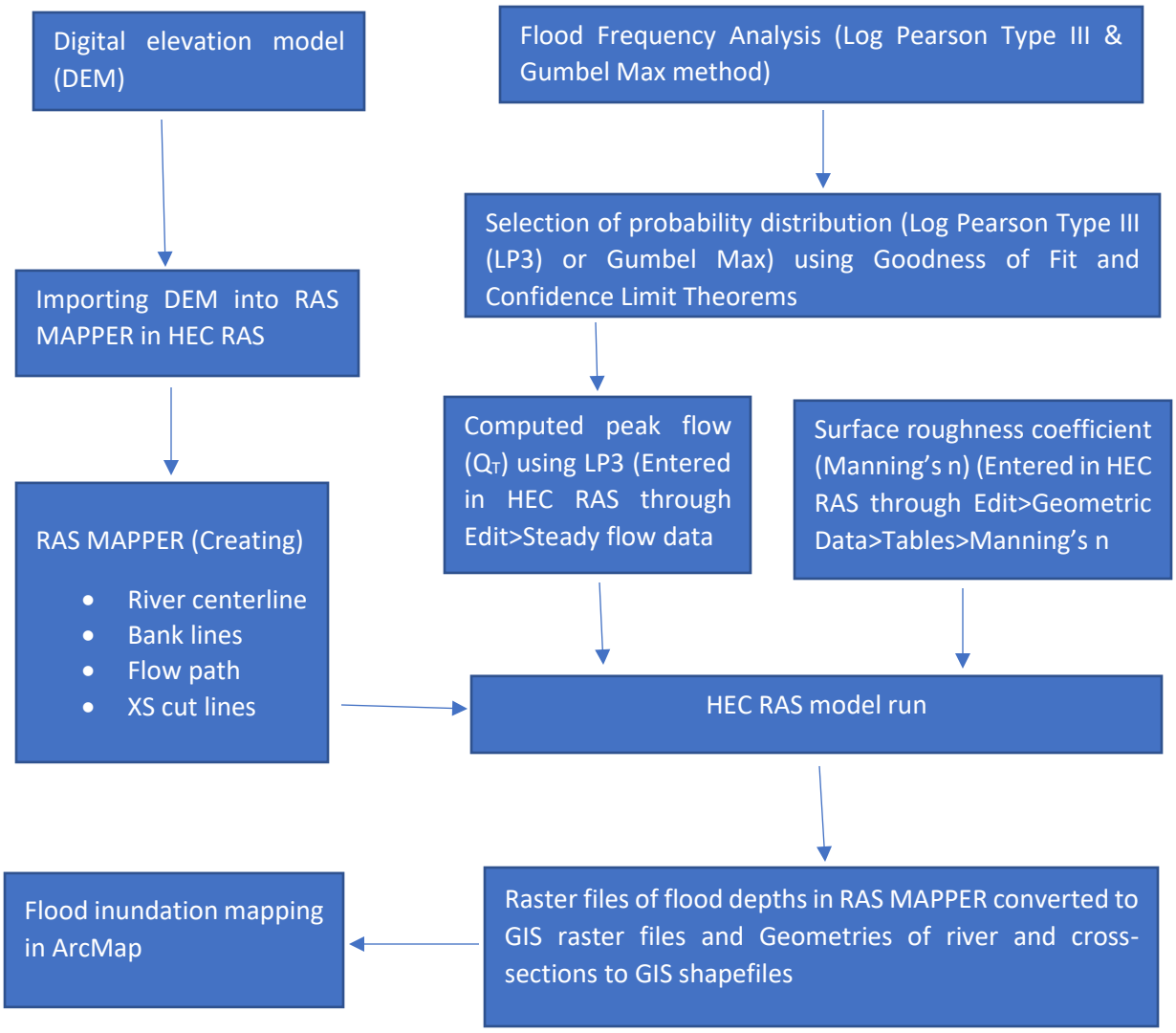

Figure 3: Methodological Flow Chart for Flood Inundation Mapping

3.9.2 Floodplain analysis

Flood occurrence is often misinterpreted based on location, necessitating precise spatial analysis to determine whether inundation has transpired within a designated floodplain. To establish floodplain boundaries, a floodplain map was generated using the Soil and Water Assessment Tool (SWAT) model. Additionally, flood inundation maps representing various

return periods developed using the HEC-RAS model were validated against the floodplain map produced by the SWAT model to assess their accuracy in identifying flood prone areas.

To further enhance the reliability of the flood inundation maps, field surveys were conducted to record geographic coordinates, particularly for villages in close proximity to the river. This data provided a crucial reference for evaluating the extent of flooding and validating model outputs, ensuring that flood hazard mapping accurately reflects areas at risk of inundation.

The methodological flow chart shown in Figure 4 describes the steps that were followed to produce a floodplain map in SWAT model.

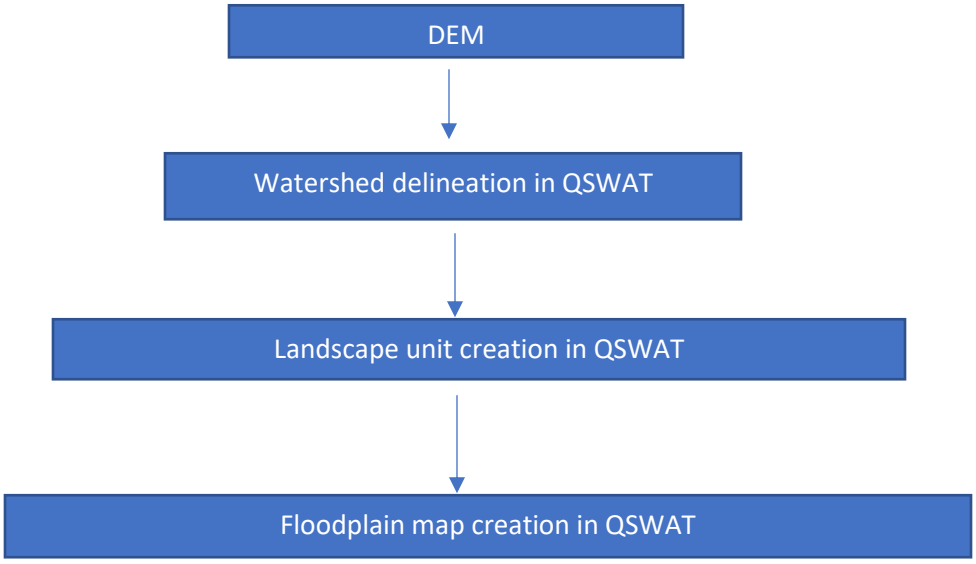

Figure 4: Methodological Flow Chart for Floodplain Mapping in SWAT model

3.10 Effectiveness of the dyke

An effective flood management strategy requires the integration of both structural and non-structural mitigation measures. Accordingly, the effectiveness of the dyke was examined to complement the insights derived from the flood inundation maps. The inundation maps were

cross-referenced to determine whether the simulated flood extents surpassed the location of the dyke, thereby indicating potential breaching. To further substantiate this analysis, a household survey was administered using semi-structured questionnaires. The survey aimed to evaluate the dyke's performance in reducing flood depth, duration, and frequency within the areas designated for protection. The questionnaire incorporated open-ended questions, thereby generating both qualitative and quantitative data, and was specifically structured to capture the flooding situation before and after the dyke's construction. The following steps were done:

3.10.1 Determining specifications of the dyke (Height)

Based on dyke specifications, a crest width of 4 m, a base width of 11.5 m, and slope gradients of 1:2 along the sea shoreline and 1:3 on the embankment's opposite side, the height of the dyke was computed, and compared against flood depths of different return periods realized from HEC-RAS model. If the flood depth was less than the dyke height it was considered effective enough to prevent water flowing to the residential area and if the flood depth was bigger than the dyke height it was deemed ineffective.

To calculate the height of the dyke the following formula was used:

$$H = \frac{B-C}{S_1+S_2} \quad \text{..... (32)}$$

Where:

H = Height of the dyke

B = Base width = 11.5 m

C = Crest width = 4 m

S_1 = Slope ratio on the shoreline = 2

S_2 = Slope ratio on the opposite side = 3

$H = \frac{11.5-4}{2+3}$

H = 1.5 m

The height of the dyke was found to be 1.5 m, and this was compared against flood depths of various return periods to evaluate the effectiveness of the dyke.

3.10.2 Determining the sample size

The Yamane formula, commonly used to determine sample size for a finite population was used to determine the sample size of the study as follows:

$$n = \frac{N*Z^2*p*(1-p)}{(N-1)*e^2+Z^2*p*(1-p)} \quad \text{..... (33)}$$

Where:

n = required sample size

N = total population size

Z = Z-score corresponding to the confidence level

p = estimated proportion of the population with the characteristic of interest

e = margin of error

In this study the population size of Karonga Township area (study area) (N) was 61,609, determined by the National Statistical Office of Malawi in 2018 (NSO), confidence level was 95% with the Z score of 1.96, the estimated proportion (p) of 0.5 and the margin of error of 5% (0.05).

$$n = \frac{61609*1.96^2*p*(1-0.5)}{(61609-1)*0.05^2+1.96^2*0.5*(1-0.5)}$$

n = 382

The initial sample size from the calculation was 382, as more questionnaires were administered during the survey up to 394, it was chosen as the sample size, further improving the precision and reliability of the results through reduced margin of error and higher confidence level.

3.11 Ethical Issues

Ethical principles were followed to ensure code of professional conduct. According to Kativhu (2016), ethical considerations serve as standards a researcher follows to avoid infringing upon other peoples' rights participating in the conduct of research. Official clearance for conducting fieldwork was obtained from the MZUNIREC. Prior to data collection, permissions were obtained from relevant authorities, including Karonga District Council and local leaders such as chiefs and village headpersons. The participants were also asked for their consent and convenient time to participate in the study.

Participation was entirely voluntary, and respondents retained the right to decline participation, withhold responses, or withdraw at any stage without prejudice. To ensure effective communication, interviews were conducted in the local language, Tumbuka, translated from English onsite. Confidentiality was preserved by not recording personal identifiers on the questionnaires such as names, and participants were assured that all data would be securely stored and used solely for academic purposes.

3.12 Summary of material and methods chapter

This chapter has presented the procedures undertaken for data collection and analysis. It starts with the explanation on estimation of river discharges for various return periods using the Log-Pearson Type III and Gumbel probability distributions. Subsequently, it elaborates on how

the flood depths at the Mwakimeme gauging station were simulated through the HEC-RAS model, and the development of flood inundation maps in ArcGIS (ArcMap). In addition, the effectiveness of the dyke in mitigating flood impacts, specifically in terms of reducing flood depth, duration, and frequency is explained, highlighting the importance of integrating physical structures such as dykes with flood inundation maps in mitigating floods.

CHAPTER 4 : RESULTS AND DISCUSSION

4.1 Introduction

This chapter presents the research study findings and discussions in four sections representing each research objective. Efforts were carefully made to ensure that the data and information acquired aligned closely with the intended objectives.

4.2 Estimating river discharges for different return periods

Streamflow data was obtained from Mwakimeme gauge station and Figure 5 shows annual peak flow data from Mwakimeme gauge station for a period of 44 years (1979 to 2022) which was used to calculate river discharges.

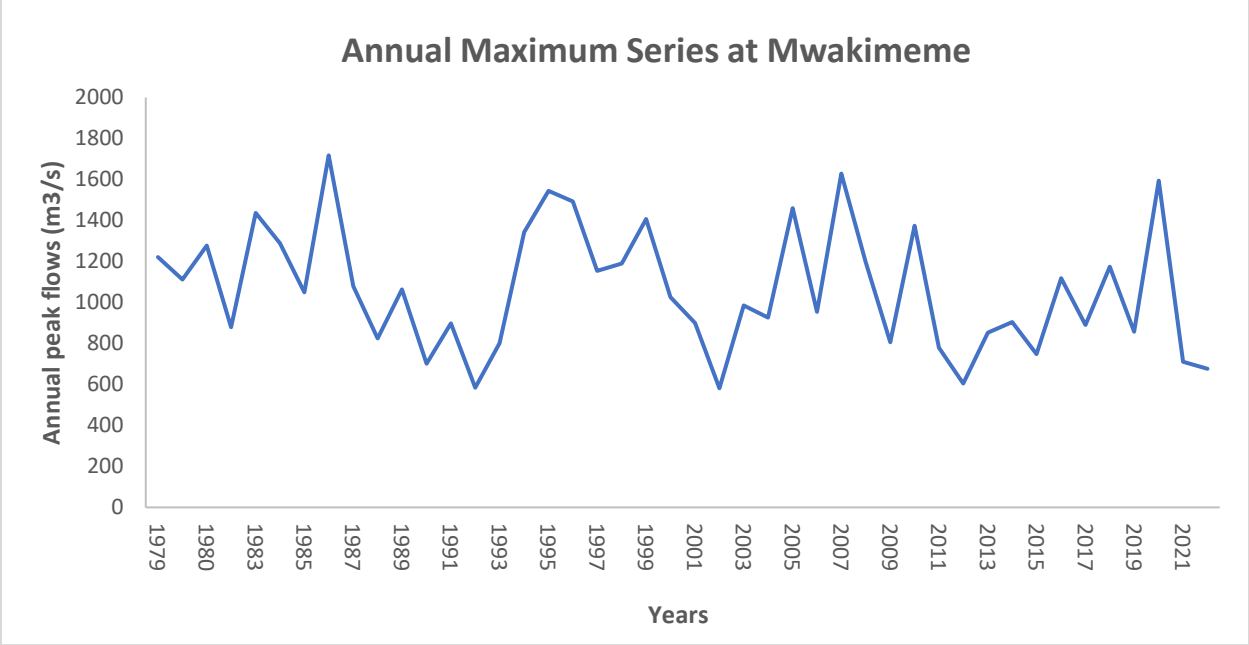

Figure 5: Annual peak flows (m3/s) at Mwakimeme

The maximum peak streamflow data is 1717.62 m^3/s realized in 1986 and the minimum streamflow data is 581.15 m^3/s recorded in 2002. The standard deviation and mean value of

streamflow data are 302.53 m^3/s and 1063.99 m^3/s, respectively. The coefficient of variation in the streamflow data is 28% which is a moderate variation and the range is 1136.47 m^3/s which suggests a high variability between the minimum and maximum discharge. Gumbel extreme value distribution and Log Pearson Type III distribution were considered to conduct flood frequency analysis as they have the potential to handle such a fair amount of variability.

Table 4 presents the estimated river discharges at the Mwakimeme gauging station on the North Rukuru River for return periods of 2, 5, 10, 25, 50, and 100 years. These values were derived using both the Gumbel Extreme Value distribution and the Log-Pearson Type III distribution.

Table 4: Estimation of Peak Floods by Gumbel Extreme Value and Log Pearson Type III

Return Period (T) years	**Gumbel Extreme Value Method**			**Log Pearson Type III Model**		
	Reduced variate (Y_T)	**Frequency factor (K)**	**Expected Discharge (X_T)**	**Frequency Factor (K_T)**	**Log Discharge (Z_T)**	**Expected Discharge (Q_T)**
2	0.366513	-0.15592	1016.82	0.02106	3.01213	1028.27
5	1.49994	0.829759	1315.02	0.847015	3.115888	1305.85
10	2.250367	1.482361	1512.46	1.266955	3.168642	1474.65
25	3.198534	2.306926	1761.92	1.706866	3.223904	1674.55
50	3.901939	2.918635	1946.98	1.986045	3.258975	1815.39
100	4.600149	3.525828	2130.68	2.233224	3.290026	1950.40

To estimate the log discharges (Z_T), the streamflow data were converted to their logarithmic base 10 values. The mean and standard deviation of the converted streamflow were 3.009484809, and 0.125621568, respectively. The coefficient of skewness (G) for the log base 10 transformed streamflow data was -0.12537. The frequency factor (K_T) which depends on the coefficient of skewness and return periods, was 0.02106, 0.847015, 1.266955, 1.706866, 1.986045, and 2.233224, for 2, 5, 10, 25, 50, and 100 year return periods, respectively. Consequently, the log discharges (reduced variate) were computed as 3.01213, 3.115888, 3.168642, 3.223904, 3.258975, and 3.290026 for 2, 5, 10, 25, 50, and 100 year return period, respectively. After finding the reduced variates (Z_T) by Eq. (2), the corresponding expected discharges (Q_T) were computed by using Eq. (9). The expected discharges by Log Pearson Type III distribution were 1028 m^3/s, 1306 m^3/s, 1474 m^3/s, 1675 m^3/s, 1815 m^3/s, and 1950 m^3/s, for 2, 5, 10, 25, 50, and 100 year return period, respectively.

To compute frequency factors (K) for various return periods using the Gumbel extreme value distribution, the reduced variates were calculated by using Eq. (21). The realized variates for 2, 5, 10, 25, 50 and 100 year return period were 0.366513, 1.49994, 2.250367, 3.198534, 3.901939, and 4.600149, respectively. The reduced mean (Y_n) and reduced standard deviation (S_n) of the sample size (n) 44 were obtained using the reduced mean and reduced standard deviation table for gumbel extreme value distribution, the results indicated 0.5458, and 1.1499, respectively. Frequency factors for various return periods, 2, 5, 10, 25, 50, and 100 years, were calculated using Eq. (22), the results were -0.15592, 0.829759, 1.482361, 2.306926, 2.918635, and 3.525828, respectively. The statistical analysis of the observed data revealed a coefficient of skewness of 0.36489872, a mean of 1063.99423, and a standard deviation of 302.533611. Using these statistical parameters and frequency factors in Eq. (23), the expected discharges

for specified return periods, 2, 5, 10, 25, 50 and 100 years, were computed as 1016.82 m^3/s, 1315.02 m^3/s, 1512.46 m^3/s, 1761.92 m^3/s, 1946.98 m^3/s, and 2130.68 m^3/s, respectively.

The expected discharges computed by the Gumbel extreme value method for return periods 5, 10, 25, 50 and 100 years are greater than the estimations predicted by the Log Pearson Type III model. Log Pearson Type III model estimated a larger peak flood than the Gumbel extreme value model in the lower return period of 2 years. Overall, Gumbel extreme value is overestimating the predicted discharge compared to Log Pearson Type III. These findings are consistent with those reported by Nasir (2025), who analyzed discharge data from the Bahadurabad river station in India for return periods of 5, 10, 25, 50, and 100 years. At shorter return periods (5 years), the Log-Pearson Type III distribution produced higher discharge estimates (79,758 m^3/s) compared to the Gumbel distribution (77,707 m^3/s). However, at longer return periods (10–100 years), the Gumbel EV-1 method yielded substantially greater discharge values (88,286–121,410 m^3/s) than those obtained using the Log-Pearson Type III distribution (79,945–95,680 m^3/s). Similarly, Shatu *et al.* (2023) analyzed 32 years of streamflow data (1979–2021) from the Teesta River to estimate discharges using the Log-Pearson Type III and Gumbel distributions for return periods of 5, 10, 50, and 100 years. Their results showed that at shorter return periods (5 years), the Log-Pearson Type III distribution produced higher discharge estimates (3,355.103 m^3/s) compared to the Gumbel distribution (3,120.958 m^3/s) and, at longer return periods (10–100 years), the Gumbel distribution yielded substantially larger values (3,879.064–6,252.887 m^3/s) than the Log-Pearson Type III distribution (3,447.332–3,474.707 m^3/s). In contrast, Singh and Chavan (2024) conducted a regional flood frequency analysis in the United States for different major rivers and observed that the Gumbel distribution tended to overestimate river discharges at

shorter return periods, whereas the Log-Pearson Type III distribution produced higher estimates at longer return periods.

4.2.1 The Goodness of Fit Test and Confidence Limits Test

In flood frequency analysis, an overestimating distribution, in this case, the Gumbel distribution is often preferred over the one that underestimates (Log Pearson Type III distribution), as this provides a margin of safety when delineating flood-prone areas and designing protective structures such as dykes. However, the choice of distribution cannot be based solely on overestimation. The reliability and accuracy of the estimates carries more weight and must be evaluated, requiring the application of goodness-of-fit tests and confidence limit analyses to identify the most appropriate distribution for discharge estimation and to adopt the predicted values with confidence.

Table 5 shows the goodness of fit results for Gumbel distribution and Log Pearson Type III distribution using Kolmogorov-Smirnov (K-S), Chi-square and Anderson-Darling (A-D) tests.

Table 5: Goodness of Fit Test for Gumbel Extreme Value and Log Pearson Type III

Distribution	Kolmogorov-Smirnov (Critical value at $a_{0.05}$ = 0.2047)			Anderson-Darling (Critical value at $a_{0.05}$ = 1.959964)			Chi-squared (Critical value at $a_{0.05}$ = 59.304)		
	Statistic	Reject	Rank	Statistic	Reject	Rank	Statistic	Reject	Rank
Log Pearson Type III	0.02378	No	1	0.242	No	1	47.224	No	1
Gumbel Extreme value	0.2060	Yes	2	0.4468	No	2	60.943	Yes	2

The selection of the appropriate flood frequency distribution was based on the comparison of the goodness of fit test results. Goodness of fit represents the distance between the observed data and the fitted distributions, the distribution with the minimum statistical value was considered as the best fit. The results of the goodness of fit test show that Gumbel extreme value distribution is rejected in the Kolmogorov-Smirnov, and Chi-square test since their statistical values are larger than the critical values. The Log Pearson type III is not rejected in both Kolmogorov-Smirnov, and Chi-square test as its statistical values are lower than the critical values. Both distributions qualify under Anderson-Darling test, statistical values are less than critical values, but Log Pearson type III gives a closer fit as its statistical value (0.242) is smaller than Gumbel's extreme value statistic (0.4468). According to the goodness of fit results, the Log Pearson Type III method is more appropriate and reliable than Gumbel's extreme value method.

To support the the goodness of fit test results based on the Kolmogorov-Smirnov (K-S), Chi-square and Anderson-Darling (A-D) tests, the coefficient of determination (R^2) test was also conducted. The coefficient of determination (R^2) between the observed and transformed data by Gumbel Extreme Value and Log Pearson Type III distribution were 0.978377 (97.84%), and 0.988565 (98.86%), respectively. These values indicate that both distributions are a very good fit for the observed data, with R^2 exceeding 0.85. Notably, the Log Pearson Type III distribution exhibits a slightly better fit compared to the Gumbel Extreme Value distribution. The high R^2 values suggest that the majority of the variability in discharge values due to different return periods is effectively captured by these models. it is important to clarify that these R^2 values do not imply that these models predict the discharge values with an accuracy

of 97.84% and 98.86%, respectively. They indicate the proportion of variance in the observed data that can be explained by the transformed data.

To complement the goodness-of-fit test conducted using the Kolmogorov-Smirnov (K-S) test, the Anderson-Darling (A-D) test, and the Chi-Square test, confidence limits of the transformed data were computed at the 95% confidence level. Confidence limits provide a statistical range within which the true value of the flood is expected to lie, with a specified level of confidence. The distribution with narrower width of limits (upper and lower limit), indicate a better fit to the data.

Using Eq. (10) and Eq. (13) for Log Pearson Type III distribution, Eq. (24) and Eq (25) for Gumbel Extreme Value distribution, Figure 5 shows the results realized for confidence limits widths.

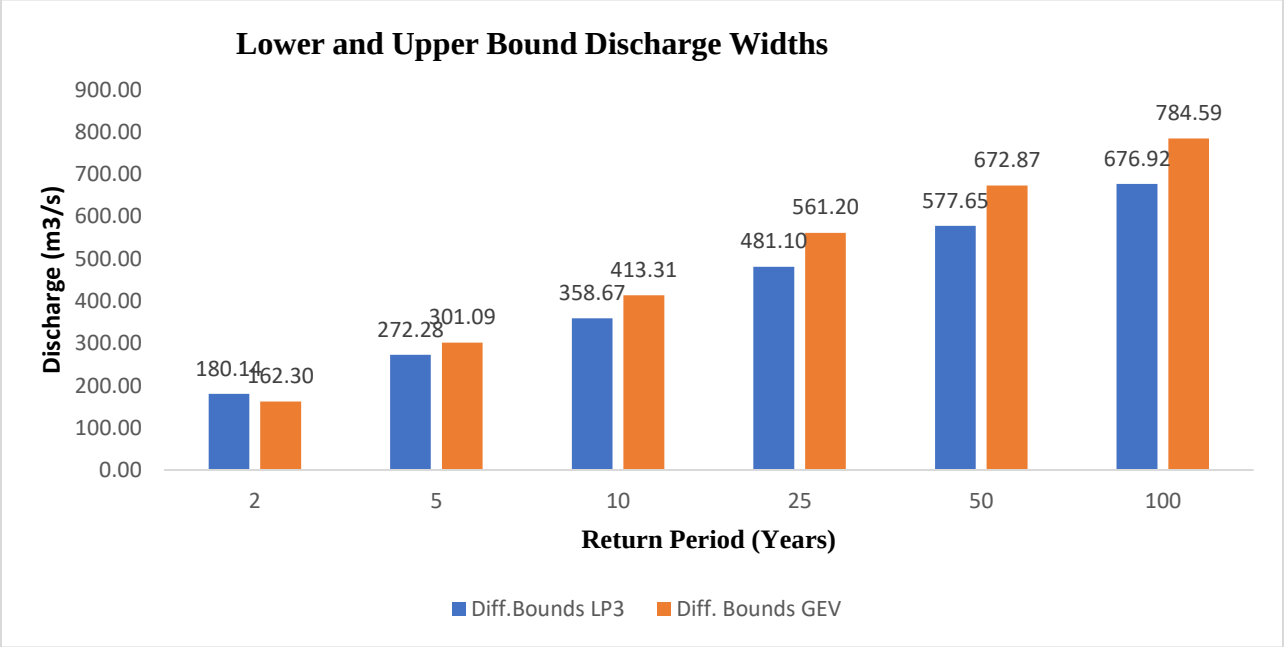

Figure 6: Differences in Upper and Lower Bounds for LP3 and GEV

In Fig. 6, smaller differences indicate less uncertainty, hence a more reliable distribution for making predictions. For the 2-year return period, Gumbel Extreme Value (GEV) shows smaller bounds (162.30 against 180.14), suggesting it has lower uncertainty for short-term predictions. From the 5-year return period onward, Log Pearson Type III (LP3) consistently displays smaller differences in bounds compared to Gumbel Extreme Value (GEV), indicating that it provides more reliable predictions for longer-term events. In hydrological studies, longer return periods are often more critical for infrastructure design and flood management. As a result, Log Pearson Type III was chosen over Gumbel Extreme Value distribution. Consequently, in goodness of fit test using Kolmogorov-Smirnov (K-S), Chi-square and Anderson-Darling (A-D) tests, coefficient of determination (R^2) test and confidence limit test, Log Pearson Type III edges Gumbel Extreme Value distribution, hence the estimated discharges for various return period from Log Pearson Type III distribution were used in this study over those of Gumbel distribution. The discharges from Log Pearson Type III which were 1028 m^3/s, 1306 m^3/s, 1474 m^3/s, 1675 m^3/s, 1815 m^3/s, and 1950 m^3/s, for 2, 5, 10-, 25-, 50-, and 100-year return period, respectively.

These findings are similar to those of Bhat *et al.* (2019), who reported that the Log-Pearson Type III distribution provided a superior fit compared to the Gumbel distribution when estimating river discharges for the Jhelum River in the Kashmir Basin. Similarly, Mkhandi *et al.* (2009) identified the Log-Pearson Type III distribution as the most appropriate model for discharge estimation in the Southern African region where Malawi is situated, outperforming other probability distributions such as the General Extreme Value, Log-Normal (three-parameter), and Gumbel distributions. However, the results from the study contrast with those of Shatu *et al.* (2023), who identified the Gumbel distribution as the most suitable method

for estimating river discharges in the Teesta River, and with Madhusudan *et al.* (2022), who similarly reported that the Gumbel distribution provided a better fit than the Log-Pearson Type III distribution when estimating flood discharges for various return periods at the Kabini Dam.

4.3 Simulation of flood water depths for the North Rukuru river (Water Surface Profiles) in HEC-RAS.

Using Ras Mapper, a GIS embedded tool in HEC RAS, a river centerline, flowpaths, river banks and cross sections were created, starting from where Mwakimeme gauging station is situated. A number of cross sections were created, specifically 207 cross sections. A cross section with a river station number of 28376 was located at Mwakimeme gauging station.

Manning's roughness coefficient (n) is an important parameter in hydraulic modelling, influencing the computation of flow resistance in open channels. In HEC RAS, the coefficient determines how water interacts with channel surfaces, affecting velocity, depth, and overall flow behavior. Through onsite observations, and remote observation using google satellite map embedded in HEC RAS, manning's values were assigned to every cross-section river station, representing the left over-bank, main river and right over-bank. The appropriate range for the manning's values for the over-banks were 0.02-0.05, representing pasture areas with short grass and high grass, and cultivated areas with no crops, and mature row crops. For the main channel, clean, straight, no rifts or deep pools and in some areas, winding and weedy, a range of Manning's values (n) selected were 0.025-0.04.

North Rukuru river HEC RAS model output flood depth (maximum channel flood depth) data was observed at the gauging station cross-section with river station 28376. Other output data such as flow area, flood velocities in the channel (Vel Chnl), minimum channel elevation (Min

Ch El), water surface elevation (W.S. Elev) and top width of the channel were also observed. The entire river reach from where the banks, cross-sections and flow paths were created was named Reach 2. Table 6 illustrates these results accompanied by total discharges (Q total) of respective return periods at the gauging station cross-section:

Table 6: North Rukuru river HEC RAS model output flow results at the gauging station

S/No	Reach	River Station	Profile	Q Total	Vel Chnl	Flow Area	Min Ch El	W.S Elev	Top Width
1	Reach 2	28376	2 Year flood	(m^3/s)	(m/s)	(m^2)	(m)	(m)	(m)
				1028	1.37	711.12	526	531.15	190.41
2	Reach 2	28376	5 Year flood	1306	1.38	876.56	526	532	197.49
3	Reach 2	28376	10 Year flood	1474	1.40	970.12	526	532.47	201.35
4	Reach 2	28376	25 Year flood	1675	1.43	1075.86	526	532.99	205.38
5	Reach 2	28376	50 Year flood	1815	1.44	1146.34	526	533.33	207.95
6	Reach 2	28376	100 Year flood	1950	1.46	1212.74	526	533.65	210.34

The maximum channel flood depths for a 2 year flood of 1028 m^3/s, 5 year flood of 1306 m^3/s, 10 year flood of 1474 m^3/s, 25 year flood of 1675 m^3/s, 50 year flood of 1815 m^3/s, and 100 year flood of 1950 m^3/s were 5.15 m, 6.00 m, 6.47 m, 6.99 m, 7.33 m, and 7.65 m, respectively, at the Mwakimeme river gauging station. A similar study conducted by Martin *et al.* (2012) at the Sironko River in Uganda examined the relationship between flood magnitude and channel depth across different return periods, the findings indicated that the maximum channel flood

depths corresponding to a 10-year flood event of 717.85 m^3/s**,** 50-year flood event of 1,230.07 m^3/s, and 100-year flood event of 1,384.24 m^3/s were 5.21 m, 6.53 m, and 6.84 m, respectively at the gauging station**.** Adugna (2020) conducted a study on flood inundation mapping and hazard assessment at Holeta river in Ethiopia, his findings indicated that a 10 year flood of 350.75 m^3/s, 25 year flood of 417.445 m^3/s, 50 year flood of 465.551 m^3/s, and 100 year flood of 511.68 m^3/s exhibited maximum flood depths of 8.38 m, 8.58 m, 8.72 m, and 8.84 m, respectively at the gauging station.

The highest water depth for the 100 year flood was 21.62878418 m, most of which lied in the stream channel, with the lowest being 0.00112915 m. The flood depth for a 2 year flood was from 0.001037598 m to 19.13500977 m, where as a 5 year flood ranged from 0.001068115 m to 19.98376465 m, 0.001037598 m to 20.45166016 m for the 10 year flood, 0.001098633 m to 20.9708252 m for the 25 year flood, and 0.00100708 m to 21.3114624 m for the 50 year flood. In a related study, Aynalem used HEC-RAS and ArcGIS to generate a floodplain map for the Muga River in the Upper Blue Nile Basin, Ethiopia (Aynalem, 2020). The analysis focused on a 100 year flood event, which resulted in a flood depth ranging from 0.001 m to 4.1215 m. Martin *et al.* (2012) conducted a flood depth analysis for the Sironko River in Uganda, assessing multiple return periods. Their findings indicated that the flood depth varied across different flood events, with ranges of 0.0082 m to 32.5901 m for the 10-year flood, 0.0016 m to 34.3357 m for the 50-year flood, 0.0071 m to 34.8347 m for the 100-year flood, 0.0084 m to 35.5957 m for the 250-year flood, and 0.0027 m to 36.0934 m for the 500-year flood. These findings show a similar trend with the present study, demonstrating that flood severity, as represented by flood depth, increases with longer return periods. This is vital in the development of effective flood mitigation strategies, as infrastructure such as dykes are

designed to withstand the worst-case flood depths, ensuring adequate resistance against floodwaters.

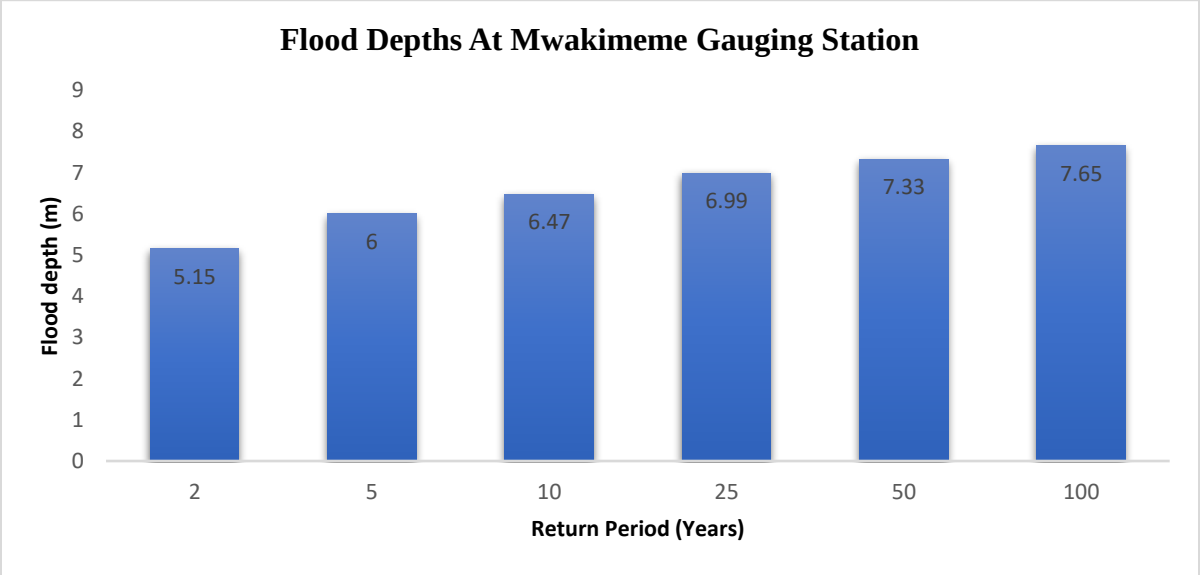

Figure 7: Flood depths of different return periods at Mwakimeme gauging station

4.4 Flood Inundation Mapping

An inundation map displays the spatial extent of probable flooding for different return periods. The RAS Mapper tool in HEC RAS was used develop spatial data file (SDF). These SDF RAS files contained the flood depths files, and the extent of flooding for different return periods. These files showed the extent of flooding with associated flood depths. The SDF RAS file was converted to a GIS read DEM file of flood depths and flood extents of different return periods.

4.4.1 Flooded Areas

The flooded areas along the North Rukuru river starting from Mwakimeme gauge station were 254209.5 m^2, 289555.8 m^2, 309817.3 m^2, 332673.4 m^2, 348384.7 m^2, and 362771.7 m^2 for 2, 5, 10, 25, 50 and 100 year return periods, respectively. During the field survey, some GPS

coordinate points were collected along the river to validate the spatial extent of flooded areas. The flood inundation maps below show the extent and depth of the 2, 5, 10, 25, 50 and 100 year floods. The maps also depict some infrastructure, and some GPS coordinate points representing houses that may experience damages during floods.

Figure 8 shows the areas of interest discussed on flood inundation maps of different periods and it is put to show a clear visual representation of the ground or earth complementing the flood inundation maps.

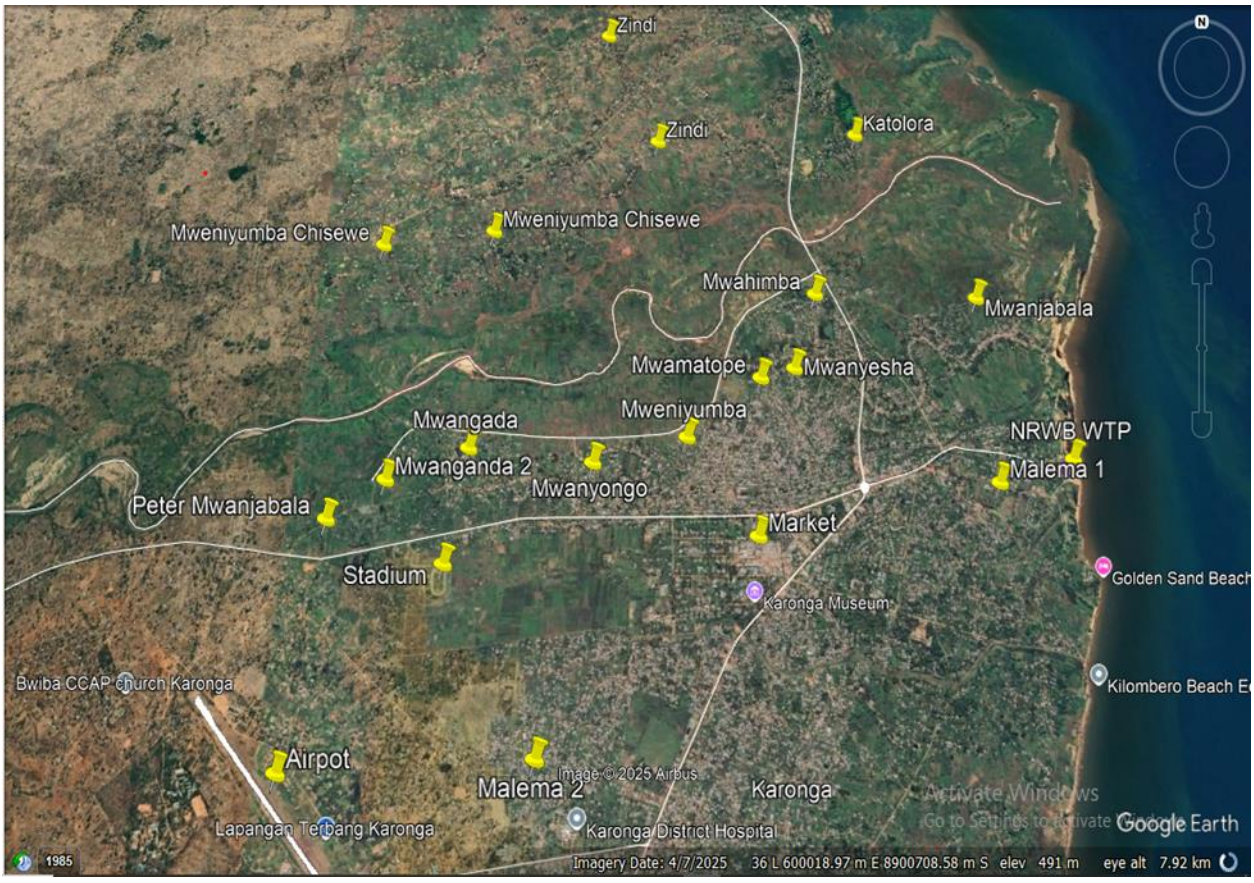

Figure 8: A Google Earth Pro image with areas of interest

4.4.2 Two-Year Flood

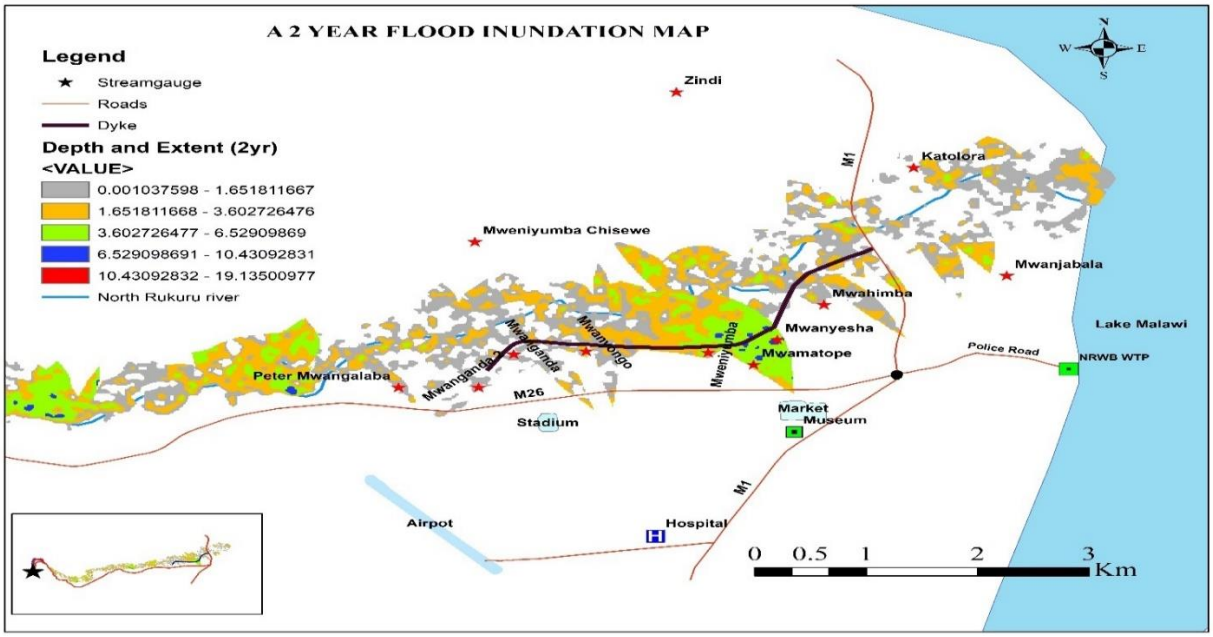

Figure 9: Flood inundation map for a 2 Year flood

4.4.3 The 5 Year Flood

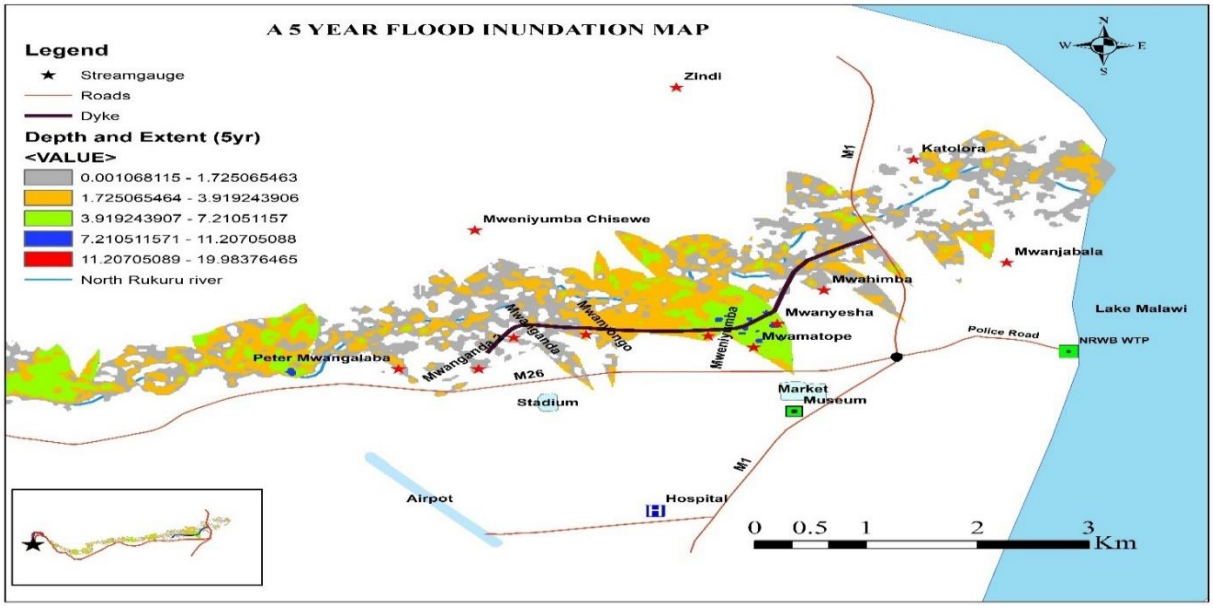

Figure 10: Flood inundation map for a 5 Year flood

4.4.4 The 10 Year Flood

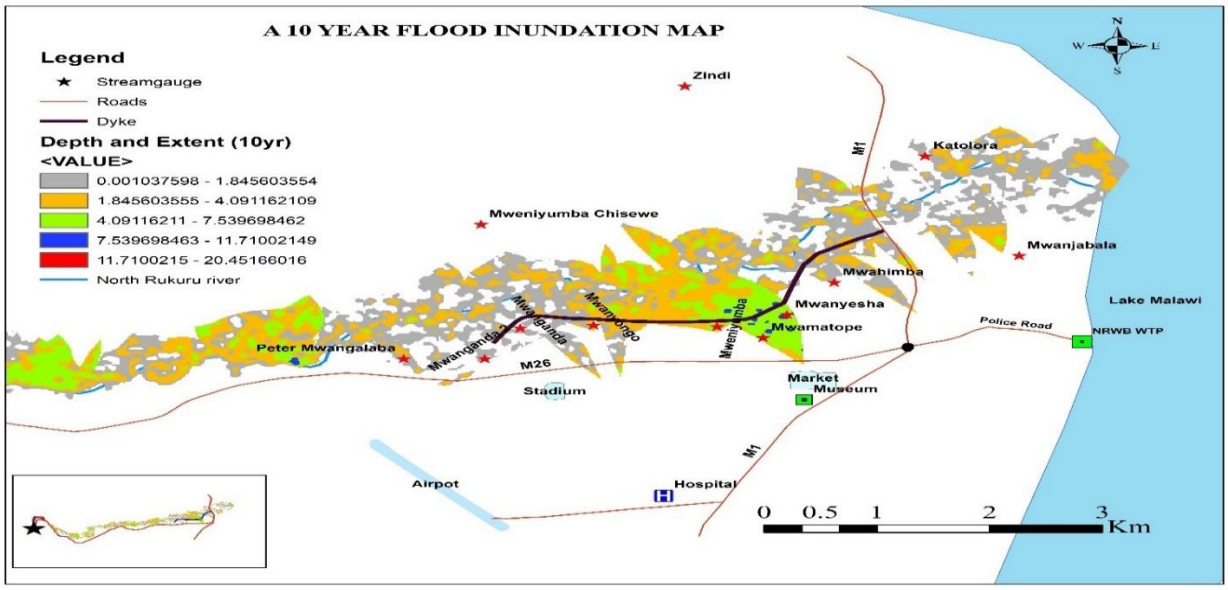

Figure 11: Flood map inundation for a 10 Year flood

4.4.5 The 25 Year Flood

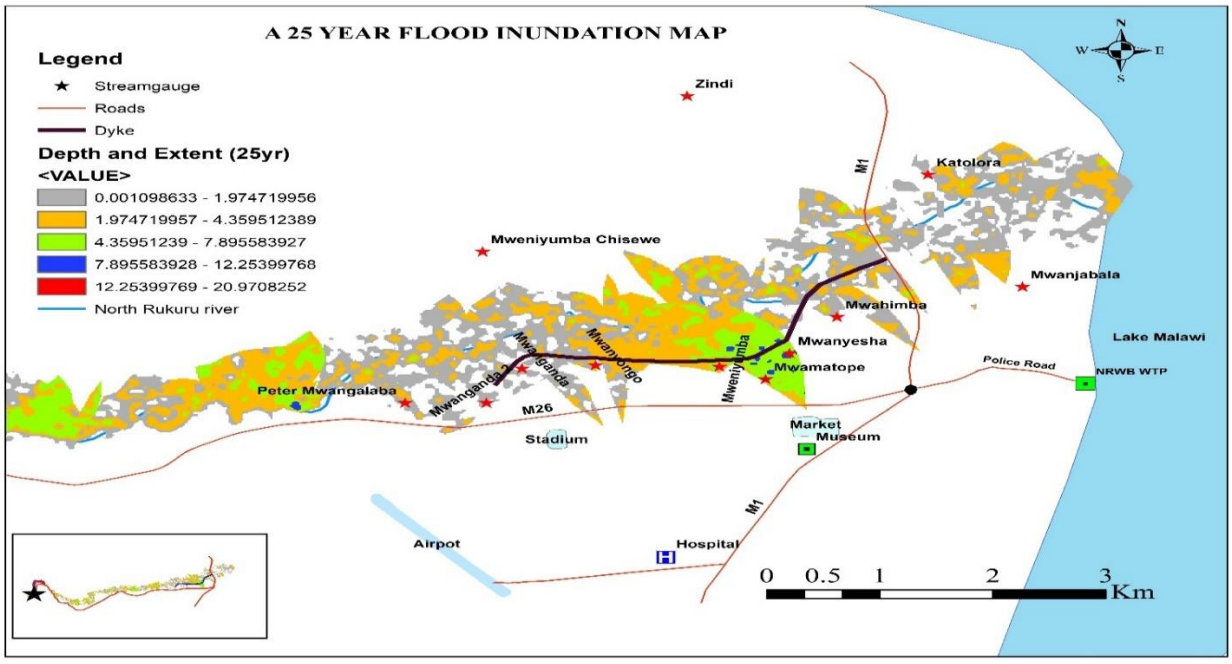

Figure 12: Flood inundation map for a 25 Year flood

4.4.6 The 50 Year Flood

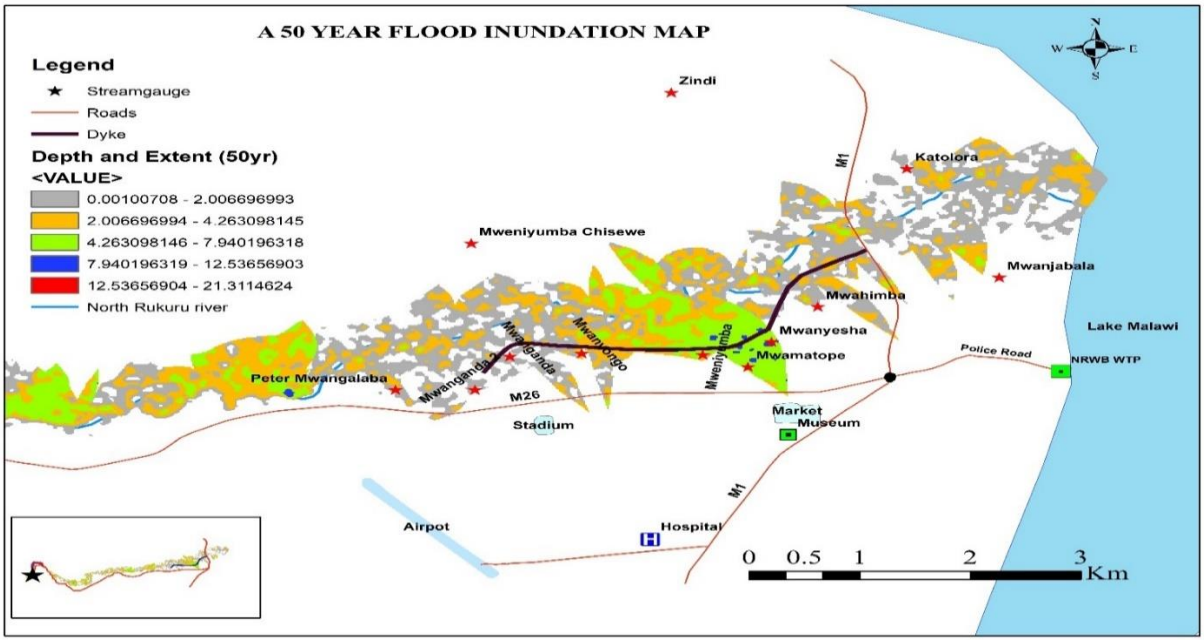

Figure 13: Flood inundation map for a 50 Year Flood

4.4.7 The 100 Year Flood

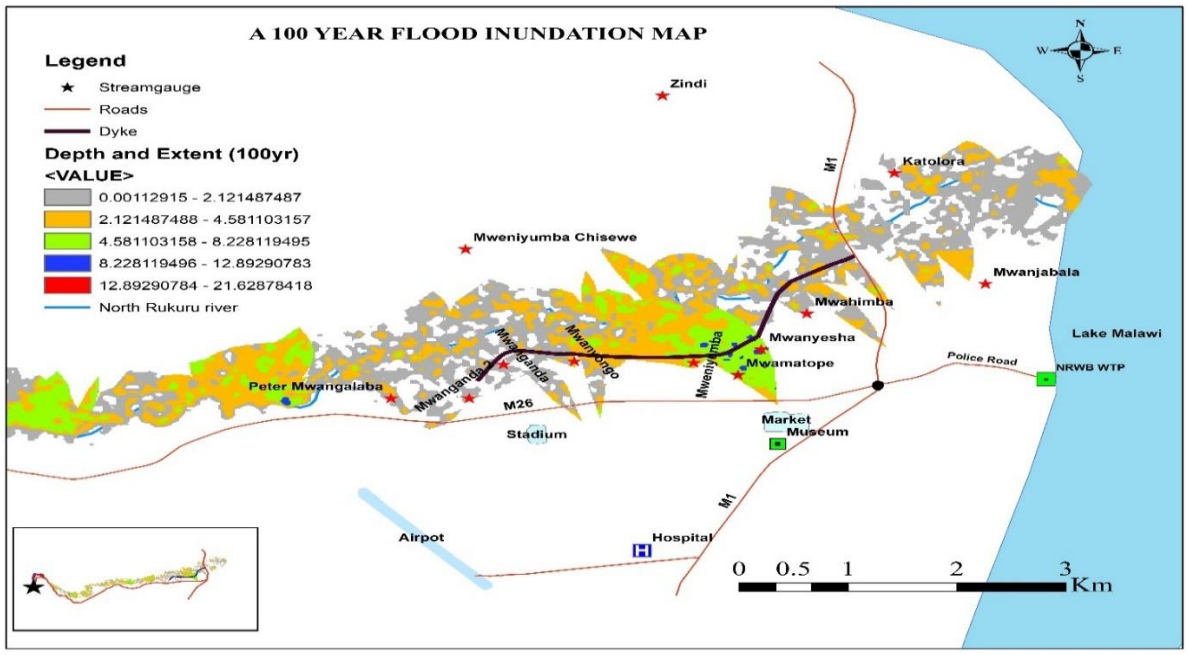

Figure 14: Flood inundation map for a 100 Year flood

The study determined that the villages of Mweniyumba, Mwahimba, Mwanyongo, Mwanganda, Mwamatope, Mwanyesha, Mwanjabala, Katolora, and Peter Mwangalaba were highly susceptible to flooding across various return periods, including the 2 year, 5 year, 10 year, 25 year, 50 year, and 100 year flood events. This susceptibility is visually represented in the respective flood inundation maps, which depict the extent of inundation at each return period.

Evidence collected through field surveys, shown through household GPS coordinates on the maps corroborates these findings, indicating that these villages frequently experience flood events, thereby validating the hec-ras model predictions. Despite the presence of a dyke approximately 4.34 km in length, extending from Mwanganda to Mwahimba, the flood maps analysis suggests that its protective capacity is limited. It was also noted that the dyke does not extend to Peter Mwangalaba and Mwanjabala villages. There was also no dyke on the other side of the river where Katolora village is located. The absence of flood protection infrastructure in these areas may have contributed to their continued exposure to flooding, as illustrated by the flood inundation mapping results.

Field observations, along with interviews conducted with the disaster officer and water officer, revealed that Zindi Village and the township area, particularly the market, are also affected by flooding. Notably, the flood inundation maps did not indicate a direct flood risk from the North Rukuru River to Zindi Village. However, a detailed focus group discussion established that the flooding in Zindi Village is indirectly linked to the North Rukuru River through one of its distributaries, Malungo River. This distributary serves as a significant conduit for floodwaters, contributing to the village's inundation. Through a thorough key informant interviews with the disaster officer and water officer, it was learned that flooding in the Karonga Township area,

particularly within the market, was primarily attributed to the clogging and sedimentation of drainage infrastructure, including the two artificial channels designed to collect runoff from the town and convey it towards the lake. The accumulation of debris and sediment in these drainage systems significantly reduced their efficiency, increasing the risk of urban flooding. This observation aligns with the findings of Gondwe *et al.* (2017), who identified clogged drainage infrastructure as a main contributing factor to flood occurrences in the Karonga Township area. This may explain why these two areas were shown not to be affected by floods of all magnitudes from the North Rukuru River on inundations yet they experienced frequent flooding.

While the hypothesis that floodwaters infiltrate the central town from the west side of the dyke at Peter Mwangalaba Village and partly Mwanganda village, where no dyke has been constructed was met with skepticism by the disaster officer and water officer, it was strongly supported through focus group discussions with village development committees. Community representatives asserted that flooding in the central town and surrounding villages was partly a consequence of the absence of the dyke in this area. These findings emphasize both the direct and indirect flood risks in terms of extent and inundation from the North Rukuru river. The flood inundation maps generated in this study are consistent with findings reported by several organizations and researchers. Previous assessments conducted by UNICEF (2017), the Malawi Red Cross (2017), the Department of Disaster Management Affairs (DoDMA 2019), ACT Alliance (2025), as well as Gondwe *et al.* (2017), identified communities such as Mwahimba, Mweniyumba, Katolora, Peter Mwangala, and Mwanjabala as being heavily and recurrently affected by flooding from the North Rukuru River.

4.4.8 Floodplain Mapping from Soil and Water Assessment Tool (SWAT) Model

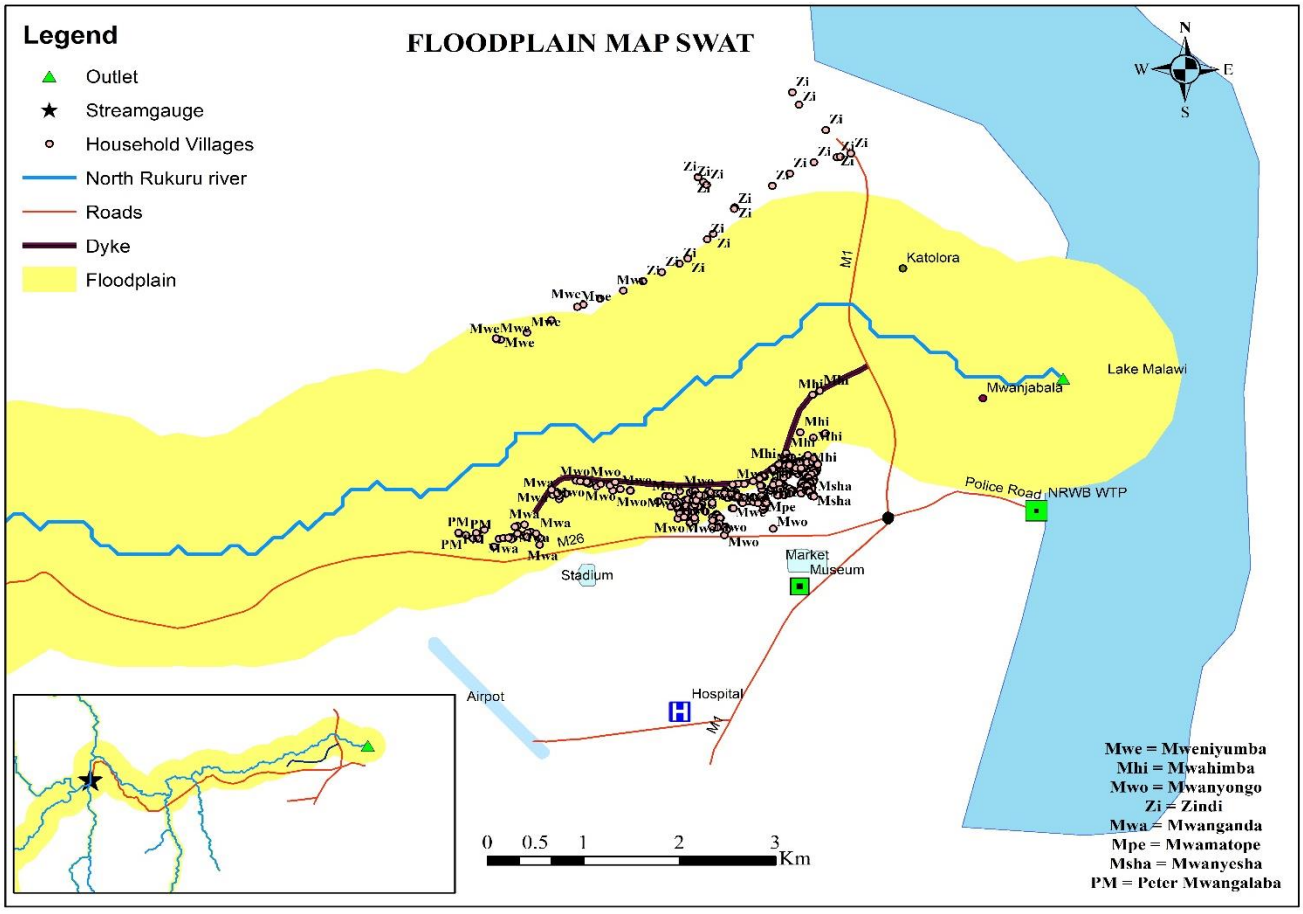

Figure 15: A map illustrating demarcations of a floodplain

The SWAT model analyzes watersheds at the Hydrologic Response Unit (HRU) level, which represents unique combinations of land use, soil type, and slope within a subbasin. This allows for detailed assessments of land management impacts on hydrology, in this case flood inundation and extents. On the other hand, HEC-RAS model operates at the subbasin level, focusing on hydraulic modeling of river systems. It uses geometric data to simulate water flow and floodplain interactions. A combination of these two models to determine the extent of flooding incorporates the effects of elevation, slope, land use, soil type, and geometric data.

The SWAT model was employed to delineate the probable floodplain of the North Rukuru River, aiming to assess whether villages currently experiencing floods are situated within the designated floodplain. The analysis revealed that settlements such as Mweniyumba, Mwahimba, Mwanyongo, Mwanganda, Mwamatope, Mwanyesha, Mwanjabala, Katolora, Peter Mwangalaba, and parts of Zindi and Mweniyumba Chisewe are located within the floodplain. This observation suggests that these areas are susceptible to floods, as illustrated by flood maps of varying return periods. The findings align with prior studies by Manda (2014), who identified construction in low-lying areas as a contributing factor to flood risk, and Gondwe *et al.* (2016), who reported that 60% of informal settlements in Karonga were established on floodplains, exacerbating flood related damages.

Furthermore, floodplain mapping indicates that the township area, including the market, as well as parts of Zindi and Mweniyumba Chisewe, are located outside the floodplain. This observation may explain why these areas were not directly impacted by flooding, as depicted in flood inundation maps across different return periods. As earlier alluded to, Karonga Town was experiencing frequent floods due to the blockage of drainage structures, and the sedimentation of the two artificial channels designed to carry runoff from the town to the lake, and not necessarily from the North Rukuru River, while Zindi was as a result of the North Rukuru River distributary called Malungo River. Manda (2014) similarly observed that artificial channels were heavily silted and encroached upon by informal settlements and agricultural activities, and the drainage structures in the township area were clogged, potentially contributing to frequent flooding in the township area.

Figure 16: Informal settlements and brick molding inside the artificial channel/canal in Karonga Township Area

4.5 Effectiveness of the dyke as a flood control structure

Mweniyumba, Mwahimba, Mwanyongo, Mwanganda, Mwamatope, Mwanyesha, and Peter Mwangalaba villages were found to be situated in the direction of the dyke or close to the dyke, indicating that they received a degree of protection from its presence. Flood depths derived from inundation maps across various magnitudes were compared with the dyke height to assess its effectiveness. To complement this analysis, a household survey targeting 394 households in the aforementioned villages was conducted to capture community perceptions regarding the dyke's role in reducing flood depth, duration, and frequency. The results are presented as follows:

4.5.1 Flood inundation map depths against the height of the dyke

Based on dyke specifications, a crest width of 4 m, a base width of 11.5 m, and slope gradients of 1:2 along the sea shoreline and 1:3 on the embankment's opposite side, the dyke height was determined to be 1.5 m. However, this height proved insufficient, as evidenced by dyke breaches observed in flood inundation maps of all return periods. The worst-case scenario, represented by the 100-year flood event, showed flood depth variations ranging from 0.001 m to 4.58 m within the location of the dyke. Flood inundation maps corresponding to other return periods displayed flood depth ranges from 0.001 m to 4 m. These findings indicate that the existing dyke height was inadequate in mitigating flood impacts and preventing inundation. A dyke height of at least 3 m to 4 m would have provided improved flood protection for local communities, limiting flood extent in vulnerable areas.

4.5.2 Flood frequency before and after construction of the dyke

Table 7 illustrates the role of the dyke in mitigating flood frequency, while also highlighting its limitations, as it was breached by floods of all magnitudes, including the 2-year event, according to flood inundation maps.

Table 7: Flood frequency before and after construction of the dyke

Flood Frequency	Prior Construction	Percentage	Post Construction	Percentage
Every year	373	94.67%	68	17.26%
Every 2 years	13	3.30%	49	12.44%
Every 3 years	1	0.25%	12	3.05%
Every 4 years	1	0.25%	0	0.00%
Every 10 years	0	0.00%	1	0.25%
Once	2	0.51%	20	5.08%
No Floods	1	0.25%	243	61.68%
I don't know	3	0.76%	1	0.25%

The findings indicate that prior to the construction of the dyke, the majority of respondents (373 out of 394), representing 94.67%, experienced annual flooding. However, post construction, a significant reduction in flood frequency was observed, with 243 out of 394 respondents (61.68%) reporting no occurrences of flooding. Despite this overall improvement, a notable proportion of respondents continued to experience flood events, with 68 out of 394 (17.26%) indicating annual floods and 49 out of 394 (12.44%) reporting flood occurrences every two years following the dyke's implementation. These results suggest that while the dyke provided substantial protection for majority of households across Mweniyumba, Mwahimba, Mwanyongo, Mwanganda, Mwamatope, Mwanyesha, and Peter Mwangalaba villages, a considerable number of residences remained vulnerable to frequent flood events.

4.5.3 Flood depth before and after construction of the dyke

Table 8 illustrates the role of the dyke in reducing flood depths, while also highlighting its limitations, as it was breached by floods of all magnitudes, including the 2 year event, according to flood inundation maps.

Table 8: Flood depth before and after construction of the dyke

Depth (m)	Prior Construction	Percentage	Post Construction	Percentage
0 m	4	1.02%	216	54.82%
0.3 m	28	7.11%	116	29.44%
0.6 m	157	39.85%	41	10.41%
0.9 m	170	43.15%	17	4.31%
1.6 m	24	6.09%	3	0.76%
1.7 m	9	2.28%	1	0.25%
1.7> m	2	0.51%	0	0.00%

The analysis reveals that prior to the construction of the dyke, a considerable proportion of respondents experienced significant flood depths. Specifically, 157 out of 394 respondents (39.85%) reported flood depths of 0.6 m, while 170 out of 394 respondents (43.15%) indicated flood depths reaching 0.9 m during flooding events. Following the dyke's construction, a notable improvement was observed, with the majority of respondents (216 out of 394, representing 54.82%) reporting no occurrences of flooding. However, a substantial number of households continued to experience flood events, even though at reduced depths. Specifically, 116 out of 394 respondents (29.44%) encountered flood levels of 0.3 m, while 41 out of 394 respondents (10.41%) reported flood depths of 0.6 m during flooding events. These findings suggest that while the dyke effectively mitigated flooding for a majority of households, flooding persisted in certain areas, highlighting potential limitations in its protective capacity.

To quantitively assess the effectiveness of the dyke in mitigating floods, flood depths data collected from 394 respondents was standardized for numerical analysis. In cases where the flood depths category was 1.7> m high, a value of 1.8 m was assigned to ensure uniformity in classification. A normality test was conducted to determine the appropriate statistical method

for analyzing flood depth reductions between Paired T-Test and Wilcoxon Signed-Rank Test. The analysis of flood depths before and after dyke construction revealed that both datasets were not normally distributed. Prior to construction, flood depths showed positive skewness of 1.087798 and after construction, skewness increased to 1.892942, where 0 indicates normal distribution. Kurtosis values further supported this where before construction Kurtosis was 1.852125 and after construction, kurtosis increased to 4.998561 with 3 indicating normal distribution. Given these findings, the Wilcoxon Signed-Rank Test was employed to assess the significance of flood depth reduction by the dyke, as it is appropriate for the data which is not normally distributed.

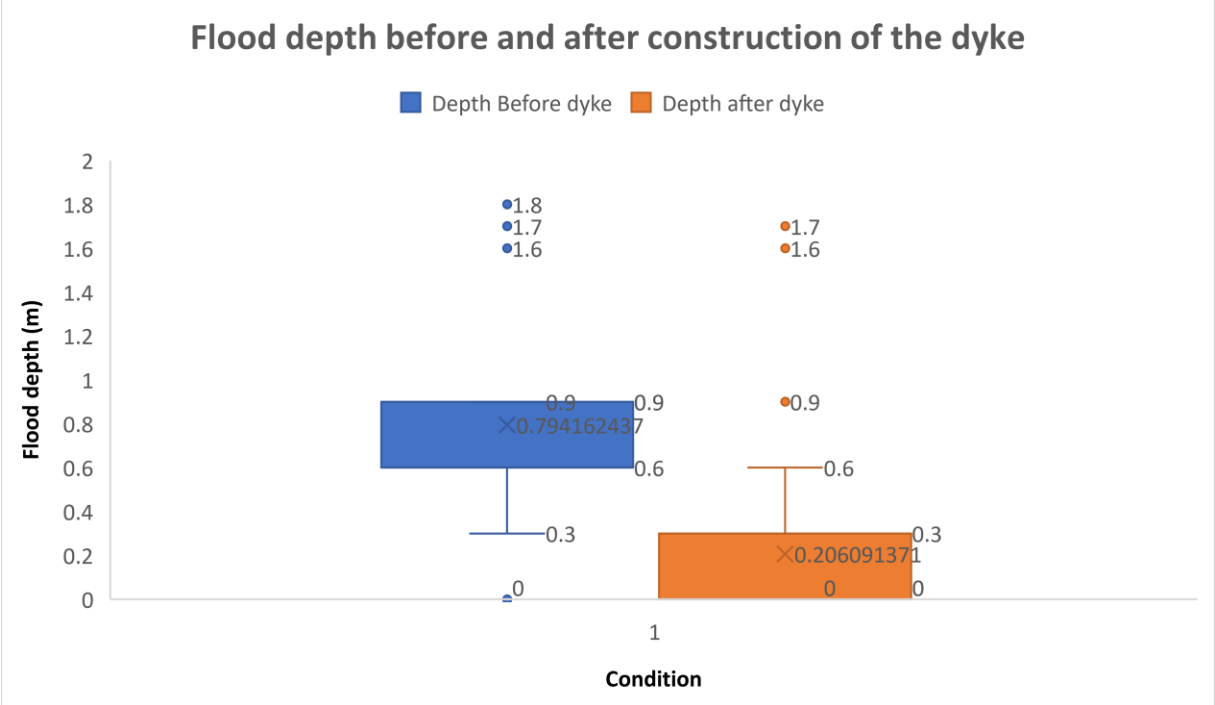

Figure 17: Boxplot depicting reduction in flood depth

The Wilcoxon Signed-Rank Test analysis yielded a test statistic value of 1627, which was less than the critical value of 34,476, leading to the rejection of the null hypothesis, which stated

that no significant difference existed in flood depths before and after construction of the dyke. This result indicates that the dyke construction led to a statistically significant reduction in flood depths.

The findings were further illustrated in a box plot, the mean flood depth before dyke construction was 0.7942 m, whereas the mean flood depth after construction was 0.2061 m, representing an approximately 74.04% reduction in flood depth, confirming a substantial decrease. Additionally, the analysis revealed that 50% of flood depth data (lower and upper quartiles) lay between 0.6 m and 0.9 m prior to dyke construction, while after construction, at least 50% of values were contained within 0 m and 0.3 m showing a significant reduction in flood depths.

4.5.4 Flood duration before and after construction of the dyke

Figure 16 illustrates the role of the dyke in reducing flood duration, while also highlighting its limitations, as it was breached by floods of all magnitudes, including the 2 year event, according to flood inundation maps.

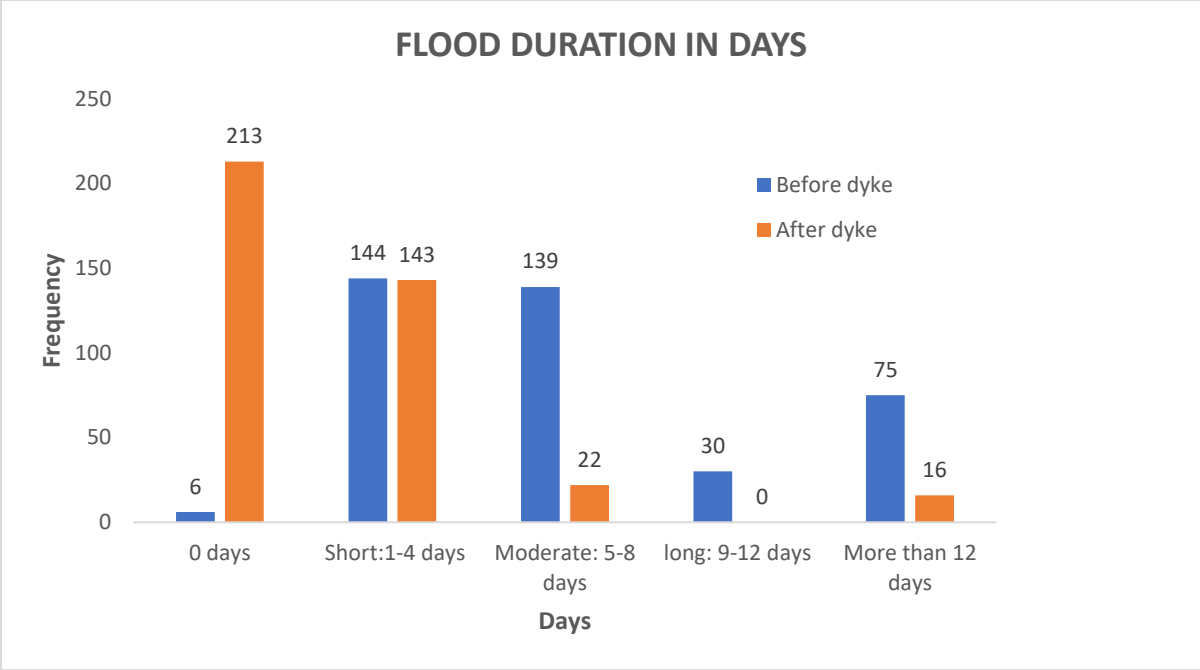

Figure 18: Flood duration before and after construction of the dyke

Prior to the construction of the dyke, flood duration varied among respondents, with 36.55% experiencing short-term inundation (1–4 days), 35.28% reporting moderate-duration flooding (5–8 days), and 19.04% affected by prolonged flooding exceeding 12 days. Following the dyke's construction, the majority of respondents (54.06%) indicated that their households had not experienced any inundation (0 days). However, a significant proportion (36.29%) reported continued exposure to short-duration flooding (1–4 days), highlighting that despite the dyke's presence, certain areas remained susceptible to flood events.

4.5.5 Overall perception on effectiveness of the dyke

Overall, the dyke provided partial protection but exhibited notable weaknesses in reducing flood frequency, duration, and depth for the surrounding villages. This was reflected in the household survey, where 381 of 394 respondents (96.7%) supported reinforcement and extension of the dyke, while only 13 respondents (3.3%) considered it adequate in its current

state. These perceptions align with the flood inundation maps, which showed the dyke being breached by floods of all magnitudes, including the 2-year event. Historical evidence further supports this, as Gondwe *et al.* (2017) reported dyke breaches during the 2010/11 floods that affected adjacent villages.

Figure 19: A dyke worn out by flood waters due to gullies created by brick molding and farming in 2023

4.6 Summary of results and discussions chapter

This chapter presented the estimation of river discharges using the Log-Pearson Type III and Gumbel distributions, with the Log-Pearson Type III selected as the preferred model based on goodness-of-fit and confidence limit tests. Flood depths at the Mwakimeme gauging station were simulated, and flood inundation maps were produced in ArcGIS identifying areas vulnerable to floods of varying magnitudes. The effectiveness of the dyke in reducing flood frequency, flood duration, and flood depth in surrounding areas was also discussed in order to complement the results produced by flood inundation maps of all flood magnitudes which showed the dyke was breached by even a 2 year flood event.

CHAPTER 5 : CONCLUSION AND RECOMMENDATIONS

5.1 Introduction

This chapter presents major findings of this research study by each research objective, recommendations and, finally, areas for further research.

5.2 Conclusion

This study determined the extent of flooding in Karonga District, with particular focus on the downstream segment of the North Rukuru River where Karonga Town Centre is located. By analyzing the spatial distribution of floods across return periods of 2, 5, 10, 25, 50, and 100 years, the research provided important insights of flood risks in the area. Furthermore, the evaluation of the dyke's performance under these varying returns periods revealed its relative effectiveness in mitigating flood depths and protecting vulnerable areas.

Complementing the technical analysis, community perceptions were gathered as well to assess the dyke's effectiveness. Respondents' experiences and insights showed both the successes and limitations of the dyke. The integration of modeling with community perspectives contributed to a holistic understanding of extent of flooding and the state of flood resilience in Karonga District. The findings offer a valuable foundation for informed decision-making concerning future dyke enhancements, the identification of other critical areas requiring flood protection infrastructures such as dykes, and the development of other mitigation strategies such as the resumption of the two artificial channels, and the improvement of the drainage channels around Karonga Town Centre.

5.2.1 Estimating the discharges for different return periods

The Log Pearson Type III distribution estimated peak discharges corresponding to return periods of 2, 5, 10, 25, 50, and 100 years were 1028, 1306, 1474, 1675, 1815, and 1950 m^3/s, respectively.

The Log Pearson Type III distribution was preferred over the Gumbel Extreme Value distribution due to its superior statistical performance. It achieved a higher coefficient of determination ($R^2 = 0.9886$) compared to Gumbel Extreme value distribution ($R^2=0.9784$) and passed both goodness-of-fit tests: Chi-square (statistic = 47.224 < critical = 59.304) and Kolmogorov-Smirnov (statistic = 0.02378 < critical = 0.2047). In contrast, Gumbel was rejected with Chi-square (statistic=60.943 > critical = 59.304) and Kolmogorov-Smirnov (statistic=0.2060 > critical= 0.2047). Additionally, Log Pearson Type III exhibited narrower confidence bounds, especially for longer return periods, demonstrating greater reliability in flood discharge prediction.

5.2.2 Simulating flood water depths

The hydraulic modelling for North Rukuru River was conducted using the HEC-RAS model. Maximum channel flood depths at Mwakimeme gauging station (River Station 28376) were 5.15 m (2-year flood), 6.00 m (5-year flood), 6.47 m (10-year flood), 6.99 m (25-year flood), 7.33 m (50-year flood), and 7.65 m (100-year flood), increasing with the return period. A total of 207 cross-sections (river stations) were used to assess flood depth behavior.

Floodplain depths showed strong spatial variability, higher near the river, decreasing with an increase in distance. For the 100-year flood, depths ranged from 0.0011 m to 21.63 m; for the

2-year flood, 0.0010 m to 19.14 m; 5-year flood, 0.0011 m to 19.98 m; 10-year flood, 0.0010 m to 20.45 m; 25-year flood, 0.0011 m to 20.97 m; and 50-year flood, 0.0010 m to 21.31 m. While the main channel carried most of the flood volume, overbank areas experienced increasing inundation with higher return periods.

5.2.3 Developing flood inundation maps for downstream North Rukuru river

Flood Inundation maps for 2 to 100-year return periods showed increasing flood extents, with Mweniyumba, Mwahimba, Mwanyongo, Mwanyesha, Peter Mwangalaba, Katolora, and Mwanganda villages exposed to floods. The validation of model outputs with GPS-based field data confirmed the spatial accuracy of the flood inundation maps. The SWAT model's North Rukuru River floodplain map further consolidated this, as it showed these areas to be situated in a floodplain, underlying their exposure to floods even the smallest floods like the 2-year event.

Zindi village and Karonga Town Centre frequently experiences floods, however their flooding was not directly linked to the North Rukuru River. All flood inundation maps from HEC-RAS model and North Rukuru River floodplain map from SWAT model placed them outside. Community consultations (FDG's with VCPC's and KII with Water and Disaster Officers) revealed Zindi's flooding was caused by the Malungo River, a distributary of North Rukuru River, while Karonga Town Centre's flooding stemmed from clogged drainage systems exacerbated by sedimentation, encroachment, and informal development within artificial channels designed to carry flooding water from the Karonga Town Centre drainage system to the lake. Some Village Civil Protection Committees (VCPC's) attributed flooding to Karonga Town Centre due to the dyke not extending to Peter Mwangalaba and Mwanganda villages,

allowing floodwaters from North Rukuru River to reach the Town Centre though this claim was disputed by technical officers (Water and Disaster Officers).

5.2.4 Evaluating effectiveness of the dyke as a flood control structure

The dyke offered meaningful but incomplete protection in reducing flood impacts along the North Rukuru River. The analysis of flood inundation maps, household survey data, and statistical tests demonstrates that while the dyke contributed to significant reductions in flood depth, frequency, and duration, its design height of 1.5 m was inadequate to withstand flood events across all return periods. The dyke was breached even during relatively minor floods, such as the 2-year event, evidenced in the 2 year flood inundation map, and the 100-year flood scenario revealed depths far exceeding its protective capacity. Although the dyke reduced mean flood depths by approximately 74%, confirmed statistically by the Wilcoxon Signed-Rank Test, and provided substantial protection for many households, persistent flooding in certain areas highlighted its structural limitations. These findings underscore the need for a higher dyke height, ideally between 3 m and 4 m, to effectively mitigate flood risks and safeguard vulnerable communities.

The dyke extended from Mwanganda to Mwahimba villages, excluding vulnerable areas such as Peter Mwangalaba, part of Mwanganda and Mwanjabala, exacerbating flood exposure to these areas. The other side of the river, where Katolora village is located did not have a flood protection structure like a dyke, even though the flood inundation maps indicated these areas prone to floods. In terms of flood frequency, the number of households experiencing annual floods dropped significantly from 94.67% (373 out of 394) before the dyke's construction to just 17.26% (68 out of 394) afterward, with 61.68% of respondents reporting no flood

occurrence. In terms of flood duration, the majority previously endured floodwaters lasting 5–8 days or longer. Following the dyke's construction, over half of the households (54.06%) reported no inundation, while those affected mostly experienced only short-term flooding (1–4 days). It was revealed that activities like brick molding and informal farming near the dyke, contributed to structural weaknesses and erosion of the dyke. Therefore, strengthening and upgrading the dyke is essential to enhance resilience, reduce vulnerability, and ensure sustainable flood protection for the affected villages.

5.3 Recommendations

From the study results the following recommendations were proposed:

The study recommends the use of Log Pearson type III distribution in conducting flood frequency analysis in North Rukuru River for related projects as it has shown to produce reliable and precise river discharge estimates for different return period under the coefficient of determination test, Kolmogorov-Smirnov test, Chi-square test, Anderson-Darling test and Confidence limit test.

The study recommends the water levels monitoring team especially the water office to be alert when the water levels at Mwakimeme gauging station reaches 5.15 m, 6.00 m, 6.47 m, 6.99 m, 7.33 m, and 7.65 m as these depths reflect 2; 5, 10, 25, 50 and 100 year floods, respectively, making villages like Peter Mwangalaba, Mwanjabala, Mweniyumba, Mwahimba, Mwanyongo, Mwanyesha, and Mwanganda, susceptible to floods, hence they have to be warned in advance once those respective water levels are reached.

The study recommends that areas in villages like Peter Mwangalaba, Mwanjabala, Mweniyumba, Mwahimba, Mwanyongo, Mwanyesha, and Mwanganda which were shown to be susceptible to floods of all magnitudes on flood inundation maps, and are situated in very low lying areas and floodplains, construction in these areas should be prohibited, where development is unavoidable infrastructures built in these areas should be of high standards capable of withstanding extreme floods such as a 100 year flood, in the worst-case scenario, resettlement to higher ground or designated safe zones should be considered, guided by flood inundation maps of severe events, such as a 100 year flood.

The dyke which experienced flood breaches with a height of 1.5 m according to flood inundation maps and community experience, needs to be reinforced and the height raised to at least 3 m to contain floods of high magnitudes.

The dyke needs to be extended to Peter Mwangalaba, parts of Mwanganda and Mwanjabala villages, who are also susceptible to floods according to flood inundation maps as well as community experience, yet the dyke only covered villages located on the same path as the Town Centre.

Dyke construction should be done on the other side of the river where villages like Zindi, Katolora and Mweniyumba Chisewe are situated to contain flooding there. A thorough research should be conducted on Marungo river when planning to construct a dyke on the other side, a distributary from North Rukuru river which directly causes flooding in Zindi village.

There should be strong governance and enforcement of laws and bylaws, deterring communities from building, brick molding and farming close to the dyke, which has worsened the state of the dyke.

Clogged drainage system around the Town Centre and the two silted artificial channels met to carry floodwater from the Town Centre to the lake needs to be rehabilitated and dredged. Community engagement and risk assessment of the people who have constructed close to the two artificial channels should be done, if possible, resettlement could be done.

5.4 Limitations

The only limitation in this study is the scarcity of data from public offices such as streamflow data, river cross-sections data, most of the data used in the models is open-source data which is widely used in this field.

However, the results remained highly accurate due to the use of reliable inputs, even though open-source data was used. The GEOGloWS Hydroviewer streamflow data, widely used in Malawi's Community-Based Flood Early Warning System (CBFEWS) and Modernized Climate Information and Early Warning Systems (M-CLIMES) projects by Department of Disaster Management Affairs (DoDMA), reliably reflects observed flows in the North Rukuru River. For instance, is has been used in a CBFEWS project by the Karonga Council, warning people in time before floods strike. In the absence of field-surveyed cross-sections, the ALOS DEM was used to define river and floodplain geometry, producing results comparable to ground-based DEMs. Azizian and Brocca (2020) found that the ALOS 30 m DEM produced results closely matching ground-based DEMs when compared with SRTM-90 m, SRTM-30 m, and ASTER-30 m DEMs, indicating its strong reliability in representing on-ground conditions.

Additionally, 207 strategically spaced cross-sections were incorporated to capture realistic river profiles, ensuring the model closely represented on-ground conditions.

5.5 Future research

A study could be done on the willingness of people from Peter Mwangalaba, Mwanjabala, Mweniyumba, Mwahimba, Mwanyongo, Mwanyesha, and Mwanganda villages to relocate to safer areas.

A thorough study focusing only on effectiveness of other flood control structures such as the two artificial channels should be done to evaluate further their condition over the years, in terms of the depth which has been silted, multiple activities hindering their actual function over the years. This could be combined with a study looking at the condition of the drainage system around the Karonga Town Centre in terms of sedimentation which has clogged it.

REFERENCES

Adugna, BA 2020, 'flood inundation mapping and hazard assessment: a case of Wera River flood plain of Boyo catchment, Ethiopia', *Journal of Hydrology*, vol.20, no.2, pp. 32-43.

Act Alliance 2025, 'Karonga floods response, Malawi', *Global Humanitarian Operations,* Geneva, Switzerland.

Ahad, U, Ali, U, Inayatullah, M & Rauf Shah, A 2022, 'Flood frequency analysis: a case study of Pohru River catchment, Kashmir Himalayas, India', *Journal of the Geological Society of India*, vol.98, no.12, pp.1754-1760.

Akhtar, H 2015, 'Pakistan needs a fresh disaster mitigation strategy', *Environmental monitoring and assessment*, vol.192, no.1, p.48.

Alaghmand, S, bin Abdullah, R, Abustan, I & Vosoogh, B 2010, 'GIS-based river flood hazard mapping in urban area: a case study in Kayu Ara River Basin, Malaysia', *International Journal of Engineering and Technology*, vol.*2*, no.6, pp.488-500.

Anwat, VK, Hire, PS, Pawar, UV & Gunjal, RP 2021, 'Analysis of magnitude and frequency of floods in the Damanganga basin: western India', *Hydrospatial Analysis*, vol.5, no.1, pp.1-11.

Asad, A, Ahmeduzzaman, M, Kar, S, Khan, A, Rahman, N & Islam, S 2013, 'Flood frequency modeling using Gumbel's and Powell's method for Dudhkumar River', *Journal of water resources and ocean science,* vol.*2*, no.2, pp.25-28.

Athulya, PS & James, KC 2017, 'Best fit probability distributions for monthly radiosonde weather data', *International Journal of Advanced in Management, Technology and Engineering Sciences*, vol.7, no.12, pp.24-31.

Aynalem, SB 2020, 'Floodplain mapping and hazard assessment of Muga River by using ArcGIS and HEC-RAS model Upper Blue Nile, Ethiopia', *Landscape Architecture and Regional Planning*, vol.*5*, no.4, pp.74-85.

Azizian, A & Brocca, L 2020, 'Determining the best remotely sensed DEM for flood inundation mapping in data sparse regions', *International Journal of Remote Sensing*, vol.41, no.5, pp.1884-1906.

Bea, K, Halchin, E, Hogue, H, Kaiser, F, Love, N, McCarthy, FX, Reese, S & Schwemle, B 2006, 'Federal emergency management policy changes after Hurricane Katrina: a summary of statutory provisions', *Defense Technical Information Center*.

Bedassa, D 2016, 'Evaluation of extreme flow quantiles estimated from global reanalysis runoff data: a case study of Blue Nile River Basin', *Environmental Science, Geography*.

Benameur, S, Benkhaled, A, Meraghni, D, Chebana, F & Necir, A 2017, 'Complete flood frequency analysis in Abiod watershed, Biskra, Algeria', *Natural hazards*, vol.86, no.2, pp.519-534.

Bhat, MS, Alam, A, Ahmad, B, Kotlia, BS, Farooq, H, Taloor, AK & Ahmad, S 2019, 'Flood frequency analysis of river Jhelum in Kashmir basin', *Quaternary International*, vol.507, pp.288-294.

Bloch, R 2013, 'Integrating flood risk management and land use planning', *Journal of hydrology,* vol.6, no.1, pp.1-17.

Brasa, BN 2023, 'Emerging issues in disaster risk reduction and building resilience in Africa: a case study of the 2023 floods', ***in 13th ICFM conference on African Floods of 2023, ICLR,* ICFM, Western University, Canada**.

Brunner, G & Bonner, V 2010, 'Hydrologic-river analysis system', *USACE,* p.411.

Butler, D & Davies JW 2004, Urban Drainage, 3rd edn, Taylor and Francis Group, London.

Chen, L, Guo, S, Yan, B, Liu, P & Fang, B 2010, 'A new seasonal design flood method based on bivariate joint distribution of flood magnitude and date of occurrence', *Hydrological Sciences Journal*, vol.55, no.8, pp.1264-1280.

Chen, L, Singh, VP and Xiong, F 2017, 'An entropy-based generalized gamma distribution for flood frequency analysis', *Entropy*, vol.19, no.6, p.239.

Chen, L, Singh, VP, Shenglian, G, Hao, Z & Li, T 2012, 'Flood coincidence risk analysis using multivariate copula functions', *Journal of Hydrologic Engineering*, vol.17, no.6, pp.742-755.

Chiu, YY, Raina, N & Chen, HE 2021, 'Evolution of flood defense strategies: toward nature-based solutions', *Environments*, vol.*9, no.*1, p.2.

Coles, D, Yu, D, Wilby, RL, Green, D $ Herring, Z 2017, 'Beyond flood hotspots: modelling emergency service accessibility during flooding in York, UK', *Journal of hydrology*, vol.546, pp.419-436.

Cowan, W.L., 2018, ‘Estimating hydraulic roughness coefficients’, *Agricultural engineering*, vol.37, no.7, pp.473-475.

Cred, UNDRR 2020, *Human cost of disasters. an overview of the last 20 years: 2000–2019*, Geneva.

Creswell, JW, 2013, ‘Steps in conducting a scholarly mixed methods study’, *DBER Series*, London.

Dal, S 2024, ‘Africa climate summit 2023: climate change and the social dimension’, *Africania*, vol.4, no.1, pp.41-61.

Desalegn, H & Mulu, A 2021, ‘Mapping flood inundation areas using GIS and HEC-RAS model at Fetam River, Upper Abbay Basin, Ethiopia’, *Scientific African*, vol.12, p.e00834.

Di Baldassarre, G, Schumann, G, Bates, PD, Freer, JE & Beven, KJ 2010, ‘Flood-plain mapping: a critical discussion of deterministic and probabilistic approaches’, *Hydrological Sciences Journal*, *vol.*55, no.3, pp.364-376.

Diaconu, DC, Costache, R, Islam, ARMT, Pandey, M, Pal, SC, Mishra, AP & Pande, CB 2024, ‘Developing flood mapping procedure through optimized machine learning techniques. case study: Prahova River basin, Romania’, *Journal of Hydrology: Regional Studies*, vol.54, p.101892.

Diop, SB, TramblaY, Y, Bodian, A, Ekolu, J, Rouché, N & Dieppois, B 2025, ‘Flood frequency analysis in West Africa’, *Journal of Flood Risk Management*, vol.18, no.1, p.e70001.

DoDMA 2019, *Malawi 2019 Floods Post Disaster Needs Assessment*, Malawi Government, Lilongwe.

Doocy, S, Daniels, A, Murray, S & Kirsch, TD 2013, 'The human impact of floods: a historical review of events 1980-2009 and systematic literature review', *PLoS currents*, vol.5.

Dottori, F, Di Baldassarre, G & Todini, E 2013, 'Detailed data is welcome, but with a pinch of salt: accuracy, precision, and uncertainty in flood inundation modeling', *Water Resources Research*, vol.49, no.9, pp.6079-6085.

Erena, SH, Worku, H & De Paola, F 2018, 'Flood hazard mapping using FLO-2D and local management strategies of Dire Dawa City, Ethiopia', *Journal of Hydrology: Regional Studies*, vol.19, pp.224-239.

European Commission 2007, 'Directive 2007/60/EC of the European Parliament and of the Council of 23 October 2007 on the assessment and management of flood risks', *Official J. Eur. Union L*, vol.288, pp.27–34.

Falade, O 2024, 'Flood vulnerability assessment using HEC-RAS and GIS in Ogbese catchment, Nigeria', *Journal of Environmental Pollution and Control*, vol.8.

Farid, M, Marlina, A & Kusuma, MSB 2017, 'Flood hazard mapping of Palembang City by using 2D model', *AIP publishing*, vol.1903, no.1, p.100009.

Ganamala, K & Kumar, PS 2017, 'A case study on flood frequency analysis', *International Journal of Civil Engineering and Technology*, vol.8, no.4, pp.1762-1767.

Garcin, M, Mdala, H & Kalebe, Y 2025, ‘Flood hazard in Malawi’, *Journal of African Earth Sciences*, vol.*223*, p.105490.

Getahun, YS & Gebre, SL 2015, ‘Flood hazard assessment and mapping of flood inundation area of the Awash River Basin in Ethiopia using GIS and HEC-GeoRAS/HEC-RAS model’’, *Journal of Civil & Environmental Engineering*, vol.5, no.4, p.1.

Ghosh, SN 2014, Flood control and drainage engineering, 4th edn, Taylor & Francis Group, London.

Gogoi, P & Patnaik, SK 2023, ‘Flood frequency analysis of Jiadhal river basin, india using log pearson type III distribution method’, *The Asian Review of Civil Engineering*, vol.*12*, no.1, pp.6-9.

Gondwe, J, Manda, M & Kamlomo, D 2017, ‘Discriminatory land use planning and flood risk management in Karonga Town, Malawi’, *Journal of Human Sciences*, vol.14, no.4, p.3343.

Government of Malawi 2023, *Malawi 2023 Tropical Cyclone Freddy Post-Disaster Needs Assessment*, Lilongwe.

Handique, A, Acharjee, S, Dhadumia, U, Gogoi, J, Das, P & Nath, B 2024, ‘Flood frequency analysis in the lower Burhi Dehing River in Assam, India using Gumbel Extreme Value and Log Pearson Type III methods’, *Discover Geoscience*, vol.2, no.1, p.75.

Hirtan, RI 2015, 'Floodplain delineation for Calnau River using HEC-RAS software', *Scientific Papers. Series E. Land Reclamation, Earth Observation & Surveying, Environmental Engineering*, vol.9, pp.84-87.

ICPDR 2021, *The 2021 updates to Danube River basin & flood Risk management plans*, Germany, Danube.

International Federation of Red Cross & Red Crescent Societies 2018, *Emergency plan of action final report Malawi: Karonga floods*, Lilongwe.

Iosub, M, Minea, I, Hapciuc, O & Romanescu, GH 2015, 'The use of Hec-Ras modelling in flood risk analysis', *Air & Water Components of the Environment*, no.20.

Islam, A & Sarkar, B 2020, 'Analyzing flood history and simulating the nature of future floods using Gumbel method and Log-Pearson Type III: the case of the Mayurakshi River Basin, India', *Bulletin of Geography. Physical Geography Series*, no.19, pp.43-69.

Izinyon, OC & Igbinoba, GE 2010, 'Comparison of Log-Pearson Type III and Gumbel probability distributions for flood frequency analysis of Ikpoba River catchment at Benin City', *Journal of the Nigerian Association of Mathematical Physics*, vol.17, pp.261-272.

Kativhu, T 2016, 'An analysis of sustainability of communally-managed rural water supply systems in Zimbabwe', Earth Science thesis, University of the Western Cape, Western Cape, https://hdl.handle.net/10566/17675

Khan, S, Al-Hussein, AA, Ncibi, K, Hamdi, N & Hamed, Y 2022, 'Flood analysis using HEC-RAS and HEC-HMS: a case study of Khazir River', *Water*, vol.14, no.22, p.3779.

Khattak, M.S, Anwar, F, Saeed, TU, Sharif, M, Sheraz, K & Ahmed, A 2016, 'Floodplain mapping using HEC-RAS and ArcGIS: a case study of Kabul River', *Arabian Journal for Science and Engineering*, vol.41, no.4, pp.1375-1390.

Khwairakpam, RS & Kundu, S 2024, 'Significance of different probability distributions in flood frequency analysis of Brahmani-Baitarani River Basin, India', *Discover Geoscience*, vol.2, no.1, p.71.

Kiba, LG, Nengzouzam, G & Ranjan, P 2023, 'Flood hazard mapping using hydraulic models and GIS: *Springer Nature*, pp.65-72.

Kingdon, MJ, Bootsma, HA, Mwita, J, Mwichande, B & Hecky, RE 1999, *Malawi River discharge and water quality*, Malawi Government, Salima.

Kumar, MK., Dharanirajan, K & Sabyasachy, S 2021, 'Application of Gumbel's distribution method for flood frequency analysis of Lower Ganga Basin, Farakka Barrage Station, West Bengal, India', *Disaster Advances,* vol.14, no.8, pp.51–58.

Kumar, S & Singh, KK 2021, 'Rain-garden infiltration rate modeling using gradient boosting machine and deep learning techniques', *Water Science and Technology*, vol.84, no.9, pp.2366-2379.

Kumar, V, Sharma, KV, Caloiero, T, Mehta, DJ & Singh, K 2022, 'Comprehensive overview of flood modeling approaches: a review of recent advances', *Hydrology*, vol.10, no.7, p.141.

Kvočka, D, Falconer, RA & Bray, M 2015, 'Appropriate model use for predicting elevations and inundation extent for extreme flood events', *Natural Hazards*, vol.79, no.3, pp.1791-1808.

Lamichhane, N & Sharma, S 2017, 'Development of flood warning system and flood inundation mapping using field survey and LiDAR data for the Grand River near the city of Painesville, Ohio', *Hydrology*, vol.4, no.2, p.24.

Larson, R 2011, *Response to Flooding in Malawi*, Malawi Government, Lilongwe.

Lumbroso, D, Rance, J, Pearce, G & Wade, S 2014, 'Emergencies-and-resilience', *Science for Humanitarian Emergencies and Resilience (SHEAR).*

Lumbroso, D, Brown, E & Ranger, N 2016, 'Stakeholder perceptions of the overall effectiveness of early warning systems and risk assessments for weather-related hazards in Africa, the Caribbean and South Asia', *Natural Hazards*, vol.84, no.3, pp.2121-2144.

Madhusudhan, MS, Surendra, HJ, Harshitha, J, Lekhana, PS & Kusumanjali, TS 2022, 'Estimation of flood discharges for various return periods at Kabini Dam using statistical approach', *Hydraulic and Civil Engineering Technology*, vol.31, pp.940-947

Malawi Meteorological Services 2020, *Climate of Malawi*, Government of Malawi, Lilongwe.

Malawi Red Cross 2017, *Emergency plan of action: Karonga flooding situation analysis report*, Malawi, Lilongwe.

Malawi Government 2019, *Floods Post Disaster Needs Assessment Report,* Government of Malawi, Lilongwe.

Malik, A & Abdalla, R 2016, 'Geospatial modeling of the impact of sea level rise on coastal communities: application of Richmond, British Columbia, Canada', *Modeling Earth Systems and Environment*, vol.2, no.3, p.146.

Manda, M & Wanda, E 2017, 'Understanding the nature and scale of risks in Karonga, Malawi', *Environment and Urbanization*, vol.29, no.1, pp.15-32.

Manda, M, Kamlomo, D, Mphande, C, Wanda, E, Msiska, O, Kaunda, J & Kushe, J 2016, 'Karonga town: growth and risk profile', *Urban Africa RIsk Knowledge*, no.9.

Manda, MZ 2014, 'Where there is no local government: addressing disaster risk reduction in a small town in Malawi', *Environment and Urbanization*, vol.26, no.2, pp.586-599.

Maranzoni, A, D'Oria, M & Rizzo, C 2023, 'Quantitative flood hazard assessment methods: a review', *Journal of Flood Risk Management*, vol.16, no.1, pp.1-31.

Martin, O, Rugumayo, A & Ovcharovichova, J 2012, 'Application of HEC HMS/RAS and GIS tools in flood modeling: a case study for river Sironko–Uganda', *Global Journal of Engineering, Design & Technology*, vol.1, no.2, pp.19-31.

Mawasha, TS 2021, ‘Combined 1D modelling with HEC-RAS for delineation floodplain area: a case study of Hennops River in the Centurion Area’, *American Journal of Mathematical and Computer Modelling*, vol.6, no.4, pp.55-62.

Merwade, V, Olivera, F, Arabi, M & Edleman, S 2008, ‘Uncertainty in flood inundation mapping: current issues and future directions’, *Journal of hydrologic engineering*, vol.13, no.7, pp.608-620.

Minywach, LT, Lohani, TK & Ayalew, A 2024, ‘Inundation mapping and flood frequency analysis using HEC-RAS hydraulic model and easyfit software’, *Journal of Water Management Modelling*, vol.10.

Mkhandi, SH, Kachroo, RK & Gunasekara, TAG 2009, ‘Flood frequency analysis of southern Africa: II. identification of regional distributions’, *Hydrological Sciences Journal*, vol.45, no.3, pp.449-464.

Moel, HD, van Alphen, EJ & Aerts, JC 2009, ‘Flood maps in Europe–methods, availability and use’, *Natural hazards and earth system sciences*, vol.9, no.2, pp.289-301.

Mokkenstorm, LC, van den Homberg, MJ, Winsemius, H & Persson, A 2021, ‘River flood detection using passive microwave remote sensing in a data-scarce environment: a case study for two river Basins in Malawi’, *Frontiers in earth science*, vol.9, p.670997.

Mujere, N 2011, ‘Flood frequency analysis using the Gumbel distribution’, *International Journal on Computer Science and Engineering*, vol.3, no.7, pp.2774-2778.

Murtaza, N, Pasha, GA, Khan, ZU, Khedher, KM & Salem, MA 2025, 'Assessing dyke and moat systems for hydrodynamic reduction in super-critical flow: a laboratory and ANN approach', *Innovative Infrastructure Solutions*, vol.10, no.1, p.14.

Mwalwimba, KI, Manda, M & Ngongondo, C 2024, 'Towards a framework for flood vulnerability assessment for Rural and Urban informal settlements in Malawi', *Journal of Geography & Natural Disasters*, vol.14, p.305.

National Statistical Office 2019, *Malawi population and housing census report-2018*, Government of Malawi, Lilongwe.

Natural Resources Canada 2018, *Federal flood mapping framework*, Government of Canada, Ottawa.

Nasir, NN 2025, 'Flood Frequency analysis using Gumbel and Log-Pearson Type-III distributions' *Springer Nature*, vol.207, pp.475-482.

NFIP 2021, *Flood insurance. U.S. national flood insurance program*, Federal Emergency Management Agency, Washington DC.

OCHA 2023, *Situation report flood risks in West and Central Africa*, United Nations, New York.

Pakhale, G, Khosa, R & Gosain, AK 2024, 'In today's world, is it worth performing flood frequency analysis using observed streamflow data?', *Environmental Advances*, vol.15, p.100485.

Patel, DP & Srivastava, PK 2013, 'Flood hazards mitigation analysis using remote sensing and GIS: correspondence with town planning scheme', *Water resources management*, vol.27, no.7, pp.2353-2368.

Pathan, AI & Agnihotri, PG 2019, 'A combined approach for 1-D hydrodynamic flood modeling by using Arc-Gis, Hec-Georas, Hec-Ras Interface-a case study on Purna River of Navsari City, Gujarat', *International Journal of Recent Technology and Engineering*, vol.8, no.1, pp.1410-1417.

Pathan, AI, Vadher, B & Agnihotri, PG 2017, 'River flood modeling using GIS, HEC-GeoRAS and HEC-RAS for Purna River, Navsari District, Gujarat, India', *International Journal of Scientific Development and Research*, vol.2, no.3, pp.216–222.

Pyae, A, Yabar, H & Richards, D 2023, 'Managing dam breach and flood inundation by HEC-RAS modeling and GIS mapping for disaster risk management', *Case Studies in Chemical and Environmental Engineering*, vol.8, p.100487

Rangari, VA Bhatt, CM & Umamahesh, NV 2021, 'Rapid assessment of the October 2020 Hyderabad urban flood and risk analysis using geospatial', *Current Science*, vol.120, no.12, pp.1840-1847.

Rentschler, J & Salhab, M 2020, *People in harm's way: Flood exposure and poverty, in 189 countries*, World Bank, Washington DC.

Robindro SK 2024, 'Comparative analysis of flood estimation using Log-Pearson Type III and Gumbel Max models in the Cauvery River, India', *International Journal of Innovative Science and Research Technology*, vol.9, no.4, pp.2170–2179.

Rossi, G, Harmanciogammalu, NB & Yevjevich, V 2012, 'Coping with floods', *Springer Science & Business Media*, vol. 257.

Šakić T, R., Grant, W, Adeloye, A, Duncan, M, J & Mwale, M 2017, 'Community based- flood risk management: experiences and challenges in Malawi', *International Water Resources Association*, pp.1–13.

Samantaray, S. and Sahoo, A., 2020, 'Estimation of flood frequency using statistical method: Mahanadi River basin, India', *H2open Journal*, vol.3, no.1, pp.189-207.

Santillan, JR, Marqueso, JT, Makinano, M & Serviano, JL 2016, 'Beyond flood hazard maps: detailed flood characterization with remote sensing, gis and 2D modelling', *The International Archives of the Photogrammetry, Remote Sensing and Spatial Information Sciences*, vol.42, pp.315-323.

Sayers, P, Galloway, G, Penning, E, Yuanyuan, L, Fuxin, S, Yiwei, C, Kang, W, Le Quesne, T, Wang, L & Guan, Y 2015, 'Strategic flood management: ten golden rules to guide a sound approach', *International Journal of River Basin Management*, vol.13, no.2, pp.137-151.

Sekani, LF 2024, 'Analysis of effective flood mitigation measures in the Lower Shire River Basin, Malawi', *International Journal of Innovative Science and Research Technology*, vol.21, no.8, pp.22-33

Senarathne, PC 2008, 'Learning to live with flood', *Journal of Hydrology*, vol.6, no.2, p.39.

Shatu, SR, Al Imran, A, Reza, E, Jahan, N & Shoma, SR 2023, 'Comparative assessment of Gumbeland, Log Pearson Type III methods: Teesta River flood frequency analysis', *International Journal of Innovative Science and Research Technology,* vol.8, no.10.

Singh, AK & Chavan, SR 2025, 'An approach to regional flood frequency analysis for general peak discharge distribution datasets', *Journal of Hydrology,* vol.650, p.132493.

Slobodan, K 2009, 'Vulnerability of Infrastructure to Climate Change', *Nature Climate Change,* vol.10, pp.488-490.

Solomon, O & Prince, O 2013, 'Flood frequency analysis of Osse River using Gumbel's distribution', *Civil and environmental research,* vol.3, no.10, pp.55-59.

Song, X, Lu, F, Wang, H., Xiao, W & Zhu, K 2018, 'Penalized maximum likelihood estimators for the nonstationary Pearson type 3 distribution', *Journal of Hydrology*, vol.567, pp.579-589.

Spachinger, K, Dorner, W, Metzka, R, Serrhini, K & Fuchs, S 2008, 'Flood risk and flood hazard maps–visualization of hydrological risks', *Earth and Environmental Science*, vol.4, no. 1, p.12043.

Thieken, AH & Gocht, M 2014, 'Flood risk mapping at the local scale: concepts and challenges, *Springer nature*, Netherlands, pp.231-251.

Tingsanchali, T & Karim, F 2010, 'Flood-hazard assessment and risk-based zoning of a tropical flood plain: case study of the Yom River, Thailand', *Hydrological Sciences Journal*, vol.55, no.2, pp.145-161.

Trogrlić, RŠ, Wright, G, Adeloye, A, Duncan, MJ & Mwale, F 2019, 'Community based-flood risk management: experiences and challenges in Malawi', *World Water Congress*, vol. 29.

Ullah, MI, Qureshi, KS, Rauf, AU & Shah, LA 2024, 'Advanced floodplain mapping: HEC-RAS and ArcGIS pro application on Swat River', *Journal of Umm Al-Qura University for Engineering and Architecture*, vol.15, no.3, pp.245-258.

UNDRR 2020, *The human cost of disasters: an overview of the last 20 years, 2000–2019*, United States of America, New York.

UNICEF 2017, *Malawi year-end humanitarian situation Report*, Malawi, Lilongwe.

UNISDR 2005, *Hyogo framework for action 2005-2015: building the resilience of nations and communities to disasters*, Japan, Hyogo.

UP DREAM 2016, *Disaster risk and exposure assessment for mitigation*, Philippines, University of the Philippines.

USGS 2018, *3D nation elevation requirements and benefits Study*, United States of America, Virginia.

Van Alphen, J, Martini, F, Loat, R, Slomp, R& Passchier, R 2009, 'Flood risk mapping in Europe, experiences and best practices', *Journal of Flood Risk Management*, vol.*2*, no.4, pp.285-292.

Vashist, K & Singh, KK 2023, 'HEC-RAS 2D modeling for flood inundation mapping: a case study of the Krishna River Basin', *Water Practice & Technology*, vol.18, no.4, pp.831-844.

Vivekanandan, N 2015, 'Flood frequency analysis using method of moments and L-moments of probability distributions', *Cogent engineering*, vol.*2*, no.1, p.1018704.

Vivekanandan, N 2017, 'Assessment of extreme rainfall using Gumbel distribution for estimation of peak flood discharge for ungauged catchments', *International Journal of Research and Innovation in Social Science*, vol.1, pp.1-5.

Wahba, M, Sharaan, M, Elsadek, WM, Kanae, S & Hassan, HS 2024, 'Examination of the efficacy of machine learning approaches in the generation of flood susceptibility maps', *Environmental Earth Sciences*, vol.83, no.14, p.429.

Wang, L, Cui, S, Li, Y, Huang, H, Manandhar, B, Nitivattananon, V, Fang, X & Huang, W 2022, 'A review of the flood management: from flood control to flood resilience', *Heliyon*, vol.*8*, no.11.

Wang, X, Xia, J, Dong, B, Zhou, M & Deng, S 2021, 'Spatiotemporal distribution of flood disasters in Asia and influencing factors in 1980–2019', *Natural Hazards*, vol.*108*, no.3, pp.2721-2738.

Water Resources Council 1976, *Guidelines for determining flood flow frequency*, United States of America, Washington DC.

Xing, Y, Shao, D, Ma, X, Zhang, S & Jiang, G 2021, 'Investigation of the importance of different factors of flood inundation modeling applied in urbanized area with variance-based global sensitivity analysis', *Science of The Total Environment*, vol.772, p.145327.

Zhang, H, Chen, L & Singh, VP 2021, 'Flood frequency analysis using generalized distributions and entropy-based model selection method', *Journal of Hydrology*, vol.595, p.125610.

Zhang, Q, Gu, X, Singh, VP, Xiao, M & Chen, X 2015, 'Evaluation of flood frequency under non-stationarity resulting from climate indices and reservoir indices in the East River basin, China', *Journal of Hydrology*, vol.527, pp.565-575.

APPENDIX

Appendix 1: Computational Table of Gumbel Extreme Value and Log Pearson Type III

Year	AMS (Q_i)	Descending order (Q_i)	Rank	P	T	Reduced Variate (Q_T)	Log(Q_i)
1979	1220.8413	1717.6198	1	0.02	45.00	3.795447	3.234927
1981	1112.2185	1628.6584	2	0.04	22.50	3.09087	3.21183
1980	1277.4463	1595.1451	3	0.07	15.00	2.673752	3.2028
1982	879.3852	1544.5869	4	0.09	11.25	2.374184	3.188812
1983	1436.0885	1492.258	5	0.11	9.00	2.138911	3.173844
1984	1288.9705	1459.54	6	0.13	7.50	1.944206	3.164216
1985	1050.1417	1436.0885	7	0.16	6.43	1.777405	3.157181
1986	1717.6198	1407.2761	8	0.18	5.63	1.630945	3.148379
1987	1079.1853	1374.7323	9	0.20	5.00	1.49994	3.138218
1988	825.00977	1343.2571	10	0.22	4.50	1.38105	3.128159
1989	1063.6971	1288.9705	11	0.24	4.09	1.271888	3.110243
1990	701.7802	1277.4463	12	0.27	3.75	1.170683	3.106343
1991	898.60834	1220.8413	13	0.29	3.46	1.076088	3.086659
1992	584.3073	1197.3318	14	0.31	3.21	0.987048	3.078215
1993	801.0114	1189.5796	15	0.33	3.00	0.90272	3.075394
1994	1343.2571	1173.782	16	0.36	2.81	0.822421	3.069587
1995	1544.5869	1154.2091	17	0.38	2.65	0.745582	3.062284
1996	1492.258	1118.3171	18	0.40	2.50	0.671727	3.048565
1997	1154.2091	1112.2185	19	0.42	2.37	0.600448	3.04619
1998	1189.5796	1079.1853	20	0.44	2.25	0.531391	3.033096
1999	1407.2761	1063.6971	21	0.47	2.14	0.464246	3.026818
2000	1026.2189	1050.1417	22	0.49	2.05	0.398735	3.021248
2001	898.852	1026.2189	23	0.51	1.96	0.334606	3.01124
2002	581.1512	986.0568	24	0.53	1.88	0.271625	2.993902
2003	986.0568	954.44275	25	0.56	1.80	0.209573	2.97975
2004	926.7205	926.7205	26	0.58	1.73	0.148241	2.966949
2005	1459.54	903.5251	27	0.60	1.67	0.087422	2.95594
2006	954.44275	898.852	28	0.62	1.61	0.02691	2.953688
2007	1628.6584	898.60834	29	0.64	1.55	-0.03351	2.95357
2008	1197.3318	890.6227	30	0.67	1.50	-0.09405	2.949694
2009	805.99976	879.3852	31	0.69	1.45	-0.15495	2.944179
2010	1374.7323	856.706	32	0.71	1.41	-0.21649	2.932832
2011	778.6164	852.4497	33	0.73	1.36	-0.27896	2.930669
2012	604.0577	825.00977	34	0.76	1.32	-0.34272	2.916459

2013	852.4497	805.99976	35	0.78	1.29	-0.40818	2.906335
2014	903.5251	801.0114	36	0.80	1.25	-0.47588	2.903639
2015	748.2664	778.6164	37	0.82	1.22	-0.54651	2.891324
2016	1118.3171	748.2664	38	0.84	1.18	-0.62098	2.874056
2017	890.6227	710.2826	39	0.87	1.15	-0.70057	2.851431
2018	1173.782	701.7802	40	0.89	1.13	-0.7872	2.846201
2019	856.706	676.7931	41	0.91	1.10	-0.88392	2.830456
2020	1595.1451	604.0577	42	0.93	1.07	-0.99623	2.781078
2021	710.2826	584.3073	43	0.96	1.05	-1.13575	2.766641
2022	676.7931	581.1512	44	0.98	1.02	-1.33675	2.764289
				Mean of Log (Qi)			3.009485
				Standard deviation of Log (Qi)			0.125622
				Skewness coefficient (G)			-0.12537

Appendix 2: Confidence limits

Exceedance Probability (%)	**LP3 Distribution curve**	**95% Lower Bound**	**95% Upper Bound**	**Diff.Bounds LP3**	**GEV Distribution curve**	**95% Lower Bound 2**	**95% Upper Bound 3**	**Diff. Bounds GEV**
2.22	1794.61	1582.38	2145.31	562.93	1918.96	1591.01	2246.91	655.90
4.44	1652.69	1472.87	1939.70	466.83	1733.59	1461.48	2005.70	544.22
6.67	1565.42	1404.21	1816.13	411.92	1623.85	1384.44	1863.26	478.82
8.89	1501.49	1353.15	1727.12	373.98	1545.03	1328.86	1761.21	432.35
11.11	1450.26	1311.69	1656.80	345.11	1483.13	1285.00	1681.27	396.26
13.33	1407.12	1276.37	1598.33	321.96	1431.91	1248.54	1615.28	366.74
15.56	1369.44	1245.19	1547.86	302.67	1388.02	1217.14	1558.91	341.77
17.78	1336.07	1217.28	1503.65	286.37	1349.49	1189.42	1509.56	320.14
20	1305.85	1191.76	1464.04	272.28	1315.02	1164.48	1465.57	301.09
22.22	1278.12	1168.10	1428.04	259.94	1283.74	1141.71	1425.78	284.08

24.44	1252.39	1145.95	1394.98	249.03	1255.02	1120.65	1389.40	268.74
26.67	1228.19	1124.91	1364.19	239.28	1228.40	1100.99	1355.80	254.81
28.89	1205.48	1104.98	1335.56	230.58	1203.51	1082.47	1324.55	242.08
31.11	1183.91	1085.89	1308.64	222.75	1180.08	1064.88	1295.29	230.41
33.33	1163.31	1067.49	1283.17	215.68	1157.90	1048.07	1267.73	219.66
35.56	1143.46	1049.59	1258.86	209.26	1136.77	1031.90	1241.65	209.75
37.78	1124.40	1032.27	1235.74	203.47	1116.56	1016.25	1216.86	200.61
40	1105.96	1015.35	1213.57	198.22	1097.13	1001.03	1193.22	192.19
42.22	1088.03	998.76	1192.23	193.47	1078.37	986.15	1170.59	184.44
44.44	1070.55	982.45	1171.61	189.16	1060.20	971.53	1148.87	177.34
46.67	1053.37	966.28	1151.54	185.26	1042.54	957.11	1127.97	170.86
48.89	1036.57	950.35	1132.10	181.75	1025.30	942.80	1107.80	165.00
51.11	1020.03	934.54	1113.14	178.61	1008.43	928.56	1088.30	159.75
53.33	1003.69	918.79	1094.59	175.80	991.86	914.31	1069.41	155.10
55.56	987.43	903.00	1076.29	173.29	975.53	900.00	1051.07	151.06
57.78	971.34	887.26	1058.35	171.10	959.40	885.57	1033.22	147.65
60	955.30	871.45	1040.63	169.18	943.40	870.96	1015.83	144.87
62.22	939.26	855.53	1023.07	167.54	927.48	856.11	998.84	142.73
64.44	923.16	839.45	1005.60	166.15	911.58	840.95	982.21	141.26
66.67	906.87	823.08	988.09	165.01	895.65	825.42	965.88	140.46
68.89	890.48	806.50	970.61	164.11	879.63	809.45	949.81	140.35
71.11	873.84	789.58	953.02	163.44	863.44	792.96	933.92	140.96
73.33	856.87	772.24	935.23	162.99	847.00	775.85	918.15	142.30

75.56	839.39	754.29	917.05	162.77	830.23	758.03	902.43	144.39
77.78	821.44	735.77	898.53	162.76	813.01	739.37	886.65	147.28
80	802.80	716.47	879.44	162.97	795.19	719.69	870.69	151.00
82.22	783.27	696.18	859.58	163.40	776.61	698.80	854.42	155.62
84.44	762.59	674.65	838.71	164.06	757.02	676.39	837.64	161.25
86.67	740.31	651.40	816.35	164.96	736.08	652.07	820.09	168.03
88.89	716.07	626.08	792.18	166.10	713.29	625.19	801.39	176.19
91.11	688.91	597.72	765.26	167.54	687.84	594.76	780.92	186.16
93.33	657.30	564.77	734.06	169.30	658.29	558.96	757.63	198.67
95.56	617.77	523.73	695.19	171.47	621.59	513.90	729.28	215.38
97.78	561.10	465.43	639.55	174.12	568.70	448.11	689.30	241.19

Appendix 3: Geometrical data model setup

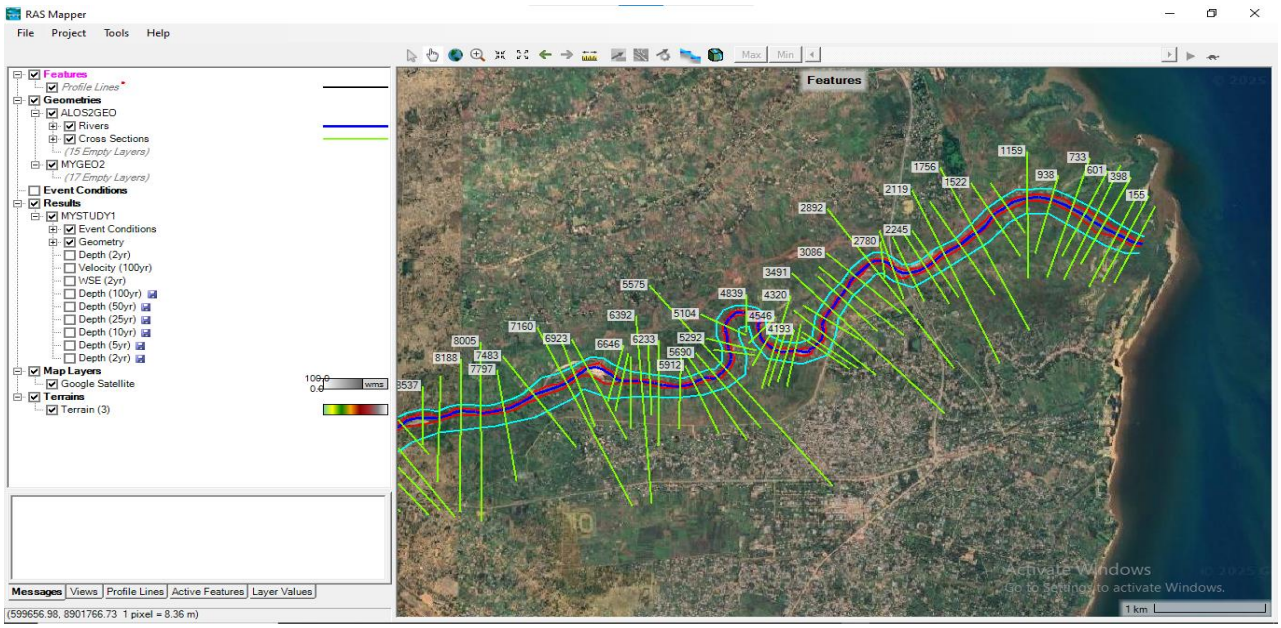

Appendix 4: Geometry data/river cross-sections

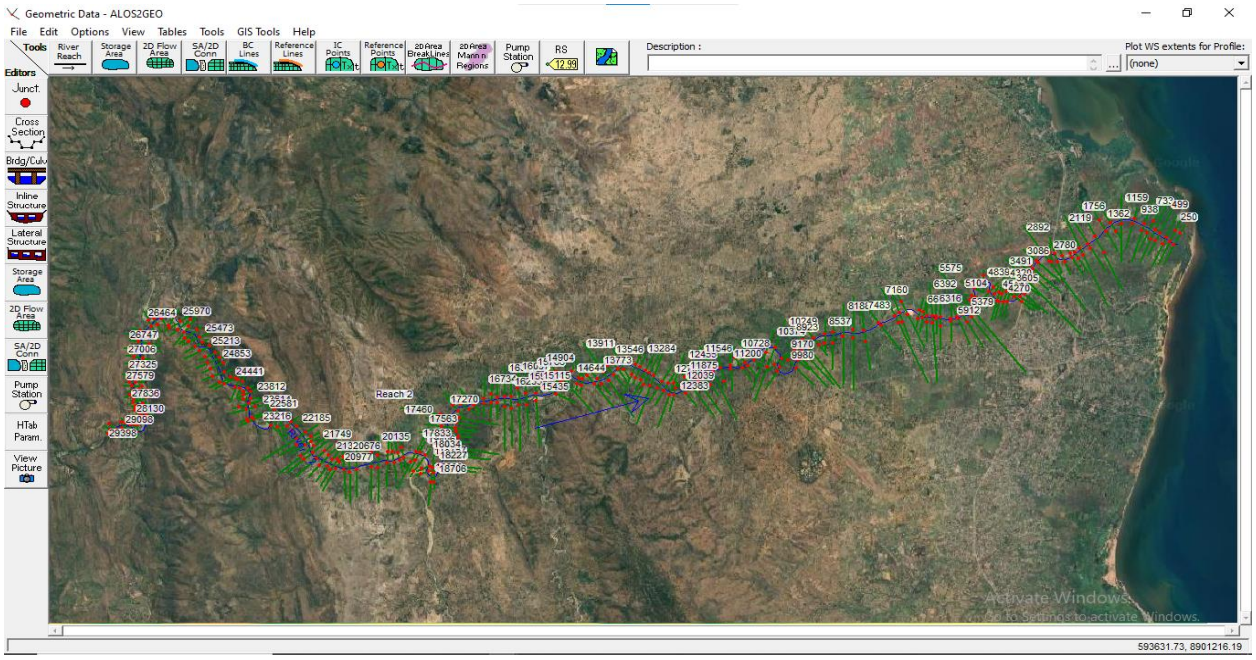

Appendix 5: HEC-RAS flood inundation maps, 2, 5, 10, 25, 50 and 100 year flood inundation maps respectively

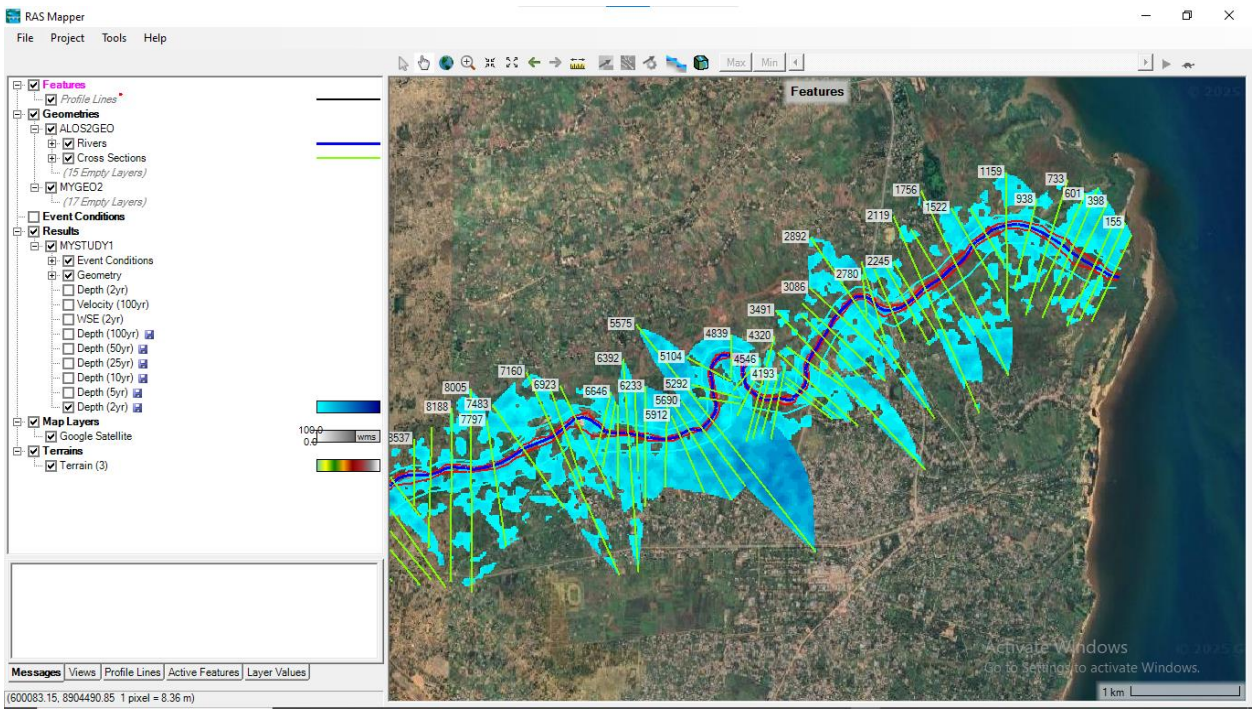

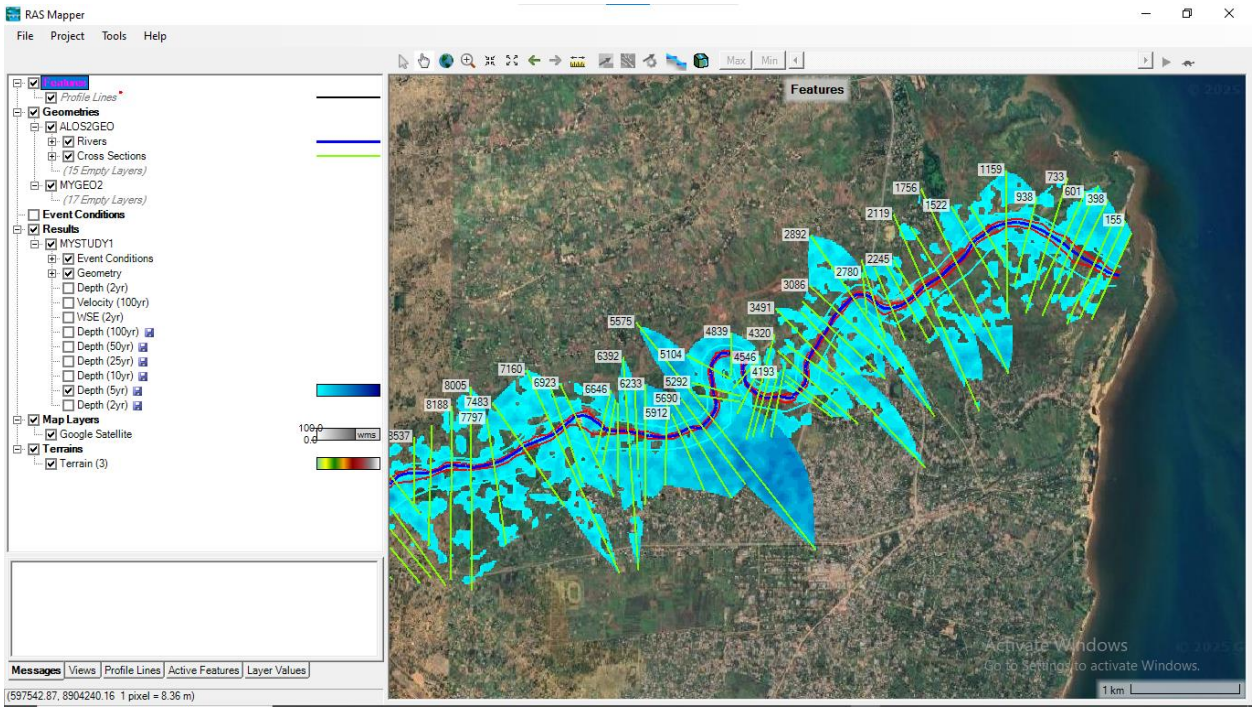
RAS Mapper
File Project Tools Help
Features
Profile Lines
Geometries
ALOS2GEO
Rivers
Cross Sections
(15 Empty Layers)
MYGEO2
(17 Empty Layers)
Event Conditions
Results
MYSTUDY1
Event Conditions
Geometry
Depth (2yr)
Velocity (100yr)
WSE (2yr)
Depth (100yr)
Depth (50yr)
Depth (25yr)
Depth (10yr)
Depth (5yr)
Depth (2yr)
Map Layers
Google Satellite
Terrains
Terrain (3)
Messages Views Profile Lines Active Features Layer Values
(597542.87, 8904240.16 1 pixel = 8.36 m)
Features
1159
733
1756
938
601
1522
398
2119
155
2892
2245
2780
3086
3491
5575
4839
4320
6392
5104
4546
4193
7160
6923
6646
6233
5292
8005
5690
8188
7483
5912
7797
8537
1 km

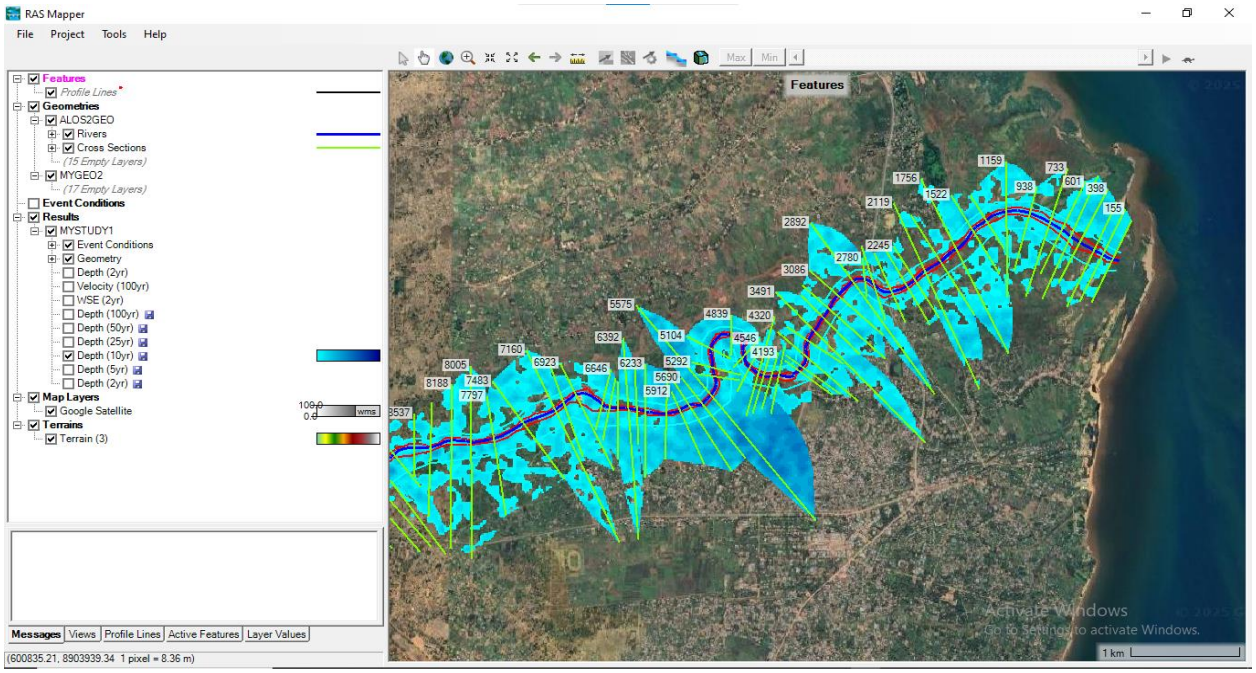
RAS Mapper
File Project Tools Help
Features
Profile Lines
Geometries
ALOS2GEO
Rivers
Cross Sections
(15 Empty Layers)
MYGEO2
(17 Empty Layers)
Event Conditions
Results
MYSTUDY1
Event Conditions
Geometry
Depth (2yr)
Velocity (100yr)
WSE (2yr)
Depth (100yr)
Depth (50yr)
Depth (25yr)
Depth (10yr)
Depth (5yr)
Depth (2yr)
Map Layers
Google Satellite
Terrains
Terrain (3)
Messages Views Profile Lines Active Features Layer Values
(600835.21, 8903939.34 1 pixel = 8.36 m)
Features
1159
733
1756
938
601
1522
398
2119
155
2892
2245
2780
3086
3491
5575
4839
4320
6392
5104
4546
4193
7160
6923
6646
6233
5292
8005
5690
8188
7483
5912
7797
8537
1 km

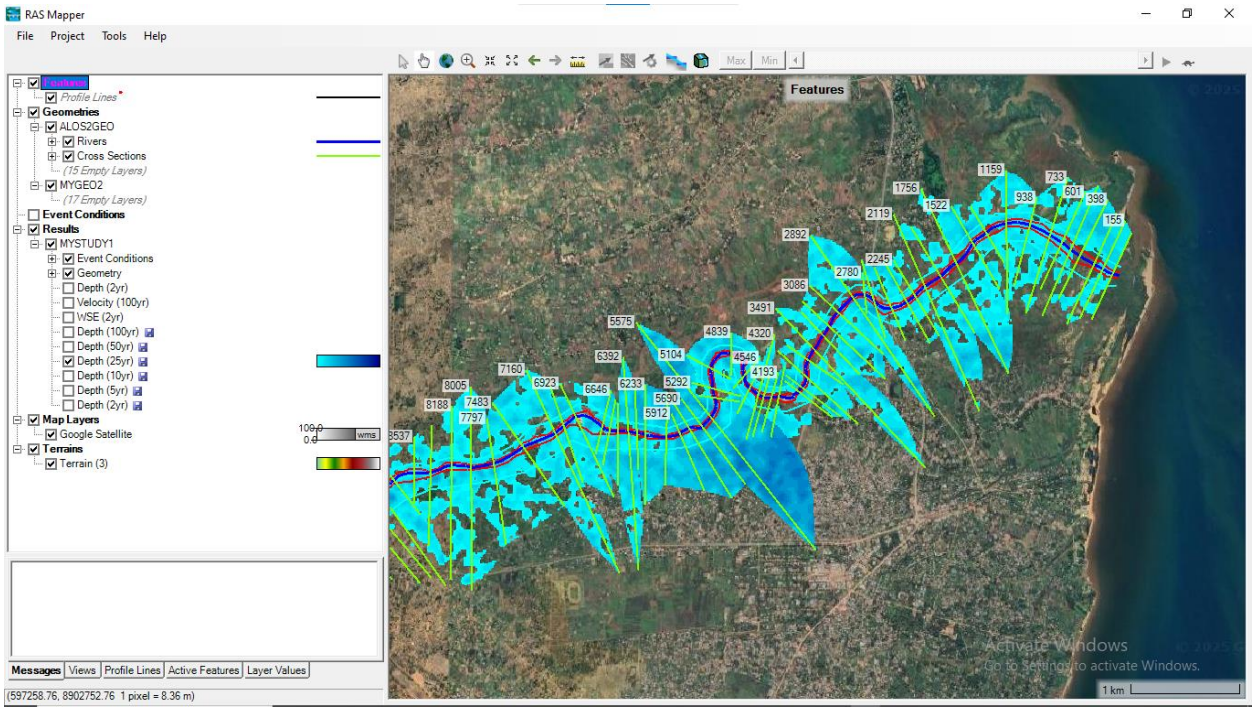
RAS Mapper
File Project Tools Help
Features
Profile Lines
Geometries
ALOS2GEO
Rivers
Cross Sections
(15 Empty Layers)
MYGEO2
(17 Empty Layers)
Event Conditions
Results
MYSTUDY1
Event Conditions
Geometry
Depth (2yr)
Velocity (100yr)
WSE (2yr)
Depth (100yr)
Depth (50yr)
Depth (25yr)
Depth (10yr)
Depth (5yr)
Depth (2yr)
Map Layers
Google Satellite
Terrains
Terrain (3)
Messages Views Profile Lines Active Features Layer Values
(597258.76, 8902752.76 1 pixel = 8.36 m)
Features
1159
733
1756
938
601
398
1522
2119
155
2892
2245
2780
3086
3491
5575
4839
4320
6392
5104
4546
4193
7160
6923
6646
6233
5292
8005
5690
8188
7483
5912
7797
8537
Activate Windows
Go to Settings to activate Windows.
1 km

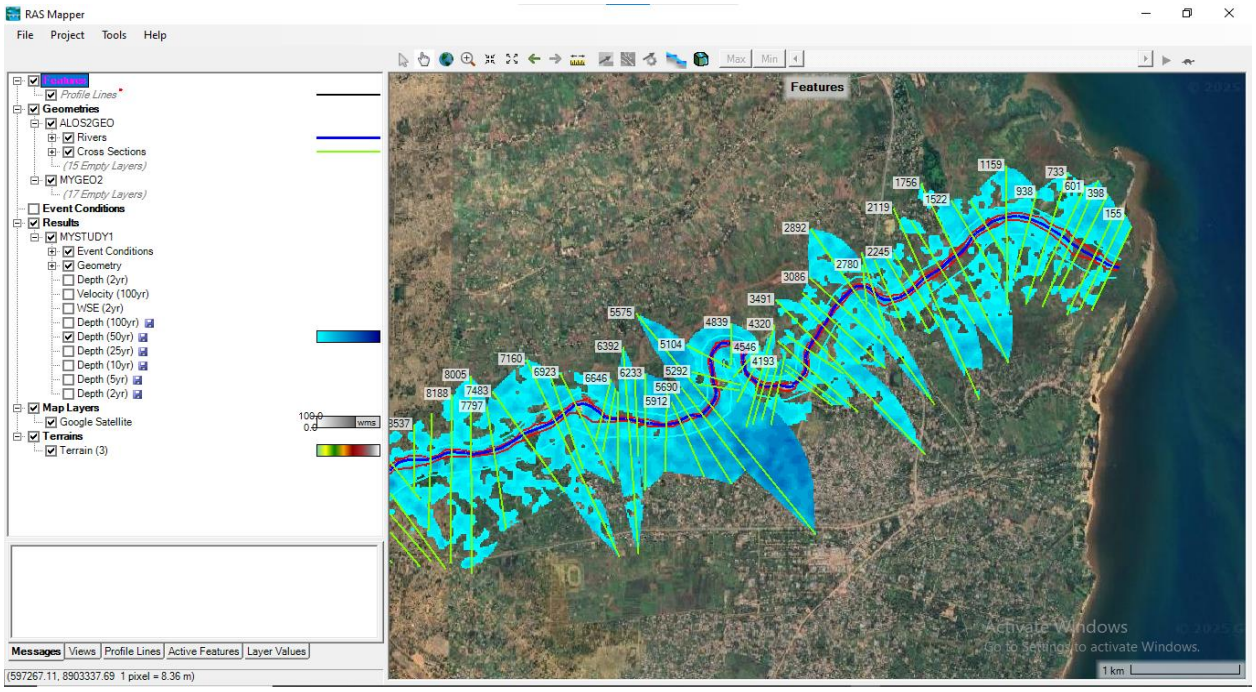
RAS Mapper
File Project Tools Help
Features
Profile Lines
Geometries
ALOS2GEO
Rivers
Cross Sections
(15 Empty Layers)
MYGEO2
(17 Empty Layers)
Event Conditions
Results
MYSTUDY1
Event Conditions
Geometry
Depth (2yr)
Velocity (100yr)
WSE (2yr)
Depth (100yr)
Depth (50yr)
Depth (25yr)
Depth (10yr)
Depth (5yr)
Depth (2yr)
Map Layers
Google Satellite
Terrains
Terrain (3)
Messages Views Profile Lines Active Features Layer Values
(597267.11, 8903337.69 1 pixel = 8.36 m)
Features
1159
733
1756
938
601
398
1522
2119
155
2892
2245
2780
3086
3491
5575
4839
4320
6392
5104
4546
4193
7160
6923
6646
6233
5292
8005
5690
8188
7483
5912
7797
8537
Activate Windows
Go to Settings to activate Windows.
1 km

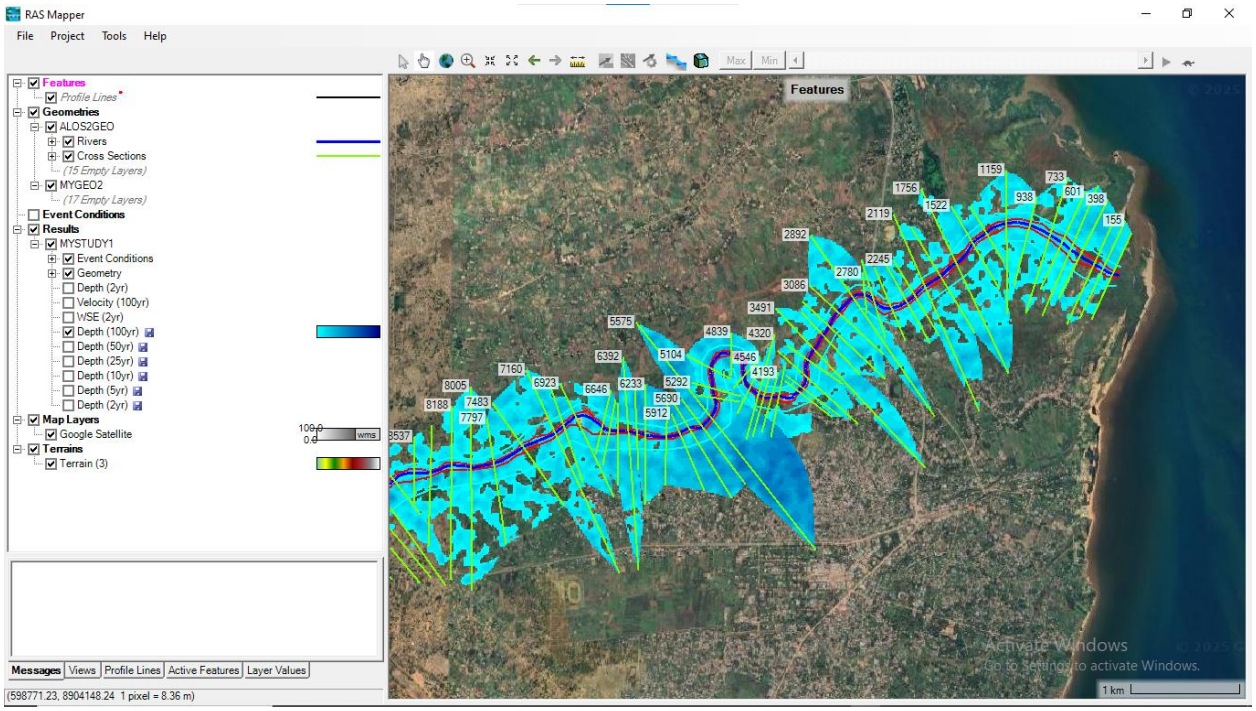

Appendix 6: Roughness or Manning's coefficient

RIVER STATION	LEFT BANK (n)	MAIN CHANNEL (n)	RIGHT BANK (n)
29398	0.035	0.03	0.035
29327	0.035	0.03	0.035
29245	0.03	0.03	0.03
29098	0.03	0.033	0.03
29042	0.03	0.033	0.03
28942	0.03	0.03	0.03
28850	0.03	0.04	0.03
28791	0.03	0.04	0.03
28480	0.03	0.04	0.03
28376	0.035	0.04	0.035
28311	0.035	0.03	0.035
28202	0.035	0.03	0.035
28160	0.035	0.033	0.035
28130	0.035	0.033	0.035
28054	0.035	0.033	0.035
28003	0.02	0.033	0.03
27901	0.02	0.033	0.03
27836	0.03	0.03	0.03

27739	0.03	0.033	0.02
27671	0.03	0.03	0.035
27579	0.03	0.033	0.03
27474	0.03	0.03	0.03
27325	0.03	0.03	0.03
27175	0.03	0.03	0.03
27006	0.03	0.03	0.05
26867	0.035	0.03	0.025
26747	0.035	0.03	0.03
26646	0.03	0.03	0.03
26464	0.025	0.03	0.025
26344	0.025	0.033	0.025
26224	0.025	0.033	0.025
25970	0.03	0.033	0.03
25838	0.025	0.033	0.025
25738	0.025	0.033	0.025
25610	0.025	0.033	0.025
25473	0.025	0.033	0.035
25338	0.03	0.033	0.03
25213	0.03	0.03	0.025
25020	0.03	0.033	0.025
24853	0.03	0.033	0.025
24735	0.03	0.033	0.03
24620	0.03	0.03	0.03
24441	0.025	0.033	0.035
24288	0.035	0.033	0.035
24222	0.03	0.033	0.03
24023	0.035	0.033	0.03
23938	0.03	0.03	0.03
23812	0.03	0.033	0.025
23739	0.025	0.033	0.035
23614	0.03	0.033	0.03
23504	0.03	0.03	0.035
23408	0.025	0.03	0.03
23216	0.03	0.033	0.025
23172	0.03	0.033	0.025
22708	0.03	0.033	0.03
22581	0.03	0.033	0.03
22484	0.03	0.033	0.03
22185	0.03	0.033	0.03
22065	0.03	0.03	0.03

21875	0.03	0.03	0.03
21749	0.02	0.033	0.05
21666	0.02	0.033	0.03
21549	0.02	0.033	0.03
21455	0.02	0.03	0.03
21312	0.03	0.033	0.03
21178	0.03	0.03	0.03
21066	0.03	0.03	0.03
20977	0.03	0.03	0.03
20911	0.03	0.03	0.03
20774	0.03	0.03	0.03
20676	0.03	0.03	0.03
20536	0.03	0.03	0.03
20264	0.03	0.03	0.03
20135	0.03	0.03	0.03
19964	0.025	0.033	0.035
19848	0.025	0.033	0.03
19739	0.03	0.033	0.03
19651	0.03	0.033	0.03
19406	0.03	0.033	0.03
19337	0.03	0.033	0.03
19222	0.03	0.033	0.03
18993	0.03	0.033	0.03
18901	0.03	0.033	0.03
18757	0.03	0.033	0.03
18706	0.03	0.033	0.03
18480	0.03	0.033	0.03
18411	0.03	0.033	0.03
18227	0.03	0.033	0.03
18133	0.03	0.033	0.03
18034	0.03	0.033	0.03
17919	0.03	0.03	0.03
17833	0.03	0.03	0.03
17749	0.03	0.03	0.03
17678	0.03	0.03	0.03
17563	0.03	0.03	0.03
17460	0.03	0.03	0.03
17270	0.03	0.033	0.03
17108	0.03	0.033	0.03
16955	0.03	0.033	0.03
16734	0.03	0.03	0.03

16603	0.03	0.03	0.03
16485	0.03	0.03	0.03
16351	0.03	0.033	0.03
16235	0.03	0.033	0.03
16097	0.03	0.03	0.03
15941	0.03	0.033	0.03
15766	0.03	0.033	0.03
15435	0.02	0.033	0.02
15288	0.02	0.033	0.02
15115	0.02	0.033	0.02
14904	0.02	0.033	0.02
14644	0.03	0.03	0.03
14472	0.03	0.03	0.03
14388	0.03	0.03	0.03
14184	0.03	0.033	0.03
14073	0.03	0.033	0.03
13911	0.03	0.033	0.03
13773	0.03	0.033	0.03
13647	0.03	0.033	0.03
13546	0.03	0.033	0.03
13284	0.03	0.03	0.03
13188	0.03	0.03	0.03
13074	0.03	0.03	0.03
12988	0.03	0.03	0.03
12884	0.03	0.03	0.03
12709	0.03	0.03	0.03
12582	0.03	0.03	0.03
12455	0.03	0.033	0.03
12383	0.03	0.033	0.03
12205	0.03	0.033	0.03
12039	0.03	0.03	0.03
11875	0.03	0.033	0.03
11737	0.03	0.03	0.03
11546	0.03	0.03	0.03
11383	0.03	0.03	0.03
11200	0.03	0.03	0.03
11007	0.03	0.03	0.03
10895	0.03	0.03	0.04
10728	0.03	0.03	0.03
10374	0.03	0.03	0.03
10249	0.025	0.033	0.025

9980	0.025	0.033	0.025
9808	0.03	0.033	0.025
9402	0.03	0.033	0.03
9263	0.03	0.03	0.025
9170	0.03	0.03	0.025
9064	0.03	0.03	0.025
8923	0.03	0.03	0.03
8748	0.03	0.03	0.03
8537	0.025	0.033	0.03
8388	0.025	0.033	0.03
8188	0.03	0.03	0.03
8005	0.03	0.033	0.03
7797	0.03	0.033	0.03
7483	0.03	0.03	0.03
7160	0.025	0.03	0.025
7058	0.025	0.033	0.025
6923	0.025	0.033	0.025
6646	0.025	0.033	0.025
6566	0.025	0.033	0.025
6483	0.025	0.03	0.025
6392	0.03	0.03	0.03
6316	0.03	0.03	0.03
6233	0.03	0.033	0.03
6041	0.025	0.025	0.025
5912	0.025	0.025	0.025
5813	0.025	0.033	0.025
5690	0.025	0.033	0.025
5575	0.025	0.033	0.025
5379	0.025	0.025	0.025
5292	0.025	0.025	0.025
5104	0.025	0.025	0.025
4839	0.025	0.033	0.025
4546	0.025	0.033	0.025
4422	0.025	0.025	0.025
4320	0.025	0.033	0.025
4270	0.025	0.033	0.025
4193	0.025	0.025	0.025
4128	0.025	0.033	0.025
3919	0.025	0.033	0.025
3870	0.025	0.033	0.025
3766	0.025	0.025	0.025

3605	0.025	0.025	0.025
3491	0.025	0.033	0.025
3339	0.025	0.033	0.025
3238	0.025	0.033	0.025
3086	0.025	0.03	0.025
2892	0.025	0.03	0.025
2780	0.025	0.03	0.025
2666	0.025	0.033	0.025
2488	0.025	0.033	0.025
2334	0.025	0.025	0.025
2245	0.025	0.025	0.025
2119	0.025	0.025	0.025
1945	0.025	0.025	0.025
1756	0.025	0.025	0.025
1522	0.025	0.033	0.025
1362	0.025	0.025	0.025
1159	0.025	0.025	0.025
938	0.025	0.025	0.025
733	0.025	0.025	0.025
601	0.025	0.025	0.025
499	0.025	0.025	0.025
398	0.025	0.025	0.025
250	0.025	0.025	0.025
155	0.025	0.025	0.025
56	0.025	0.025	0.025

Appendix 7: Goodness of Fit test

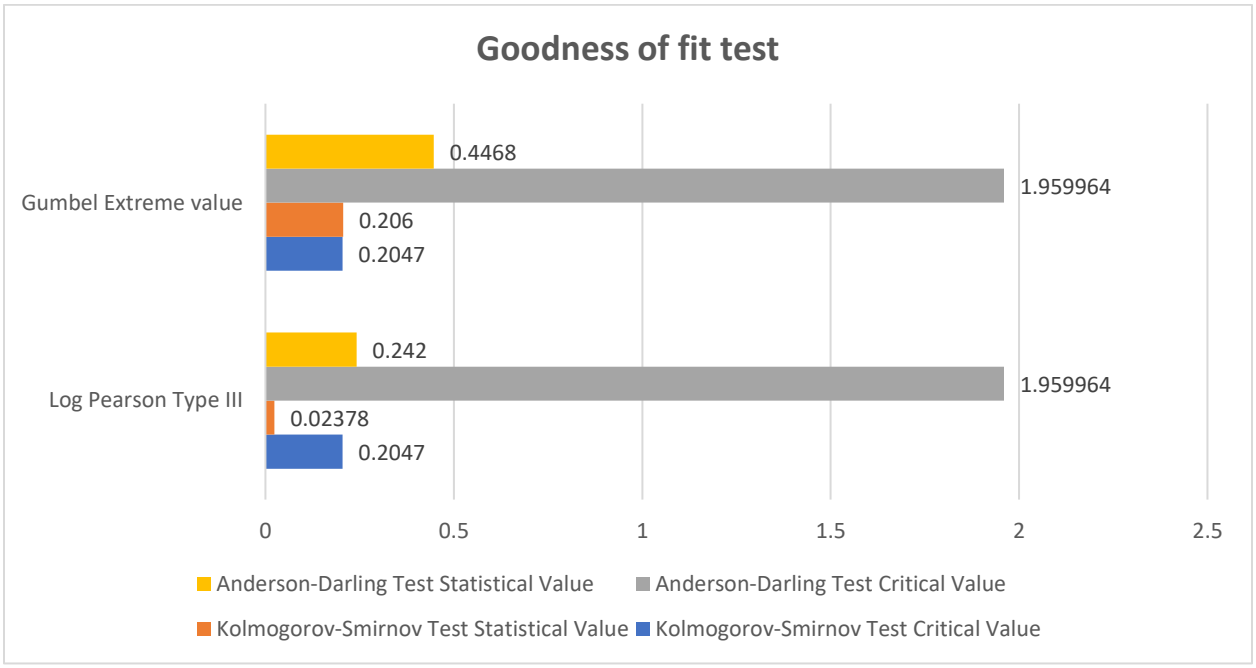

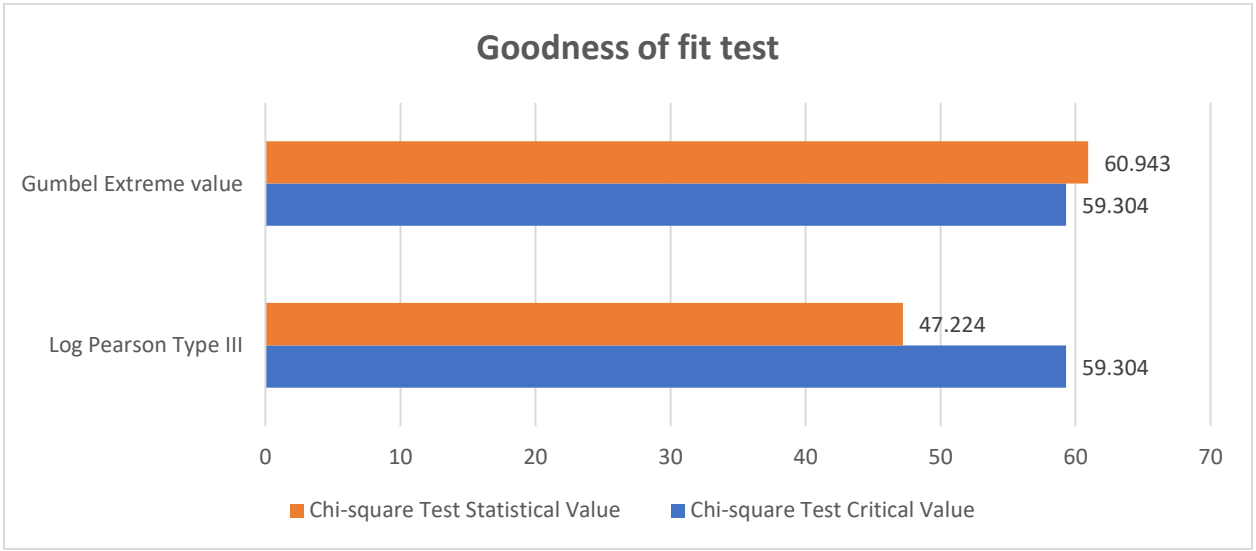

Appendix 8: Descriptive statistics for annual maximum series data (flowrate) from 1979 to 2022 at Mwakimeme.

Statistic	**Value**	**Percentile**	**Value**
Sample size	44	Minimum	581.15
Range	1136.47	5%	614.97
Mean	1063.99	10%	704.33
Variance	91526.59	25% (Q1)	845.59
Standard deviation	302.53	50% (Median)	1038.18
Standard error	45.61	75% (Q3)	1280.33
Coefficient of Variation	0.284	90%	1482.44
Skewness	0.365	95%	1587.56
Kurtosis	-0.748	Maximum	1717.62

Appendix 9: Estimation of Peak Floods by Gumbel extreme value and Log Pearson Type III at Mwenitete gauge

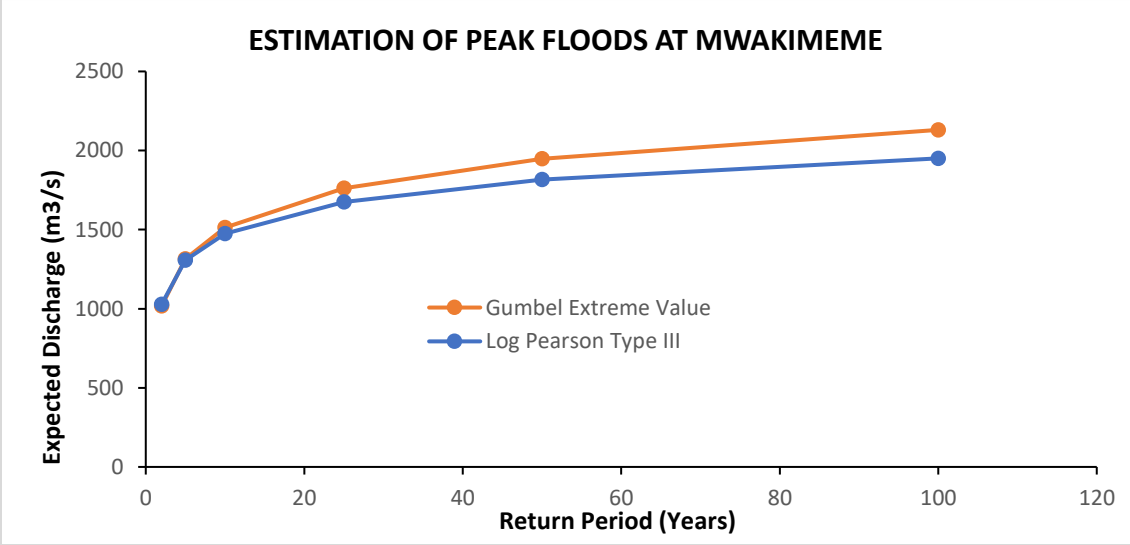

Appendix 10: Confidence limits of LP3 data series, n (44) at 95% confidence level

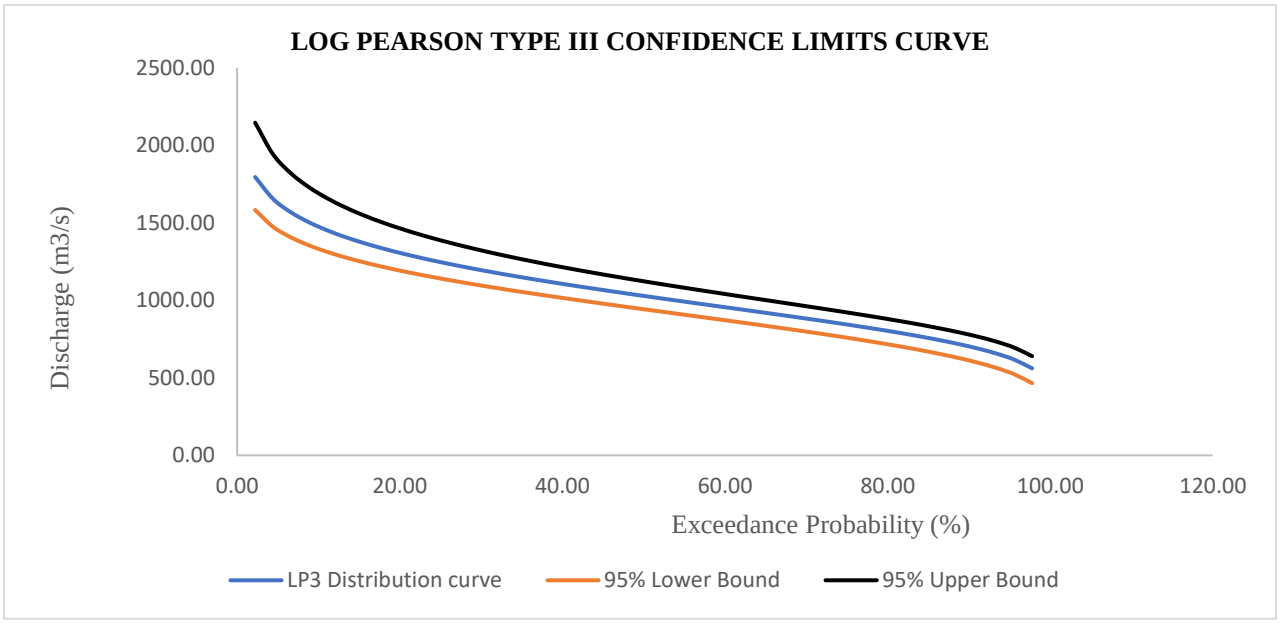

Appendix 11: Confidence limits of GEV data series, n (44) at 95% confidence level

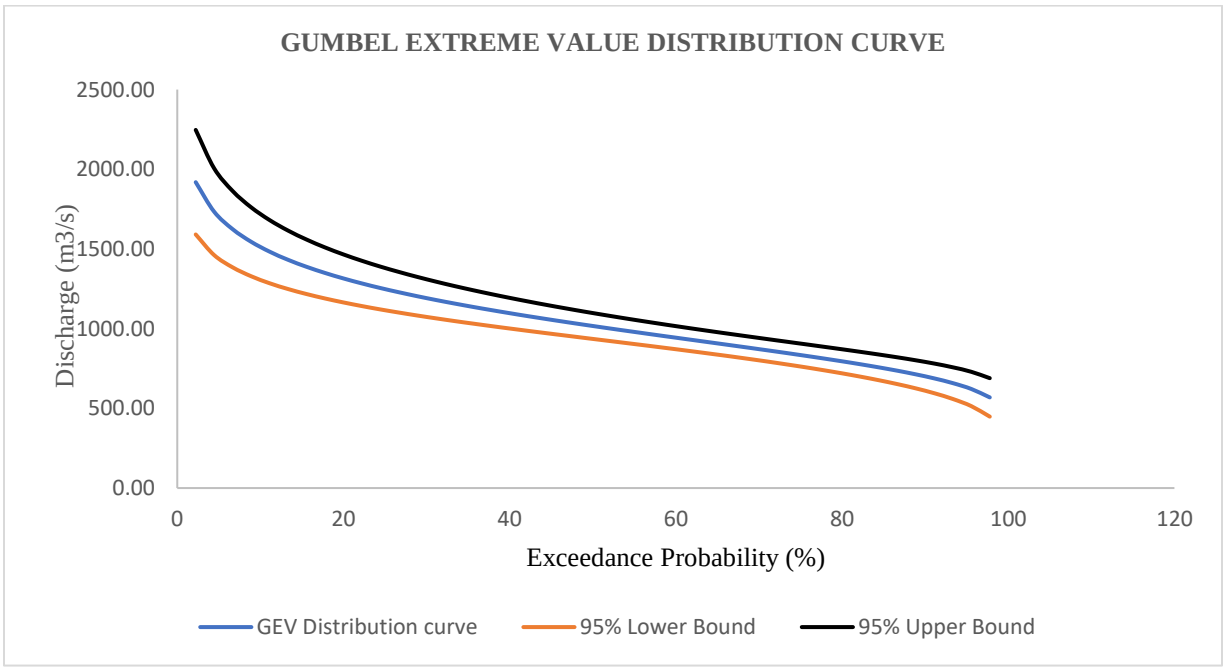

Appendix 12: Differences in Upper and Lower Bounds for LP3 and GEV

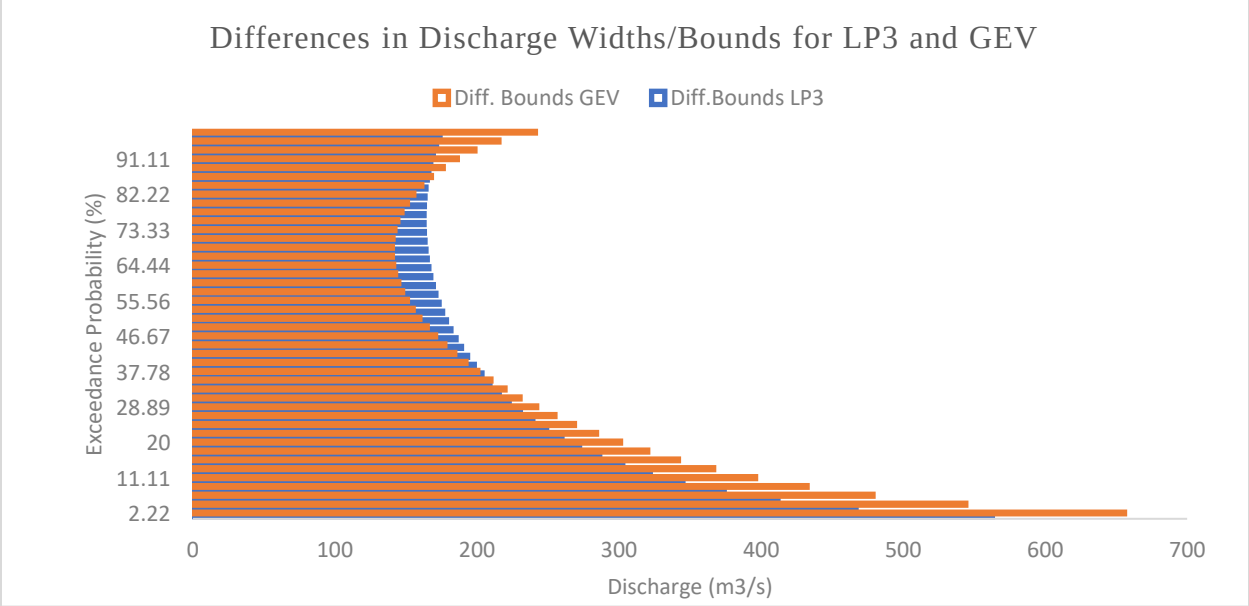

Appendix 13: Confidence limits for Gumbel Extreme Value and Log Pearson Type III

EP (%)	**RP (Years)**	**Log Pearson Type III (Bulletin 17B)**						**Gumbel Extreme Value**				
Exceedance probability (%)	Return Period (Years)	a	b	LP3 Distribution	95% Lower Bound LP3	95% Upper Bound LP3	Diff. Bounds LP3	Probable Error (Se)	GEV Distribution	95% Lower Bound GEV	95% Upper Bound GEV	Diff. Bounds GEV
50	2	0.96	-0.09	1028.27	942.43	1122.57	180.14	41.40	1016.82	935.68	1097.97	162.30
20	5	0.96	0.63	1305.85	1191.76	1464.04	272.28	76.81	1315.02	1164.48	1465.57	301.09
10	10	0.96	1.52	1474.65	1331.49	1690.16	358.67	105.44	1512.46	1305.80	1719.11	413.31
4	25	0.96	2.83	1674.55	1489.90	1971.00	481.10	143.16	1761.92	1481.32	2042.52	561.20
2	50	0.96	3.86	1815.39	1598.22	2175.87	577.65	171.65	1946.98	1610.54	2283.42	672.87
1	100	0.96	4.90	1950.40	1700.06	2376.98	676.92	200.15	2130.68	1738.38	2522.97	784.59